Trace Elements in Magnetite and Hematite for Improving Pathfinder Element Selection of the Hillside copper mineralisation, Yorke Peninsula

Benjamin Thomas

Centre for Tectonics, Resources and Exploration
Department of Geology and Geophysics
School of Earth and Environmental Sciences
University of Adelaide, South Australia
benjamin.thomas@student.adelaide.edu.au

Table of Contents

1 Abstract 4
2 Introduction 5
2.1 Mining and exploration history 6
2.2 Geological setting 8
2.4 Local geology and previous studies 9
2.5 Proterzoic 10
3 Structural Setting 10
4 Project aims 11
5 Core logging study 12
5.1 Host rocks 12
6 Analytical procedures 14
6.1 Petrography 14
6.2 Scanning electron Microscope (SEM) 14
6.3 Electron Probe Micro Analysis (EPMA) 15
6.4 LA-ICPMS operating procedure 16
7 Results 17
7.1 Petrography 17
7.1.1 Iron oxide 17
7.1.2 Sulphides 17
7.2 Ore petrography 18
7.3 Accessory Minerals 18
7.4 Iron oxides 19
7.4.1 Replacement of magnetite by hematite 19
7.4.2 Primary, newly formed Hematite 19
7.4.3 Rare Earth Elements 20
7.4.4 Trace elements 21
7.5 Correlation of Elements 21
7.5.1 Trace element variation in Fe-oxides 21
7.5.2 Trace element variation in sulphides 22
7.6 Magnetite-Hematite Element Comparison 23
7.7 Sulphides 24
7.7.1 Petrography 24

7.7.2 Trace Elements 24
7.8 Sulphur Isotopes 25
8 Interpretation of results: 26
8.1 Iron Oxides 26
8.2 Co/Ni Ratio: 28
8.3 Trace element comparison 28
8.4 Sulphur Isotopes 28
8.5 Comparison of Analytical Technique 29
9 Discussion 30
9.1 Hillside ore Paragenesis 30
9.2 Magnetite to Hematite reaction 30
9.2.1 Non-redox 30
9.2.2 Redox reactions 31
9.3 Possible Pathfinder Elements 32
9.4 Hillsides Relationship with IOCG Deposits in the Gawler Craton 33
9.5 Genetic model for the Hillside mineralisation 34
9.6 Future Study Recommendations 35
10 Conclusion 35
Acknowledgements 36
References 37
Figure Captions 40
Table Captions 41

1 Abstract

The Hillside deposit is located in the southern part of the Olympic Province onthe Gawler Craton, South Australia. This area has a history of IOCG-U style deposits, including the word class Olympic Dam deposit. Several other deposits and prospects have also been identified within this Olympic Dam domain. The Hillside deposit was discovered in the 1800s but recent work by Rex Minerals has expanded the mineralisation zone and have categorised this deposit as part of the IOCG-U family. A prominent characteristic of the Hillside IOCG mineralisation is the conversion of magnetite to hematite which in previous works on IOCG-U deposits has shown to be related to the mineralisation process. Two main mineralizing episodes can be distinguished, an earlier one was extremely Fe rich and allowed the formation of magnetite and pyrite. The second stage of mineralisation involved the injection of copper mineralizing fluids concurrent with the widespread replacement of magnetite by hematite. Analysis of the iron oxides was carried out using optical methods as well as, trace element and rare earth element analysis by Electron Probe Micro Analysis and Laser Ablation ICP MS. The trace elements were used to identify compositional signature variation between the different iron oxide minerals. The rare earth element analysis showed a distinct overall enrichment in the hematite samples compared to the magnetite. The trace element analysis showed that several elements are distributed differently between the two oxides and sulphides. These elements include Cr, Zn, V, Ti, Ni, Pb and Co which show anomalies in both the oxides and sulphides. A variation between what elements are enriched is depent on the mineral they are found within. This is suggested to reflect changes in composition of the mineralising fluid from the early magnetite-pyrite to the late hematite-chalcopyrite stage. The sulphides showed that chalcopyrite was enriched in several trace elements compared to pyrite,. Sulphur isotope data were derived for pyrite and chalcopyrite also to characterise the source of the fluids. There was no systematic difference between chalcopyrite and pyrite. The data did show negative values between -2.6 $\delta^{34}S$ and -6.6 $\delta^{34}S$ which indicates that the source of the sulphur is most likely magmatic. This study gives an indication into the change in conditions that caused the replacement of magnetite by hematite and therefore the changes that caused mineralisation. An element signature was also collected to

indentify the difference between the iron oxides that will help in future works on this deposit.

2 Introduction

The Hillside Cu-Au deposit is located 170km from Adelaide on the Yorke Peninsula, South Australia, 12 km from the township of Ardrossan (Rex Minerals 2010). The deposit lies on the eastern border of the Olympic Cu-Au region on the eastern margin of the Gawler Craton. The Hillside deposit has been classified as an IOCG-(U) style deposit similar to other deposits within the Gawler Craton such as Olympic Dam and Prominent Hill (Cerlienco 2009).

The Olympic Cu-Au province contains two operating IOCG mines, the original supergiant IOCG deposit Olympic Dam and the smaller Prominent Hill. There are many prospective mineralized zones such as Oak Dam, Emmie Bluff, Carrapateena, Acropolis and Punt Hill (Fairclough 2005; Bastrakov et al. 2007; Belperio et al. 2007).

The Moonta-Wallaroo district which Hillside is situated in has a long history of copper mining dating back to the 1847 (Wade & Cochrane 1954). In recent times activity has been very limited although Wheal Hughes at Moonta was operating in 1990 (Rex Minerals 2010). The Hillside deposit itself is located within the Pine Point Copper Belt which has had historical mining of the Hillside mine prior to 1916 (Wade & Cochrane 1954). This was the incentive for renewed exploration in 2007 by Rex Minerals ltd. The exploration concept was applied along the Pine Point Fault zone following the identification of combined gravity and magnetic anomalism, which has lead to the successful discovery of the Olympic Dam and Prominent Hill deposits as well as several other identified, known occurrences (Budd et al. 1998). The Pine Point fault it's self runs approximately North-South and is ~100m wide (Flöttmann et al. 1998). The fault borders the eastern side of the Yorke Peninsula and continues along the whole coast (Flöttmann et al. 1998). The historic workings in the area were very small and were restricted to normally just one vein of high grade copper containing chalcocite, cuprite

and malachite, very little information was gathered from these workings such as the host rock geology, alteration and structural control (Wade & Cochrane 1954).

The genetic model for the large and comprehensive group of IOCG-U deposits is not fully understood (Groves et al. 2010), due to the variations between the deposits catergrised as IOCG-U there is no unifying genetic model that covers all the dofferent deposits. this study will hopefully give an indication on the processes that formed the Hillside deposit. The identification of possible pathfinder elements will also be valuable for future works and exploration processes.

This study focuses on compositional and mineralogical variation of the iron oxides within the Hillside deposit to determine mobilisation and fixation of trace and ultra-trace elements during the mineralising history. This will identify possible pathfinder elements that may improve exploration success and help distinguishing 'fertile' from 'barren' Fe-oxide Cu mineralising systems. Previous work on the deposit has identified four different stages of iron oxide formation. These include: 1. primary magnetite, 2. magnetite, 3. Hematite (replacement of magnetite) and 4. bladed hematite (primary, newly formed hematite) (Graham Teale 2010). The study of these and how they relate to mineralisation will hopefully give an indication to the conditions that caused the change to the iron oxides and caused mineralisation. The replacement of magnetite by hematite is seen at most IOCG-U deposits and this process will be looked at in greater detail to see how this replacement occurred (Belperio et al. 2007) (Oreskes and Einaudi 1990). The way that this replacement is related to the mineralisation process will also be looked at in detail. Sulphide minerals found within the deposit such as pyrite and chalcopyrite are also analysed for trace element content and variation to characterise the mineralizing event and indentify possible sources of metals and fluids. Trace elements can be used to identify compositional changes that occurred to the fluid during the mineral formation.

2.1 Mining and exploration history

The area 1-2 kilometres north of Pine Point has three historical workings: the Hillside, Phillip's and Hart's Mines (Wade & Cochrane 1954). Hart's Mine was only a small a

working following a copper vein in the cliff face near the coast. The mineralisation style here is closer to the later secondary mineralisation at Hillside and not the main mineralizing event (Wade & Cochrane 1954). Phillip and Hillside mines on the other hand were larger and had shafts sunk. Due to the age of these mines information on these is scarce until 1916, the Hart's Mine is believed to be started in 1847 but there is no information when the Hillside Mine was started (Wade & Cochrane 1954). The discovery of Hillside was by a farmer ploughing his field copper was overturned during ploughing, two shafts were sunk some time prior to 1916 (Wade & Cochrane 1954). Work had ceased between 1916 and the next Department of Mines inspection in 1929 but started again soon after 1929. The two shafts at Hillside were sunk to 26m and 48m during the period between 1929 and 1932. There is no information on when this mine was abandoned but must have occurred shortly after the last Department of mines visit in 1932 (Wade & Cochrane 1954). During the period mining 57 tons of handpicked copper ore was removed from the Hillside Mine at a very high grade of 13% copper yielding approximately 8 tons of copper (Wade & Cochrane 1954; Drexel 1979). Two lodes were identified, one at .3m and the other at 4m. The ore is in irregular shaped lenses which consist of chalcopyrite and bornite. Several other copper minerals are also present in much smaller amounts and only in certain zones, these minerals include malachite, chalcocite, covellite and atacamite (Wade & Cochrane 1954).

Exploration has been carried out sporadically since 1957 with the Department of Mines (Woodmansee 1957), then Shaw River Minerals (Drexel 1979), BHP, CRA and Dampier Mining Co. (Dampier Mining Co. Ltd et al. 1986). In more recent times companies such as MIM Exploration Pty Ltd (MIM Exploration Pty Ltd 1997), Avoca Resources (Avoca Resources Limited 2006) and most recently Rex Minerals (Rex Minerals 2009b) have all taken an interest in the area. These more recent exploration attempts have recognised the area has been genetically related to the IOCG family (Cerlienco 2009). Recent works using a scintillometer and rock chip surveys has identified Uranium is present but has yet to be found in any sort of economic volume (Mumme 1955; Rowley 1955; MIM Exploration Pty Ltd 1997). Rex Minerals which is the current tenement holder has been conducting a large amount of diamond and RC drilling in an area that was first identified from geophysical surveys which indicated a gravity and magnetic high, which has found to be an indicator of a IOCG-U deposit..

Drilling has identified five separate, broadly parallel smaller faults running approximately N-S; the Dart, Zanoni, Marion, Parsee and Songvaar faults. The Dart, Zanoni, Marion and Parsee host copper mineralisation, while the Songvaar has significant intervals of uranium mineralisation. Grades in the Dart Zone range from 0.2-1.5% Cu over 7-70 m intervals, in the Zanoni from 0.2-3.2% Cu over 8-259 m, 0.4% Cu over 200 m in the Parsee and 0.5% Cu over 55m in the Songvaar. (Rex Minerals 2010a). On July 28th Rex Minerals released there maiden resource estimation of 100Mt at 0.7% copper and 0.2 g/t of gold (Rex Minerals 2010b).

2.2 Geological setting

The Hillside deposit is located within the Pine Point Copper Belt region which is on the south-eastern edge of the Gawler Craton (Flöttmann et al. 1998). In the Craton's geological history there has been several stages of rifting and collision dating back to the Late Archaean (2560-2500 Ma) (Hand et al. 2007). Due to this complex tectonic history several tectonic subdomains are identified based on structural and tectonic differences (Ferris et al. 2002). Major events that occurred around the approximate time of the deposits formation are the Paleoproterzoic rifting events that created several basins within the Gawler Craton. The rifting events were then followed by the Kimban Orogeny (1730 – 1690 Ma) which halted the formation of the basins. The Kimban Orogeny also caused a great deal of crustal-scale shear zones, granitic magmatism and low- to high-grade metamorphism. The Orogeny was followed by a period of extension during 1680 – 1640 Ma which is associated with local magmatism and sedimentation. Post dating the Kimban Orogeny is the Kararan Orogeny 1570 – 1540 Ma, this overlaps the magmatic period of the Hiltaba Suite ofwhich representative intrusive rocks are found at Hillside. The Hillside deposit sits within the Olympic Domain which contains the Wallaroo Group metasediments (1740-1760 Ma) and metavolcanic units (Hand et al. 2007). The Wallaroo metasediments are intruded by the Mesoproterozoic Hiltaba Suit granitoids (1595-1570 Ma). This is believed to be fundamental in the formation of Oylmpic Dam deposit and is linked to other IOCG style deposits within the Gawler Craton (Ferris et al. 2002; Zang et al. 2002). The Hillside area is also intruded by another magmatic suite of the Arthurton Granite (1582±2Ma) and Tickera Granite (ca

1600-1575MA) and possibly Curramulka Gabbronorite at 1589 ± 5 Ma (Zang et al 2007), all of these units are associated with the Hiltaba suite.

The Hillside deposit sits on the very eastern edge of the Olympic Cu-Au province which covers most of the Olympic Domain (see figure 11), parts of the Mt Woods Inlier, Cleve Domian and Gawler Range Volcanics Domain (Skirrow et al. 2002) and it is the southernmost established IOCG style mineralisation of the province.

The Hillside deposit is believed to be related to the Moonta- Wallaroo district which has a long history of high grade Cu-Au mineralisation (Conor 1995). These deposits are believed to have formed through early hydrothermal alteration of iron oxides and have been related to an IOCG style mineralising process (Ruano *et al.* 2002; Skirrow *et al.* 2002). The geology of the Moonta-Wallaroo district is similar to that at Hillside with Wallaroo group metasediments and metavolcanics. These groups overlie the Mid-Palaeoproterozoic Gleesons' Landing Granite in the south west of the peninsula. The Hiltaba Suite Granitoids intrude the Wallaroo Group in the Moonta-Wallaroo district just as they do at Hillside. Outcrops of basement are rare and are largely covered by Cambrian and Tertiary sediments of the Stansbury and St Vincent Basins. Alteration at Moonta Wallaroo is complex and has been closely studied by Conor (1995); Zang (2002); Zang *et al.(* 2002). The alteration consists of calcsilicate, magnetite-biotite, chlorite dominated assemblages and later epithermal and carbonate veining. Mineralisation is associated with both the biotite and chlorite dominated assemblages (Zang *et al.* 2002).

2.4 Local geology and previous studies

The geology directly surrounding the Hillside area has had very little work carried out on it and is poorly understood, mainly due to the poor outcrop situation on the peninsula which makes it difficult to study the basement units.

During their exploration campaign Rex Minerals has carried out a large amount of drilling in 2008 - 2010 which has increased the amount of information about the basement geology. In 2009 two honours projects were carried out at the Hillside deposit

increasing the knowledge of the deposit. Rex has also employed a contract petrographer to gain further insight into how this deposit formed.

2.5 Proterzoic

The basement units in the Hillside area have been examined using geophysical methods carried out in recent times; a study has also been carried along the coast at the only basement outcrops (Raymond 2001).This showed that the basement is made up of undifferentiated Wallaroo Group with intrusions from the Hiltaba Suite Graintoids (Teakle 1983; Zang et al. 2006). A rhyolite unit was noticed during a thin section analysis of waste from the historic Hillside Mine and Harts Mine. These mines are believed to be part of the Moonta Porphyry, this indicates that Wallaroo Group-aged volcanic similar to those at the historic Moonta mines (Drexel 1979). It was also discovered that the rhyolites were the host rock at these mineralized areas.

The IOCG related Mesoproterozoic Hiltaba Suite granites which intrude the Wallaroo Group are the Arthurton sub-suite (1582 ± 7 Ma) in this case (Creaser & Cooper 1993). The Arthurton granite is described as adamellite to quartz monzonite and has a quartz, microcline, plagioclase, mica, sphene, tourmaline, magnetite and chlorite composition (Conor 1995; Zang 2002). There are two different mafic units documented in the vicinity of Hilllside area. The first is the Renowden Metabasalt Member which is of Wallaroo Group age and the second the Mesoproterozoic Curramulka Gabbronorite. The Gabbronorite has possibly been identified within the mineralized zone, due to the high degree of alteration it is difficult confidently identify this unit. The Curramulka Gabbronorite is believed to of intruded into the Wallaroo Group at 1589 ± 5 Ma. This is a similar time to that of the intrusion of the Arthurton Granite (Zang et al.)

3 Structural Setting

The large scale structural control in the area is the Pine Point Fault; this structure encloses the Hillside mineralisation making it an important factor in the creation of the Hillside deposit. This is a major structure dominating the eastern edge of the peninsula. This major structure has had very little data published on it. The main work completed on the fault zone was commissioned by PIRSA and undertaken by SRK Consulting,

who used integrated geophysical methods to better understand the architecture of the Stansbury Basin.

Features caused by Kimban Orogeny (1859-1700 Ma) can be seen within the Gawler Craton and the Wallaroo Group. These features are truncated by the Pine Point Fault, which indicates that the first period of movement occurred post the Kimban Orogeny. The fault creates the border between the Gawler Craton and the St. Vincent Block. The exact age of the formation of this fault is not known but is believed to be of Mesoproterzoic age. The fault was reactivated in the Neoproterozoic and the early Cambrian as an east dipping oblique normal fault (Teasdale et al. 2001). The Delamerian Orogeny reactivated the fault zone once again, creating a high angle oblique reverse fault with dextral movement (Teakle 1983; Zang et al. 2006). Evidence for these fault reactivations is only visible from the coastal outcrops due to the tertiary cover. During the Tertiary the fault was reactivated twice which caused grabens to form. The grabens were then in filled with Tertiary sediments and created the topography of the Yorke Peninsula seen today.

4 Project aims

The aim of this project is to develop a geochemical signature for both hematite and magnetite formation in the hillside mineralisation. The trace and rare earth elements will be examined to identify compositional difference between the two iron oxides. The trace element composition will also be examined for comparisons with the sulphides.

The REE characteristics give an indication of the compositional changes of mineral forming fluids that caused the replacement of magnetite by hematite which is related to the deposition of sulphides.

In addition, sulphur isotope samples will be analysed to complement the existing data set of sulphur isotope ratios (Talylor 2009) to further our understanding of the fluid/sulphur isotope evolution and to characterise the sulphur source. All samples collected were taken in context with the lithological setting recorded by drill core logging. The results of this study will then be compared with other IOCG-U deposits within the Gawler Craton.

5 Core logging study

A core logging study was undertaken to identify suitable samples for the iron oxide analysis and sulphur isotope study. Hole number HDD044 was selected under Rex Minerals' guidance because it contained most of the units encountered within the deposit. This hole was first logged than a range of samples were selected. Holes HDD062 and HDD033 were also logged to help gain a better understanding of the deposit. No samples were gathered from these holes but a detailed log was important in the relationship of the units found within the deposit.

5.1 Host rocks

Core logging established that the alteration was so prominent that identification of original rock units was quite difficult. Three main rock units were identified through the alteration, the first is a black/grey metasediment with metasandstone and schistose lithologies present. The metasediment is strongly banded in sections; the darker bands are dominated by biotite. The green colour that can be seen in the bands is due to the presence of amphibole. The banding in some sections changes from being perpendicular to closer to parallel to the core axis. This unit is believed to be part of the Wallaroo Group

The second is a felsic intrusive granitoid, this dominated hole HDD062. The composition of this unit is dominated by pods of coarse quartz-feldspar ± tourmaline pegmatite and fine grained quartz-feldspar aplite is also present. In sections of these units sphene can be seen, this appears to be present in the sections that show higher counts on the scintillometer which indicates a higher uranium content. This unit is the Arthurton Granite which is part of the Hiltaba Suite which is linked to many IOCG style deposits in the Gawler Craton.

The third type of lithology intersected by the drill hole HDD033 at several points is a gabbro. A small amount of this unit is also present towards the base of hole HDD044, due to the high degree of alteration the identification of the exact abundance of the gabbro was difficult. The gabbro is very rich in amphibole, pyroxene and plagioclase. It is coarse to medium gained with a grains size of approximately 1mm. This could possibly be part of the Curramulka Gabbronorite that intruded at a similar time to that of

the Arthurton Granite. This unit may be an important factor in the mineralising process of the deposit.

There are several alteration styles identified within the three holes logged. The most prominent alteration style is K-feldspar alteration which dominates large sections of the core. The specific rock unit type didn't appear to make any difference on the amount of alteration. This alteration can often be found in layered patterns, this layering does not appear to be related to the replacement that is taking place.

The metasediment is intruded by the granite and the gabbro, however the granite and gabbro are seen to intersect each other. The gabbro which is believed to be part of Curramulka Gabbronorite which has intrusion dates very similar to that of Arthurton Granite.

6 Analytical procedures

6.1 Petrography

For the petrography study 8 samples were used that had previously been collected by Graham Teale from a series of holes showing different lithologies within the deposit. A sampling session was then carried out for the sole purpose of this study with Fe oxide rich samples collected from hole HDD044 (see Table 11). This involved the collection of 15 samples and a polished block and thin sections were prepared of each sample. The polished blocks were selected because they are required for several of the analytical techniques. The thin sections allow the study of non ore minerals and are important to the petrography research section of the project.

6.2 Scanning electron Microscope (SEM)

The SEM instrument that was used was a Philips XL30 FEGSEM equipped with an Oxford CT1500HF Cryo stage, EDAX DX4 integrated Energy Dispersive X-ray Analyser with mapping capability and HKL Channel 5 Electron Back Scatter Diffraction System (EBSD). The EDAX system was used to identify minerals within the samples. The SEM was set to 25 KV for improved contrast between the magnetite and hematite which was important to the project. The spot size was set to 4µm and the back scatter method was selected for mineral distinction.

The work carried out on the SEM was used to examine features within the polished block samples that would not be visible through optical microscopes. The iron oxides and sulphides were examined for internal variations so correct microprobe locations could be selected. The SEM was also used for looking for small grained minerals that could not be seen in the optical microscope. Any minerals that were examined in the optical microscope but their identity not known were examined to obtain a chemical signature and then identify the mineral.

The iron oxides replacement textures were examined and showed that the replacements were very distinct and defined. The magnetite grains showed to be very uniform and would be perfect for microprobe analysis. The hematite is a lot harder to find due to it

normally only surrounding the much larger magnetite grains. This means that most of the hematite is too small for laser ablation ICPMS analysis as it requires a ~80µm diameter ablation spot size. Some samples show a high degree of martitization where the magnetite has been almost completely replaced by hematite. This can give hematite samples big enough but where the hematite replaces magnetite the grains are pitted

6.3 Electron Probe Micro Analysis (EPMA)

A trace and ultra trace element analysis was carried out on six representative polished block samples from the 25 samples available. These were selected on the basis for the most suitable samples to be used in the Laser Ablation Inductively Coupled Plasma Mass Spectrometer analysis (LA-ICPMS). This required large mineral grains of over 80µm that would be selected for analysis. Hematite and magnetite were both selected for the iron oxide analysis in what had been identified in preliminary studies as different generations. The sulphides were also examined and a series of chalcopyrite and pyrite grains were selected for EPMA and LA-ICPMS analysis. Several garnet grains were also used in the analysis due to their believed importance in the location of the ore body.

The elements examined in the analysis varied between the sulphides and the oxides examined. The elements analysed in the Fe-oxides included: O, Na, Mg, Al, Si, K, Ca, Ti, V, Cr, Mn, Fe, Cu, Zn, As, Ce, Pb. Elements such as Na, Mg, Al and Si were examined as a check to confirm that the sample that is been examined was an iron oxide and none of the surrounding silicates had mistakeable been analysed. The other elements were used to distinguish a compositional difference between magnetite and hematite.

The elements examined during the sulphide analysis include P, S, V, Mn, Fe, Co, Ni, Cu, Zn, As, Mo, Ag, Cd, Sb, Pd and Bi. These elements were selected as they are commonly found within sulphides. The variations between these elements within the pyrite or chalcopyrite are indications of fluid variations over time and during the mineralizing event.

6.4 LA-ICPMS operating procedure

The trace and rare earth element concentrations within the iron oxides were obtained using a Laser Ablation System coupled with an Agilent 7500 Series ICP-MS at Adelaide Microscopy, University of Adelaide. Laser settings used during the analyses were: continuous beam at 5 Hz, an 80 µm spot diameter and 75 % power level. An internal standard BHVO-1 was implemented and a known sample BCR-2 used as secondary standard to fit a linear curve. Iron oxide grains were selected prior to using the LA ICP-MS, this was done by microscope work as well as SEM and microprobe. The SEM was important to see if there were any inclusions or variations in the replacement of magnetite by hematite. This was not a problem with magnetite because of its abundance and pristine condition; hematite on the other hand was not as common and difficult to get zones large enough (100 µm) for the laser ablation procedure and is often filled with pits.

30 samples of magnetite and hematite were analysed. A large number of elements were analysed including: ^{24}Mg, ^{27}Al, ^{29}Si, ^{31}P, ^{34}S, ^{43}Ca, ^{49}Ti, ^{51}V, ^{52}Cr, ^{57}Fe, ^{59}Co, ^{60}Ni, ^{65}Cu, ^{66}Zn, ^{75}As, ^{139}La, ^{140}Ce,^{146} Nd, ^{147}Sm, ^{153}Eu, ^{157}Gd, ^{163}Dy, ^{166}Er, ^{172}Yb, ^{197}Au, ^{208}Pb, ^{209}Bi, ^{238}U. Elements such as Mg24, Al27, Si29, P31, S34 and Ca43 were analysed not so much for data for the iron oxides but as indicators if a mineral inclusion was encounted during ablation.

40 sulphide samples were examined, 20 of chalcopyrite and 20 of pyrite. A glass standard of Mass-1 was used for the calibration but no known sample was used to create a linear fit. Laser settings used during the analyses were: continuous beam at 5Hz, a 65 µm spot diameter and 75 % power level. The sulphides were identified prior to the laser by optical microscopy but due to the high abundance of sulphides in the samples this was relatively easy. The low melting point meant that the laser burned the sulphides covering the surrounding area in remains of the burning sulphides necessitating that the sample was cleaned during analysis.

7 Results

7.1 Petrography

The detailed report of ore mineral petrography can be found in Appendix A.

7.1.1 Iron oxide

There are several different iron oxide stages that have previously been identified by previous studies on the Hillside deposit. Graham Teale in preliminary studies has identified 4 iron oxide stages (Teale 2010). The first stage is a primary magnetite growth stage that is related to the mafic intrusions that have occurred in this area. These intrusions are believed to be related to the Hiltaba suite which is an important feature for the formation of IOCG deposits within the Gawler Craton. A second Magnetite formation event marks the commencement of the hydrothermal event. The period has been classified as a "skarn" formation period which is important to the mineralized zone (Cerlienco 2009). During the main mineralising event the first hematite formed by the replacement of magnetite. This is a very important factor in the IOCG formation process, this replacement is often believed to be related to copper and gold mineralisation. This process is therefore very important to understand because understanding this can help define the mineralized zone. The fourth iron oxide event is also during the main mineralizing event and is relatively late in the overall deposits formation. The fourth iron oxide event consists of primary bladed hematite (see figure 31) growth that is very obvious. This stage is only observed within a certain mineral zones such as quartz veins and carbonate veins. These bladed hematite grains are often very small, normally less than 50 microns across.

7.1.2 Sulphides

The sulphide samples were selected for sulphur isotope work with a mixture of chalcopyrite and pyrite samples used. Each rock sample collected from a different depth had a sulphur sample taken if possible. This gave 12 sulphur isotope samples to use and gave the best variation possible. The samples were collected using a tungsten carbide drill bit on a small mounted dental drill. To reduce the chance of contamination gloves were worn during collection and after every sample was collected the drill was wiped

down with ethanol. A few of the sample had both chalcopyrite and pyrite so a sample of both was collected.

7.2 Ore petrography

Magnetite is the dominate iron oxide ore mineral present within the samples collected at Hillside. Hematite replacement is visible in almost all samples in varying degrees. The martite replacement textures vary throughout the samples with two clear distinct replacement styles. The hematitic replacement in certain samples is controlled by the joints and fractures within the magnetite and replacement occurs from the outside of individual grains inward (see figure 7). The second replacement texture seen is where the hematite replacement doesn't follow the fractures within the grains and appears to follow porous zones within the magnetite grains (see figure 4). "Replacement wave fronts" can be seen where the hematite replacement front has flown through. The replacement appears random in sections as the fluid flows through the most porous sections within the magnetite grains.

7.3 Accessory Minerals

Samples show high degrees of alteration making the identification of precursor difficult. Slides dominated by plagioclase, K-feldspar, clinopyroxene, quartz, chlorite, garnet and biotite. The metasediments appear to be dominated by plagioclase and "red rock alteration" which is found throughout the hole and doesn't appear to have a preference in the protoliths it is most prominent (see figure 10). This type of alteration is seen in varying degrees throughout the entire slide BT015. The mineralized zone appears to be rich in garnet and clinopyroxene, these zones are part of the skarn mineralisation. All samples show some degree of brecciation and fracturing (see figure 10). A late stage of carbonate veining can be seen in every sample, occasionally containing chalcopyrite.

A uranium oxide was identified using the SEM as its high density made it very bright and easy to identify. The grains were very small but consistent throughout most samples and were hosted in several different minerals. Galena was also a mineral that was identified that was not seen in before. Galena was only identified in some samples and only in very fine grain size. Unidentifiable accessory rare earth rich minerals were also

identified. These minerals were not identifiable due to their very small size of less than 5µm.

7.4 Iron oxides

The iron oxides, magnetite and hematite, are a dominant feature of the deposit and many of the samples collected. The relationship between the oxidation state of the iron oxides and chalcopyrite is very evident because the places where the iron oxide and chalcopyrite are in contact only hematite is present, magnetite is never in contact with chalcopyrite. Replacement of magnetite by hematite is prevalent in varying degrees throughout all the samples examined.

7.4.1 Replacement of magnetite by hematite

The replacement pattern is found to be controlled by two different physical characteristics: fractures that run through the magnetite (see figure 7) and what appears to be a porosity of the magnetite (see figure 4). In most cases the replacement was confined to the surrounding edges of the magnetite grains (see figure 2 & 3). The degree of the replacement varies from almost one hundred percent in some zones and in other sections the replacement is only on the very edge of the magnetite grains or not present at all in some parts. When chalcopyrite is present and makes grain to grain contact with the iron oxides there is always some hematite replacement even if it's only a few µm across.. The replacement texture that appears to follow a porous path within the magnetite is only present in some samples. The wave front of fluid can be seen as a ring of hematite replacement within the magnetite grains with no sign of fractures within the grains (see figure 4).

7.4.2 Primary, newly formed Hematite

A primary hematite is also present within several of the samples. This hematite is clearly identifiable by the bladed shape and lack off remanent magnetite with the grains. The bladed hematite has a lot less pits within it compared to the hematite that replaces magnetite (see figure 10). The primary hematite appears to be in a quartz influx which is

later in the deposits formation. The bladed hematite is always seen to have a ring of quartz surrounding it.

7.4.3 Rare Earth Elements

The rare earth element data gives information about the changes in conditions that caused the change from magnetite to hematite. The magnetite REE analyses did not work as well as hoped because of accuracy of the LA-ICPMS, data gathered were often close to the detection limits of the method (see table 5). Due to the very low values the data cannot be viewed as accurate but can be used to give an indication of values and a comparison between the magnetite data and hematite data.

REE content of hematite was distinctly higher, commonly an order of magnitude above detection limit of the method and thus the data can be considered more reliable.. (see table 6). The hematite has a total REE content of 1.275 against chondrite and magnetite having a value of 0.086 against chondrite (see table 13&14). This is a large difference of two orders of magnitude show a clear enrichment of REE in the later hematite. This means the problems with the magnetite samples was not present with the hematite samples. The hematite samples are the ones that would give the indication of the fluids responsible for the copper mineralisation as the relationship between the replacement of magnetite by hematite and chalcopyrite has been documented. The large Ce anomaly seen within magnetite is an indication of redox fluctuation; the anomaly is not seen in the hematite samples (see figure 6 & 7). The Eu anomaly that is seen in other IOCG deposits is seen within the magnetite yet it is not seen within the hematite samples (see figure 6 & 7)

The hematite samples showed a very flat REE (Boynton 1984) pattern and this is similar to that of chondrite (see figure 6). There is a very slight inflection upwards within the light rare earth elements. The large difference in the shape between the two graphs is seen in the large difference in the LaN/YbN values, the hematite has a LaN/YbN value of 5.01 and magnetite has a LaN/YbN value of 1.10 (see table 13&14). The LREE show the biggest difference between the two iron oxides with the hematite having a LaN/SmN value of 3.27 and magnetite having a value of 0.78 (see table 13&14). This indicates that the largest difference between the two plots involves the LREE.

7.4.4 Trace elements

Trace element concentrations were analysed via Electron Probe Micro Analysis (EPMA) and ultra trace elements were collected using the LA-ICPMS. Graphing of these elements against each other allows for a comparison between the two different oxides. The trace element study identified distinct differences of element variations between the magnetite and hematite. The graphs of the samples that have showed the anomalies are in "Figures and Tables" (see figure 8&9).

7.5 Correlation of Elements

7.5.1 Trace element variation in Fe-oxides

Correlation between the different elements within the iron oxides was carried out to identify possible compositional relationships. Several element pairs showed a clear difference between the two different iron oxides. The elements include we're very close to the detection limit such as Au and Ca. Elements that were used to identify possible contamination or mineral incusion such as Mg, Al, Si, K and Na were excluded .

Magnetite and hematite show several distinct element correlations. The biggest difference is the correlation between Ti and V, the correlation value for hematite is high at 0.76 showing a strong correlation between the two elements. Magnetite's correlation value for Ti and V considerably lower at .032, this indicates almost no correlation between these two elements (see figure 10&11).

A similar difference is also seen for the Co and V correlation with magnetite having a higher value of 0.80 (see figure 15). Hematite has a lower value of 0.56 indicating a slight difference between the correlations, however both correlation coefficients are relatively high showing that there is a relationship between these two elements in the iron oxides (see figure 6).

The Co and As values also show a higher value of the correlation coefficient in the magnetite samples of 0.76 compared to the hematite value of 0.38. This is again seen in

the Pb and As correlation with magnetite having a higher value of 0.75 (see figure 10). Hematite has a much lower value of 0.57 shows a clear difference in the elements distribution (see figure 11). The Pb and Co correlation values are higher within the hematite samples with a value of 0.74 compared to the magnetite value of 0.46 (see figure 10&11).

These strong differences in the correlation values between magnetite and hematite show a clear difference in the elemental distribution within the samples. This data shows that the elements within the two different oxides are different and there is variations in their concentrations. This may be a reflection of the different conditions during the formation of each of these minerals.

7.5.2 Trace element variation in sulphides

The sulphides were also examined for trace element content and results were compared to establish differences and similarities in trace element content., The trace element variation of the sulphides does not show the same trends as found for the oxides. This is mainly due to the different capacity for trace element incorporation of chalcopyrite and pyrite compared to the Fe-oxides.

The trace elements in pyrite show very little distinct correlation values. The only high correlation value within the pyrite is between V and Mn with a correlation value of 0.81 (see figure 13). The chalcopyrite has several strong correlations values within its major elements. The strongest is between Co, Ni and Cu with all values been above 0.66, the Co/Ni relationship has been well documented and in this case it has a 1.00 correlation value (Campbell and Valerie, 1984) (see figure 12). Pb, W and Ir also have a high degree of correlation with all values above 0.72, indicating a very strong correlation between these elements (see figure 12). There is also a strong correlation between Pb and Bi with a value of 0.86, indicating a very strong relationship between these two elements (see figure 12).

7.6 Magnetite-Hematite Element Comparison

By comparing the elemental composition between the two iron oxides a changing elemental signature can be identified. These compositional differences may indicate a change that has occurred in the mineralising fluid system or elements that can be used to identify the environments the two elements are found in.

The chromium values of magnetite and hematite show a large difference between them, the hematite values are consistently lower than that of magnetite (see figure 14). The hematite values are mostly below 2ppm, compared to that of magnetite where most values range from between 1.5ppm-4.5ppm. The zinc values show a similar relationship to that of chromium, all hematite values are very low (below 20ppm) (see figure 14). The magnetite values of zinc range from 10ppm to 140ppm with most values well above that of hematite. The values of both zinc and chromium are significantly higher in the magnetite compared to that of hematite.

The vanadium concentration shows a unique difference between the hematite and magnetite. The Vanadium values of hematite have a large range of 0ppm-350ppm (see figure 15). The magnetite on the other hand has a very narrow range of 60-130ppm, showing a clear difference between the two oxides. Studies have shown that the variation of vanadium concentrations is small between magnetite and hematite (Schuiling and Feenstra 1980). Hematite may have a slightly higher concentration of vanadium but this does not explain the large difference seen here.

A binary plot of Ni and Ti in magnetite and hematite illustrates the different compositions. The magnetite has a lower value of nickel compared to hematite but a large variation of titanium content. Alternatively hematite has nickel values of 40-90ppm and a higher titanium concentration on average (see figure 16). The titanium values also have a much larger variation with values ranging from 60-490ppm (see figure 16). When graphed against each other two distinct zones can be identified that separate the magnetite and hematite.

A binary lead and cobalt plot (see Figure 17) shows a difference in the magnetite and hematite values. The Pb and Co concentrations in magnetite are consistently low with a few outliers and are grouped tightly on the graph. The lead values are all very low and

the cobalt values have a tight range with values between 22-30ppm (see figure 17). The hematite values show a slight correlation between the lead and cobalt. The lead values in hematite are consistently higher than that of magnetite.

7.7 Sulphides

7.7.1 Petrography

There are two main sulphide minerals that dominate the deposit, there is the non economically important pyrite and the economically important chalcopyrite. The pyrite formed well before the chalcopyrite was introduced to the system. The pyrite grains are massive and may show a euhedral shape indicating that the crystals grow in open space. Pyrite grains are very large in size (<4 cm). The later chalcopyrite has invaded a lot of the area that was occupied by the pyrite grains. The chalcopyrite floods this area with the pyrite and causes the fracturing of the pyrite grains. This relationship can be clearly seen as the ghost shape of the pyrite grains is still present. The chalcopyrite is seen to infill small grains within many of the oxides and these areas are also strongly related to the hematite replacement. All the chalcopyrite is seen to have formed in between other mineral grains (see figure 33). There is a very late carbonate event that has also carried some chalcopyrite with it. The chalcopyrite is found as small grains on the edge of carbonate veins that cut across all other minerals.

7.7.2 Trace Elements

The trace elements of both pyrite and chalcopyrite were analysed via EPMA and LA-ICPMS. The elements examined in each method were not exactly the same giving a variation in the number of samples for each element. The trace elements were examined and plotted, any anomalies between the two sulphide minerals were looked at more closely.

The cobalt values between the two sulphides show are clear anomaly within cobalt values, the chalcopyrite values are all over 500ppm (see figure 19). The pyrite values for cobalt are much lower and are all bellow 150ppm. The chromium concentrations show an opposite trend, the pyrite values are much higher than chalcopyrite. The pyrite values range from 1.5ppm to 3.5ppm, the chalcopyrite is all bellow 1ppm (see figure 19).

When comparing the cobalt and nickel values it is clear to see that the pyrite has a much higher level of enrichment of both elements compared to chalcopyrite (see figure 21). The distribution of cobalt and nickel in these sulphides is known to be non-uniform (Campbell and Valerie 1984) some difference in enrichment is expected. The Co/Ni ratio (see figure 14) shows that the two sulphides are very similar which is what would be expected even with a large enrichment difference.

7.8 Sulphur Isotopes

The sulphur isotope values were collected using a mass spectrometer GVI IsoPrime mass spectrometer. The results gave surprisingly consistent values for both pyrite and chalcopyrite (see table 10). The rage of the sulphur isotope values was -2.6 to -6.6 $\delta^{34}S$ which is a relatively small range. There was a very small spread with the data, most of it between -6.6 and -5. The two values that were much lower than the others both came from pyrite. This data was added and compared with that collected by Taylor (2009), the samples collected during this project have a much smaller range compared to Taylor's (2009) (see figure 32). Taylor (2009) had a range of $\delta^{34}S$ of -26 to +4 compared to -6.6 to -2.6 for samples collected during this project (see figure 32). This may indicate a large range in sulphur values within the deposit or errors in the collection of some of the samples with very low δ34S which appear as they may be outliers.

8 Interpretation of results:

The objective of this study is to determine distinct trace element signatures for hematite and magnetite in the Hillside mineralisation. These elements can then be used as pathfinder elements for the purpose of exploration.

8.1 Iron Oxides

The study of the iron oxides has involved a detailed petrography study on the iron oxides and their relationship with the sulphide minerals in the deposit. The iron oxides were also examined using SEM to identify zoning within the grains. The selected grains were then analysis using the microprobe and LA-ICPMS to get the elemental signature of the different oxides.

The rare earth element values are a key to understand the mineralisation event of the Hillside deposit. The chondrite normalised REE patterns point out significant differences between the hematite samples and the magnetite samples (see figures 1&2). The REE plot for hematite shows an extremely primitive REE signature that was very close to chondrite values (see figure 6). This REE signature is distinctly different from that of magnetite indicating that the REE uptake of hematite involved a change in the composition of the fluids that also caused the hematite to become enriched in REE. This replacement of the oxides is strongly related to the fluid influx that caused the mineralisation of this deposit. Therefore an idea of the composition of the mineralizing fluid can be gathered from the iron oxide race and REE composition. The mineralising fluids are suggested to have carried a primitive signature inherited from the source rock, indicated by the primitive signature of the hematite REE.

An important part of the mineralizing process is the involvement of the Hiltaba Suite magmatic rocks. Recent studies have established a REE pattern for the Arthurton Granite which is the part of the Hiltaba Suite found within and in the vicinity of the Hillside deposit (Taylor 2009) (see figure 24). The Arthurton Granite was shown to have a low total REE content and a rather flat or “primitive” pattern is (see Figure 24). In contrast, a study by Oreskes and Einaudi (1990) on the Olympic Dam granite and the hematite breccias of the Olympic Dam deposit found that the granit as well as the

hematite were enriched in REE and especially LREE. The origin of the REE enrichment of the hematite is not clear but it is reasonable to believe that it was caused by a hydrothermal process (Oreskes, Einaudi, 1990).
Comparison of REE patterns of hematite at Hillside and Olympic Dam shows distinct differences but also similarities.. This can be explained through the compositional variations within the Hiltaba Suite (Budd et al. 1998).
A study by Taylor (2009) revealed that that the REE composition of the granite in the area of the Hillside deposit is not as differentiated and enriched as the Olympic Dam Granite (see figure 24).
The primitive REE pattern of hematite from Hillside suggests that the fluid involved in the oxidation of magnetite to hematite had a primitive REE signature with low total LREE content, while at other Gawler Craton IOCG-U deposits e.g. Olympic Dam the REE content was high.
The REE pattern of magnetite at Hillside allowed for several interpretations to be made. One key aspect is the intense variability of the Cerium content which is a key indicator of redox reactions due to the possible 4+ redox state of Ce (German and Elderfield 1990). The anomaly does not show a consistent positive or negative anomaly, but rather a strong variation from positive to negative values., This suggests fluctuating redox conditions during the mineralising event. Whether this Ce variation is a primary property of the magnetite or due to secondary disturbance of the Ce content may have to be further evaluated.
The europium anomaly shows very different values between the magnetite and hematite, there is almost no europium anomaly in the hematite with a value of 1.13 Eu/Eu* while magnetite has a distinct negative anomaly of 0.75 Eu/Eu* (see table 13&14). This difference helps interpreting the change in the fluid composition or its redox state as the deposit developed.

The trace element analysis of the iron oxides shows that several elements vary considerable between the magnetite and hematite. These elements included Ti, Cr, Co, Zn, V, Ni and Pb, some give an indication on the variation in conditions that these elements were formed.

8.2 Co/Ni Ratio:

The cobalt-nickel ratio can be used to characterise the source of the metals in the system (Campbell and Valerie 1984). A value >5 is suggested to indicate a magmatic source for the sulphur (see figure 22). The values determined for Hillside are rather variable, possibly indicating mixed sources for the metals transported by fluids from different sources.

8.3 Trace element comparison

Several trace elements were compared between the oxides and sulphides, this was to look for a relationship that would help identify the different events that formed the deposit. Magnetite and chalcopyrite are both enriched in chromium compared to the sulphides that are believed to have formed during the same period as each iron oxide. This may indicate that the fluid that oxidized the magnetite may have also mobilised or removed elements such as chromium. These fluids may have then become enriched in the elements that it removed from the magnetite, as the chalcopyrite precipitated from the fluid it therefore became enriched in these elements.

Pyrite and hematite are both enriched in nickel, these two minerals formed during different event so the reason behind the enrichment is not clear. Pyrite and magnetite both have enrichment in cobalt which is expected due to the fact they are both believed to have formed during the same fluid injection. This indicates that the first phase of fluid injection was enriched in cobalt compared to the later fluid.

The chalcopyrite is enriched in several trace elements compared to pyrite. These trace elements give the indication that the fluid that formed the chalcopyrite must have been enriched in these elements. This fluid has changed in composition compared to the first fluid in some way, weather it was interaction with surrounding rocks or an intrusion source can be deduced that these were enriched in these minor trace elements.

8.4 Sulphur Isotopes

The sulphur isotopes were used to characterise possible fluid sources and evolution of the sulphur source. The small variation in values indicates that there was most likely one sulphur source. The low negative numbers can also give an indication of the source of the sulphur, these numbers give an indication that the source of the sulphur is

magmatic, possibly mafic (Bastrakov et al. 2007). Comparing these values to other IOCG deposits/prospects within the Gawler Craton it can clearly be seen that this deposit fits into the IOCG category. This deposit has similar values as Olympic Dam, Cairn Hill and Oak Dam (see figure 23) (Bastrakov et al. 2007).

8.5 Comparison of Analytical Technique

The two micro analytical techniques used in this project were the LA-ICMPS and the electron microprobe. The elements analysed in each method were slightly different yet there are several elements that were analysed by both methods. A comparison between these two different techniques reveals a clear difference in the values each gives (see figure 24, 25, 26 and 27). The microprobe results are significantly higher than the LA-ICPMS, the average values are higher and so is the max value recorded (see figure 24, 25, 26 and 27). The relationship between the max value and the average appear to be constant between both analytical methods. The discrepancy in the results indicates a systematic error within one of the methods. The LA-ICPMS is the most likely source of the errors as a large area is analysed with this method (80μm), the laser also burns into the sample collecting material under the surface that has not been examined for mineral purity. The samples below the surface may cause a slight dilution in the values recorded. The sulphides show a slightly larger difference when comparing the two analytical techniques, this may be due to the fact that the sulphides have a lower melting point and the laser penetrates to a greater depth increasing the dilution. In comparison the Electron Microprobe is able to target a small area of several microns and interacts with a much smaller depth. This allows for a much purer sample decreasing the risk of dilution giving slightly higher values.

9 Discussion

9.1 Hillside ore Paragenesis

The paragenesis of the Hillside deposit has been well documented in 2009-2010 by studies carried out by Rex Minerals and that by 2009 honours students Cerlienco and Taylor. This study however looks closely at the ore minerals and evidence of their proposed relationship.

9.2 Magnetite to Hematite reaction

To change magnetite to hematite a process needs to occur where the combination of Fe^{2+} and Fe^{3+} are converted into just Fe^{3+}. The commonly proposed way for this to occur is by an oxidation reaction to alter the magnetite to hematite (Mucke and Cabral 2005) (Ohmoto 2003) (Otake et al. 2010).

$$2Fe_3O_{4\,(Mag)} + O_2 = 3Fe_2O_{3\,(Hem)}$$

In this case an environmental change to more oxidising conditions would cause the oxidation of magnetite and therefore create hematite. A second scenario where the change from magnetite to hematite could occur is in non-redox reaction. A non-redox reaction is one which is not controlled by the oxidation state but is based on a pH change. To cause the replacement of magnetite by hematite a pH decrease to make an acidic environment is required.

$$Fe_3O_{4\,(Mag)} + 2H^+ = Fe_2O_{3\,(Hem)} + H_2O + Fe^{2+}$$

9.2.1 Non-redox

An acidic environment is required for this process to take place. The pH decrease allows the Fe^{2+} ion to be dissolved from the magnetite crystal structure. This gives the end product of hematite and water with Fe^{2+} as a free ion. It is unclear what happens to this ion but would be carried by the acidic fluid until it reached an environment where by it could be oxidized. An effect of this process is a decrease in volume of 32.22% due to the lost ion from the iron oxide (Ohmoto 2003). The size difference would be much

closer to 2-5% and an increase in porosity of up to 30% (Ohmoto 2003) (Otake et al. 2010).

This process would cause a decrease in the iron oxides volume as the magnetite is converted to hematite. This could explain the intense hydrothermal brecciation that is commonly observed in all of the IOCG deposits in the Gawler Craton. The degree of brecciation and the size of clasts vary from deposit to deposit, this could be due to the variation in original magnetite and the pH and temperature that this process took place. The porosity of the iron oxides would also be increased because of the hematite been forced to filling the spaced caused by the 32.22% volume reduction (Ohmoto 2003). This extra space and increased porosity allows for the acidic fluid to continue to flow on and replace more magnetite by hematite causing a cascade effect. This possibly could be the reason that such a large zones of magnetite are able to be brecciated and fluids responsible for replacement area able to move into a zone of relatively non porous magnetite. The mineralizing fluids which could be the same as the acidic fluid or a later intrusion is now able to easily move through the deposit causing this conversion. Studies by Otake (2010) have shown that this style of reaction can occur over a wide range of pressure and temperatures, but as with most acidic reactions it favours high temperatures. A temperature of mineralisation of 461.6°C was proposed by Cerlienco (2009), hot enough to allow this reaction to take place. The magnetite can be seen from the petrography study to be uniform within the grains and appear to be relatively non-porous (see figure 2). The hematite is seen to have many pits within it (see figure 28) which could be due to a high porosity which further supports the non-redox reaction theory. As the Fe^{2+} ions are removed from the magnetite and it becomes hematite it's crystal structure is open to other elements. This could explain the increase in REE content compared to the magnetite as the acidic hydrothermal fluid may be enriched in REE.

9.2.2 Redox reactions

The commonly accepted process that the magnetite is transformed into hematite is by oxidation of magnetite. This involves the change from reducing environment that the magnetite had formed within to an oxidising environment. The oxidising environment involves magnetite and oxygen combining to form hematite.

The fluid within the hydrothermal system needs to contain enough oxygen to cause the oxidation of the magnetite. The believed source of the hydrothermal system is the Arthurton Granite which is part of the Hiltaba Suite, this magmatic intrusion is from great depth so it is very unlikely that the fluids from it would be oxidized. The most likely way that an oxidizing fluid would be incorporated into the hydrothermal system is if the fluid came from meteoric water. The water from the surface would be able to carry oxygen that could then oxidize the magnetite. The fluid would need a way to move down to the required depth, the large crustal structure of the Pine Point Fault is a very feasible way for these fluids to intrude to the granite.

9.3 Possible Pathfinder Elements

The study of major, minor and trace elements within the oxides and sulphides have given an indication on elements that could be used as pathfinder elements. The elements that are likely pathfinder elements are Cr, Zn, V and Pb within the oxides. The chromium values are almost twice as high in the magnetite compared to the hematite with magnetite having an average value of 152ppm and hematite having an average value 268ppm (See Table 1&2). The zinc values for magnetite have an average value of 429ppm and hematite only having a value of 346ppm (see table 1&2). Vanadium is different because hematite has a much higher value compared to magnetite, magnetite has a value of 152ppm and hematite has a value of 268ppm (see table 1&2). Hematite is also enriched in lead with a value of 385.30ppm and magnetite having a value of 204.54ppm. A lower concentration of chromium and zinc as well as an increased concentration of vanadium and lead would be suitable indicators for hematite rich zone. The hematite rich zone are the zones that mineralisation is also most prominent.

The sulphides also contain several trace elements that could be used as pathfinder elements, these elements are Co, Mn and Cr. There is a huge difference between the cobalt values of the chalcopyrite and pyrite, chalcopyrite has a value of 414ppm compared to 20474ppm in pyrite (see table 3&4). Chalcopyrite on average is found to have elevated cobalt content but the two orders of magnitude difference seen here shows clear signs of enrichment (Campbell and Valerie 1984). Pyrite is also enriched in manganese, with an average value of 123.11ppm and chalcopyrite having an average value of 70.90ppm. This is a 57.5% difference between the chalcopyrite and pyrite. The

chalcopyrite has a chromium enrichment with the average value of 2.25ppm and pyrite has an average value of 0.73ppm. The enrichment variations may be strongly affected by the sulphides ability to incorporate these elements into their structure. This makes it difficult to use these elements as path finding elements.

9.4 Hillsides Relationship with IOCG Deposits in the Gawler Craton

It has been suggested by previous work (Cerlienco 2009) that the Hillside deposit is part of the broad IOCG-U family. Although it appears to be very different from that of Olympic Dam and Prominent Hill, which are the two big deposits within the Gawler Craton. A recent study by Groves, et al (2010) has discussed the issues of classification of IOCG-U deposits encompassing a huge number of different styles of setting and mineral assemblages (see figure 25). To overcome this problem the classification of IOCG-U deposits has been broken up into 5 different categories (see table 12). Deposits such as Olympic Dam and Ernest Henry are categorised as IOCG sensu stricto, these style of deposits have several characteristics such as LREE enrichment and low S sulphides (Groves et al. 2010). Although Hillside has the low S sulphides it also has a considerable amount of pyrite present, it also has a lack of LREE enrichment when compared to deposits such as Olympic Dam (Groves et al. 2010). Although Hillside does meet several other characteristics requirement such as abundant Fe oxides (magnetite/hematite) and hydrothermal style mineralisation it doesn't match them all. One of the five IOCG categories is that of skarn mineralisation. Hillside mineralised zones are dominated by skarns, most of these are garnet skarns and several CPX skarns (see table 11). This therefore makes this deposit similar to those found within the IOCG skarn category, although the Hillside deposit is Paleoproterozoic in which is older than many of the skarn deposits (see table 11). The age of the skarn deposits seem to be well constrained between Mesozoic-Paleozoic, Hillside is outside this age making it one of only three (Groves et al 2010). The Hillside deposit does not clearly fit into one of these IOCG sub-categories and appears to be a mixture of both.

The Hillside mineralisation indicates that the deposit formed at a much greater depth than that of Olympic Dam. Olympic Dam is seen to have zonation of copper mineralisation related to depth. From the surface downwards the copper mineralisation is chalcocite, then bornite, then chalcopyrite with a final pyrite rich zone (Johnson and

Malcolm 1995). The Hillside deposit is believed to have formed at a greater depth compared to that of Olympic Dam (Cerlienco 2009), this is indicated also in the copper mineralisation as chalcocite is not seen within the samples of the deposit and very little if any bornite is seen. The mineralisation is dominated by chalcopyrite and is also pyrite rich which is found a great depth within the Olympic Dam deposit. A study of the different types of IOCG-U by Groves et al. (2010) showed IOCG-U style deposits and their relationship with depth within the overall system. The possible location of the Hillside deposit is identified within figure 30, this it at much greater depth than the Olympic Dam deposit. At this depth there is both the mafic units and the felsic units intermixing with each other.

9.5 Genetic model for the Hillside mineralisation

The Genetic model for all IOCG deposits is one of much controversy with many different models been hypothesised. The intrusion of the Arthurton Granite at 1582 ± 7 Ma started the first stage of deposits formation (Zang 2002). This intrusion created a hydrothermal that system which may have precipitated out the magnetite and pyrite. It is also possible that the magnetite may have been part of a banded iron formation that formed well before the magmatic intrusion.

This hydrothermal fluid continued to circulate and changed in composition. It is not clear where this compositional change came from, it may have been due to interactions with surrounding rocks or mixing with a second magmatic intrusion. The effect that this process had on the fluid is that it became an oxidizing fluid and became enriched in copper and sulphur. As this fluid moved through the magnetite + pyrite zone they caused the oxidation of the magnetite which changed the magnetite to hematite. This oxidation process is documented in the cerium values within the magnetite as they show a strong redox variation (see figure 2). As the fluid moved around the system slight replacement of pyrite occurred as it was replaced in sections by chalcopyrite. This fluid slowly cooled and caused the precipitation of chalcopyrite out of system and some minor pyrite. The relationship between the oxidation of hematite and the formation of chalcopyrite is extremely strong. The relationship can be seen petrographically as the

chalcopyrite is only in contact only hematite, this suggests that the same fluid that oxidised the magnetite also contained the copper.

9.6 Future Study Recommendations

The elements that are possible pathfinder elements have been identified within the iron oxides. The hematite rich zones are associated with the high grade copper mineralisation, the hope is to be able to easily identify the hematite rich zones. The elements to target are Cr, Zn, V and Pb, as they show discrepancies between the iron oxides. Future studies would need to examine if these elemental anomalies are also found in the surrounding minerals. The identification of these pathfinder element rich zones can be used to identify the hematite and copper mineralisation area. Work carried out on surface soils can be used to identify these pathfinder element rich zones as minerals under the ground may have been exposed to the same conditions that caused that hematite replacement and copper mineralisation. All of these future studies must be combined with this project before a deduction on whether these elements can be used as path finding elements.

10 Conclusion

This study has examined the composition of magnetite, hematite, chalcopyrite and pyrite in the Hillside Cu-Au deposit. Several elements have been identified as possible pathfinder elements that can be used for future exploration work. More knowledge needs to be gathered if the enrichment pattern of these elements in the iron oxides can be detected in the surrounding host rock. The rare earth elements and petrological study have identified possible processes and condition changes that have caused the replacement of magnetite by hematite. This data can be used in conjunction with future studies to identify the copper rich zones within the Hillside deposit.

The magnetite replacement by hematite is most likely due to an oxidation change due to a fluid change or influx of a different fluid. This oxidation change is recorded in the distinct variation of Ce content documented in the magnetite REE patterns. This anomaly is not found in the hematite samples, therefore hematite was in a stable oxidation state compared to magnetite that experience a much more variable oxidation state.

Hillside's position in the IOCG-U family is still not fully understood as its characteristics don't match the proposed groups correctly. The age of this deposit also makes it difficult as it is much older than other deposits similar to it.

Acknowledgements

I would like to first and foremost thank my supervisor Andreas Schmidt Mumm and my co supervisor Nigel Cook for their assistance throughout the year in field and laboratory work. Rex Minerals has funded this project as well as supplied ideal samples for this project to be undertaken. I would like to make special mention of Graham Teale whose guidance and insight on the Hillside Deposit has been invaluable. I also thank both Ben Wade and Angus Netting at Adelaide Microscopy for their tutorials and guidance in the use of the Electron Microprobe and LA-ICPMS.

References

Avoca Resources Limited 2006. Fourth Quater Activities Report.

Bastrakov E. N., Skirrow R. G. & Didson G. J. 2007. Fluid evolution and origins of iron oxide Cu-Au prospects in the Olympic Dam district, Gawler craton, South Australia. Economic Geology 102, 1415-1440.

Belperio A., Flint R. & Freeman H. 2007. Prominent Hill: A hematite-dominated, iron oxide copper-gold system. Economic Geology 102, 1499-1510.

Boynton, W.V., 1984. Cosmochemistry of the rare earth elements: meteorite studies. In: Henderson, P. (Ed.), Rare Earth Element Geochemistry. Elsevier, Amsterdam, pp. 63–114.

Budd, A., Wyborn, L., Bastrakova, I., 1998. "Exploration Significance of the Hiltaba Suite, South Australia." AGSO Research Newsletter No.22, Nov-1998.

Campbell, F.A., Valerie, E.G., 1984. Nickel and Cobalt in Pyrrhotite and Pyrite from the Faro and Sullivan Orebodies. Canadian Mineralogist Vol.22, pp. 503-505 1984.

Cerlienco, B., 2009. Geological setting and alteration characteristics of the Hillside mineralising system, Yorke Peninsula. The University of Adelaide.

Conor C. H. H. 1995. Moonta–Wallaroo region, an interpretation of the geology of the Maitland and Wallaroo 1:100 000 map sheet areas. South Australia. Department of Primary Industry and Resources. Open File Envelope 8886.

Creaser R. A. & Cooper J. A. 1993. U-Pb Geochronology of Middle Proterozoic Felsic Magmatism Surrounding the Olympic Dam Cu-U-Au-Ag and Moonta Cu-Au-Ag Deposits, South Australia Economic Geology 88, 186-197.

Dampier Mining CO. LTD, BHP Minerals LTD & CRA Exploration PTY LTD 1986. Open File Envelope No. 3567: EL 499, EL 906 And EL 1112, Curramulka-Pine Point Area

Drexel J. F. 1979. Mineral occurrences south of Ardrossan - Hillside, Phillips and Harts mines. South Australia. Department of Mines and Energy. Report Book, 79/77.

Fairclough M. 2005. Geological and metallogenic setting of the Carrapateena FeO-Cu-Au prospect - a PACE success story. MESA Journal 38, 4-7.

Ferris G. M., Schwarz M. P. & Heithersay P. 2002. The Geological Framework, Distribution and Controls Of Fe-Oxide-Cu-Au Mineralisation In The Gawler Craton, South Australia. Part I - Geological And Tectonic Framework. In:Porter T. M. ed. Hydrothermal Iron Oxide Copper-Gold & Related Deposits: A Global Perspective 2 PGC Publishing, Adelaide.

Flöttmann, T., Haines, P.W., Cockshell, C.D. and Preiss, W.V. 1998. 'Reassessment of the seismic stratigraphy of the Early Palaeozoic Stansbury Basin, Gulf St Vincent, South Australia', Australian Journal of Earth Sciences, 45: 4, 547 — 557

German, C.R., Elderfield, H., 1990. "Application of the Ce anomaly as a paleoredox indicator: The ground rules" PALEOCEANOGRAPHY, VOL. 5, NO. 5, PP. 823-833, 1990

Hand M., Reid A. & Jagodzinski L. 2007. Tectonic framework and evolution of the Gawler craton, southern Australia. Economic Geology 102, 1377-1395.

Johnson J.P., Malcolm M.T., 1995. Sources of mineralising fluids for the Olympic Dam deposit (South Australia) Sm-Nd isotopic constraints. Chemical Geology 121 177-199.

MIM Exploration PTY LTD 1997. Open File Envelope No. 9166. EL 1785 Maitland. First Partial Relinquishment Report For The Period 7/9/1992 To 6/3/1996.

Mucke, A., Cabral, A.R., 2005. "Redox and nonredox reactions of magnetite and hematite in rocks." Chemine der Erda 65, p. 271-278.

Mumme I. A. 1955. Ground scintillation survey at the Hillside, Harts and Parara copper mines, and a copper prospect on section 39 Hd of Muloowurtie, Ardrossan. South Australia. Department of Mines. Report Book, 39/22.

Ohimoto, H., 2003. "Nonredox Transformations of Magnetite-Hematite in Hydrothermal Systems." Economic Geology Vol. 98, p. 157-161.

Oreskes, N., Einaudi, M (1990). "Origin of Rare Earth Element Enriched Hematite Breccias at the Olympic Dam Cu-Au-Ag Deposite, Roxby Downs, South Australia." Bulletin of the Society of Economic Geologists 85(1).

Otake,T.,etal. "Mechanisms of iron oxide transformations in hydrothermal systems." Geochim.Cosmo-chim.Acta (2010).

Rex Minerals 2009b. Quarterly Activities Report - for the period ended 30 June 2009. Online www.rexminerals.com.au

Rex Minerals ltd., 2010a. Corporate Overview Booklet – March 2010. Online. www.rexminerals.com.au

Rex Minerals ltd., 2010b. Maiden Copper Resource - Hillside Project, South Australia – July 28th. Online. www.rexminerals.com.au

Rowley R. 1955. Uranium occurrence, Hillside copper mine, Ardrossan. South Australia. Department of Mines. Report Book, 39/8.

Ruano S. M., Both R. A. & Golding S. D. 2002. A fluid inclusion and stable isotope study of the Moonta copper-gold deposits, South Australia: evidence for fluid immiscibility in a magmatic hydrothermal system. Chemical Geology 192, 211-226.

Schuiling R.D., Feenstra A., 1980. Geochemical Behaviour of Vanadium in Iron ~ -Titanium Oxides. Chemical Geology, 30 143-150.

Skirrow R. G., Bastrakov E. N., Davidson G. J., Raymond O. L. & Heithersay P. 2002. The Geological Framework, Distribution and Controls of Fe-oxide Cu-Au Mineralisation in the Gawler Craton, South Australia. Part II - Alteration and Mineralisation. In: Porter T. M. ed. Hydrothermal Iron Oxide Copper-Gold & Related Deposits: A Global Perspective, pp. 33-47. 2 PGC Publishing, Adelaide.

Stuart W. J. 1970. The Cainozoic stratigraphy of the eastern coastal area of Yorke Peninsula, South Australia. Transactions of the Royal Society of South Australia 94, 151-178.

Talylor, C., 2009. The Source of Fluids and Metals at the Hillside Copper-Gold Mineralisation, Ardrossan, South Australia. The University of Adelaide (unpublished).

Teakle R. P. 1983. Hydrocarbon Potential of the Cambrian Succession on Yorke Peninsula, South Australia. University of Adelaide, Adelaide (unpublished).

Teale, G., 2010. Preliminary Observations on the Hillside Cu (-Au-U-REE) Project, Yorke Peninsula, South Australia. (unpublished).

Teasdale J., Pryer L., Etheridge M., Romine K., Stuart-Smith P., Cowan J., Loutit T., Vizy J. & Henley P. 2001. Western Stansbury Basin SEEBASE Project SRK Consulting & Primary Industries and Resources, South Australia, Adelaide.

Wade M. L. & Cochrane G. W. 1954. Hillside copper mine, Ardrossan (21/10/52). Mining Review, Adelaide 97, 55-59.

Woodmansee W. 1957. Diamond drilling at the Hillside copper mine, Ardrossan. South Australia. Department of Mines. Report Book, 41/61.

Zang W. L. 2002. Late Palaeoproterozoic Wallaroo Group and early Mesoproterozoic mineralisation in the Moonta Subdomain, eastern Gawler Craton, South Australia. Report Book, 2002/001. Department of Primary Industries and Resources, South Australia.

Zang W. L., Raymond O. L. & Conor C. H. H. 2002. Geology of Yorke Peninsula and Cu–Au mineralisation at Moonta and Wallaroo. In: 16th Australian Geological Convention, Adelaide, Excursion Guide A1 Geological Society of Australia, Adelaide.

Zang, W.L., Fanning, C.M., Purvis, A.C., Raymond, O.L., Both, R.A., 2007. "Early Mesoproterzoic bimodal plutonism in the southeastern Gawler Craton, South Australia." Australian Journal of Earth Sciences 54, p. 661-674.

Figure Captions

Figure 1: Location of Hillside and tenements.
Figure 2: Large magnetite grains surrounded by hematite. Magnetite is seen to be free from impurities and no signs of porous spaces compared to the hematite.
Figure 3: Replacement texture of magnetite-hematite. Replacement follows fractures within the magnetite
Figure 4:Hematite wave front replacement.
Figure 5: Plagioclase rich zone with "red rock alteration". Brecciated texture with minor late vein cutting through the sample.
Figure 6: Rare earth element plot of hematite samples. Indicating a very primitive source.
Figure 7: Rare earth element plot of magnetite. Very large Ce anomaly indicating redox change. Small negative Eu anomaly not seen in hematite samples. Several samples close to detection limit and must be viewed with caution.
Figure 8: LA-ICPMS data comparing magnetite and hematite using all elements analysed. Trace elements can be seen to have some minor variations between the two minerals. The rare earth element section of the graph can be seen to show a large difference between the two minerals.
Figure 9: PPM counts from LA-ICPMS data. Chalcopyrite seen to have higher concentrations than pyrite in many different elements.
Figure 10: Magnetite correlation plot with all major elements.
Figure 11: Hematite correlation plot with all major elements.
Figure 12: Chalcopyrite correlation plot with all major and minor elements.
Figure 13: Pyrite element correlation plot with all major and minor elements.
Figure 14: magnetite and hematite graph of chromium vs zinc. The magnetite can be seen to consistently higher values of chromium and zinc. The variation of the magnetite is very large compared to that of hematite. The hematite has much lower values compared to magnetite and the values appear to be very uniform.
Figure 15: This graph shows the relationship between magnetite and hematite between zinc and Vanadium. The hematite consistently has a lower value of zinc compared to magnetite but has a large variation of vanadium. The magnetite appears to have a consistent level of vanadium but a large range of zinc.
Figure 16: Magnetite and hematite graph shows Ni versus Ti. The two different minerals can be seen to form two different zones within the plot area.
Figure 17: Magnetite and hematite graph with cobalt (Co) versus lead (Pb). The Pb and Co contents of magnetite are very consistent, a tight range can clearly be seen. The hematite values have a slight correlation between lead and cobalt.
Figure 18: Chalcopyrite comparison between the two analytical techniques (Microprobe vs. LA-ICPMS).
Figure 19: Chromium versus Cobalt in Chalcopyrite and Pyrite. Chalcopyrite showing high concentrations of chromium and very low cobalt. pyrite very high in Cobalt but chromium levels low.
Figure 20: Both pyrite and chalcopyrite with low amounts of vanadium but varying amounts of chromium.
Figure 21: Chalcopyrite and pyrite data from the microprobe, showing levels in cobalt and nickel are much higher in pyrite.
Figure 22: Cobalt- Nickel ratio of sulphides. Both pyrite and chalcopyrite have similar ratios.

Figure 23: Sulphur isotope data for several deposits/ prospects in the Olympic Dam domain. (Bastrakov et al 2007)
Figure 24: A REE plot of granite samples collected from C. Taylor 2009. This shows the relatively flat shape of the REE plot (Taylor 2009).
Figure 25: Magnetite comparison of analytical techniques (Microprobe vs. LA-ICPMS).
Figure 26: Hematite comparison of analytical methods (Microprobe vs. LA-ICPMS).
Figure 27: Pyrite comparisons between the two analytical techniques (Microprobe vs. LA-ICPMS).
Figure 28: Hematite with chalcopyrite infilling hematite grain fractures
Figure 29: Chalcopyrite and pyrite. Antinomy vs indium shows a clear variation in the concentration of indium in pyrite but low concentration and little variation in chalcopyrite. Antinomy has a distinct variation in chalcopyrite but low concentration and little variation in pyrite.
Figure 30: IOCG-U system and locations of known deposits within the system. (Groves et al 2010)
Figure 31:Primary hematite within quartz rich zone. Surrounded by chalcopyrite, hematite always has a small quartz ring surrounding the grains.
Figure 32: Sulphur isotope data from this study and Taylor (2009).
Figure 33: Chalcopyrite filling in space with primary hematite within quartz.

Table Captions

Table 1: Magnetite electron microprobe data summary.
Table 2: Hematite electron microprobe data summary.
Table 3: Chalcopyrite electron microprobe data summary.
Table 4: Pyrite electron microprobe probe data summary.
Table 5: Magnetite LA-ICPMS data summary.
Table 6: Hematite LA-ICPMS data summary.
Table 7: Magnetite LA-ICPMS data summary.
Table 8: Chalcopyrite LA-ICPMS data summary.
Table 9: Pyrite LA-ICPMS data summary.
Table 10: Sulphur isotope data.
Table 11: Sample collected from Hillside and specimen notes from the field.
Table12: Classification of IOCG-U style deposits from around the world (Groves et al 2010).
Table 13: Hematite REE summary.
Table 14: Magnetite REE summary.

Figures and Tables

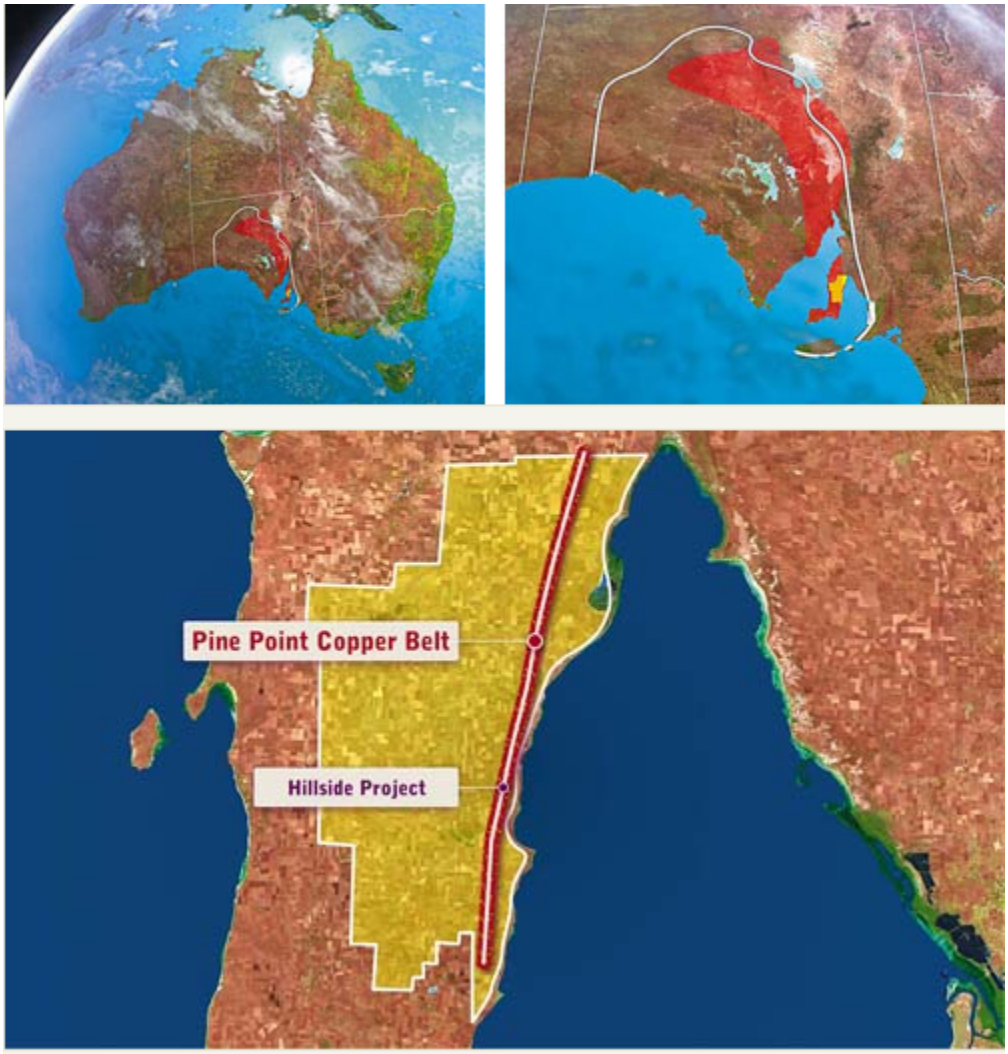

Figure 1: Location of Hillside and tenements.

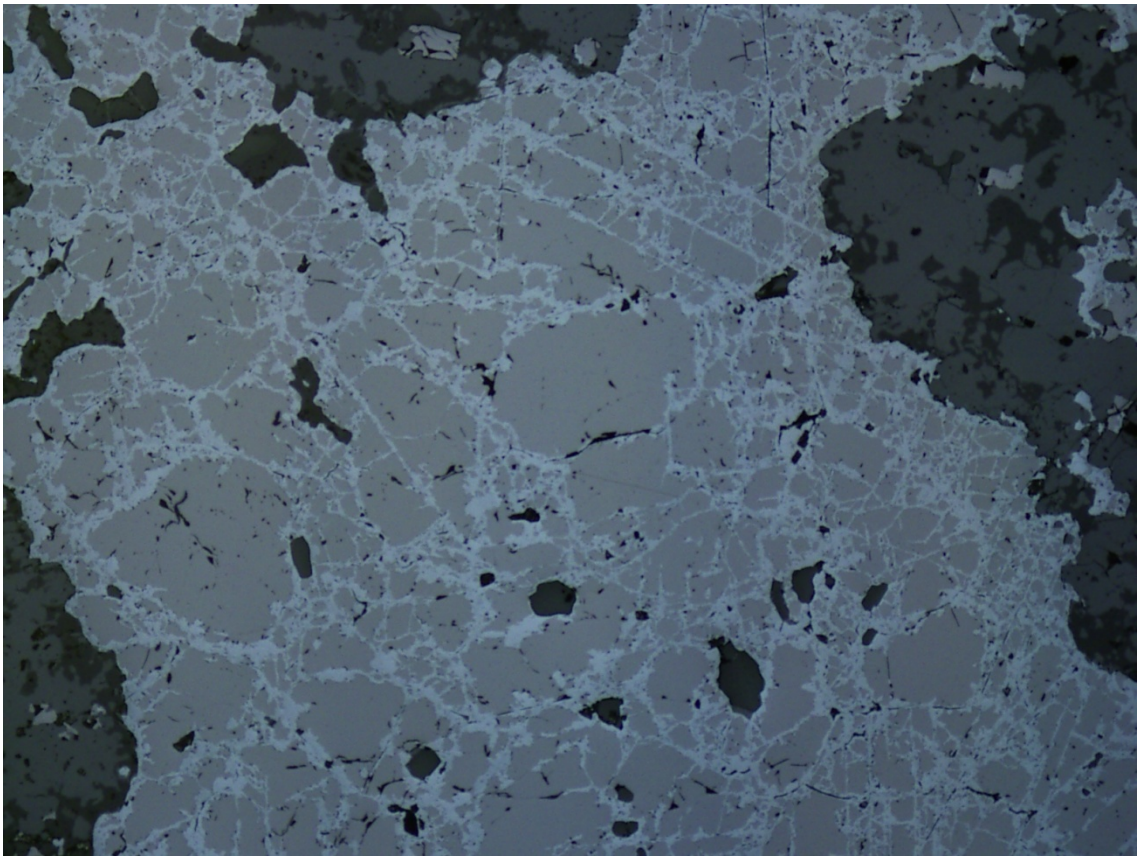

Figure 2: Large magnetite grains surrounded by hematite. Magnetite is seen to be free from impurities and no signs of porous spaces compared to the hematite.

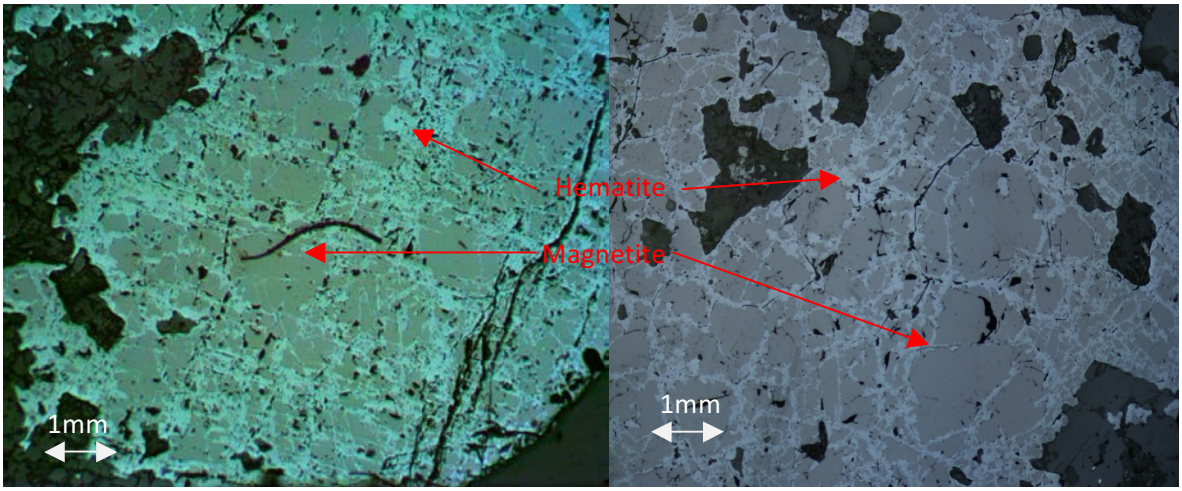

Figure 3: Replacement texture of magnetite-hematite. Replacement follows fractures within the magnetite

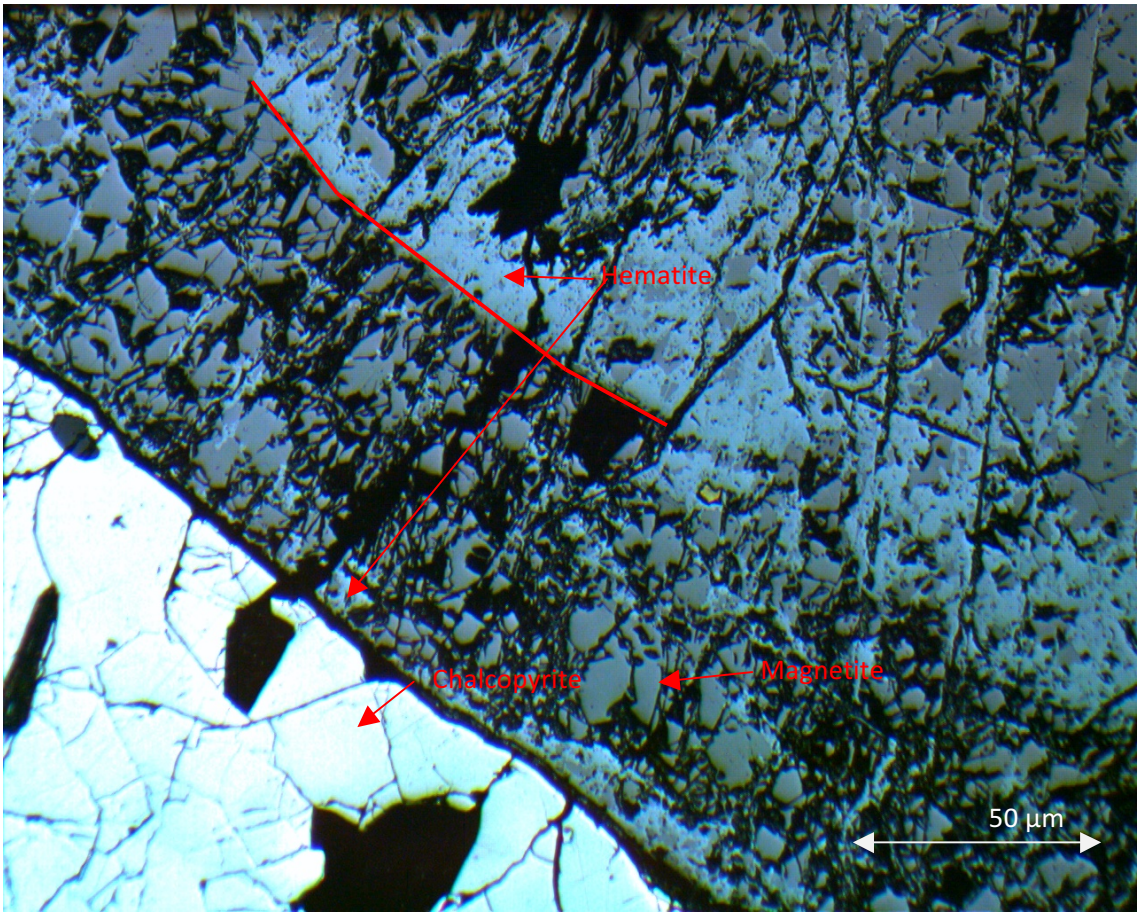

Figure 4:Hematite wave front replacement.

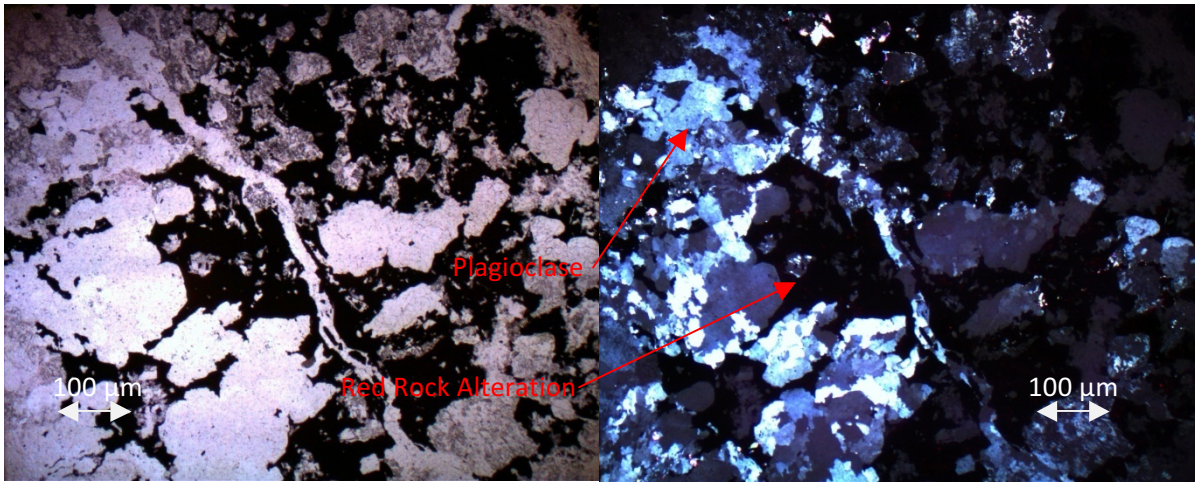

Figure 5: Plagioclase rich zone with "red rock alteration". Brecciated texture with minor late vein cutting through the sample.

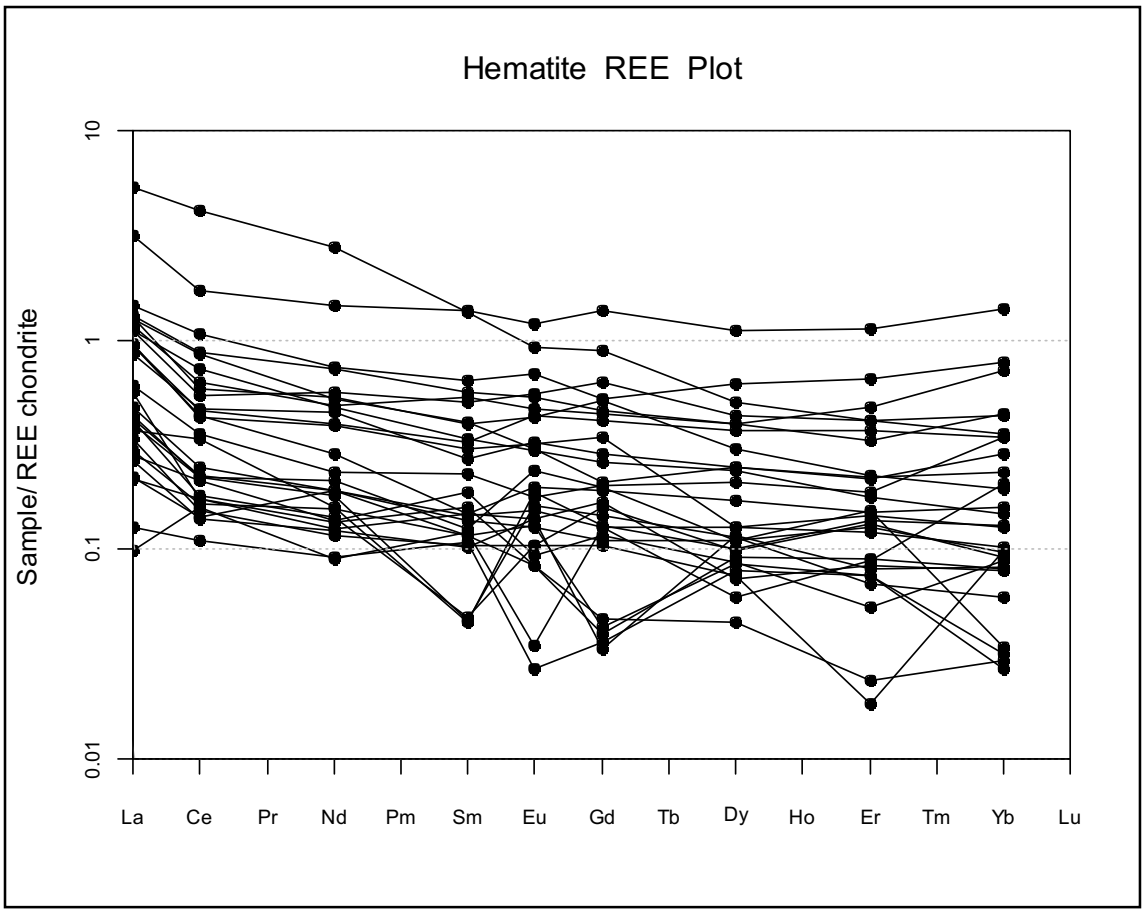

Figure 6: Rare earth element plot of hematite samples. Indicating a very primitive source.

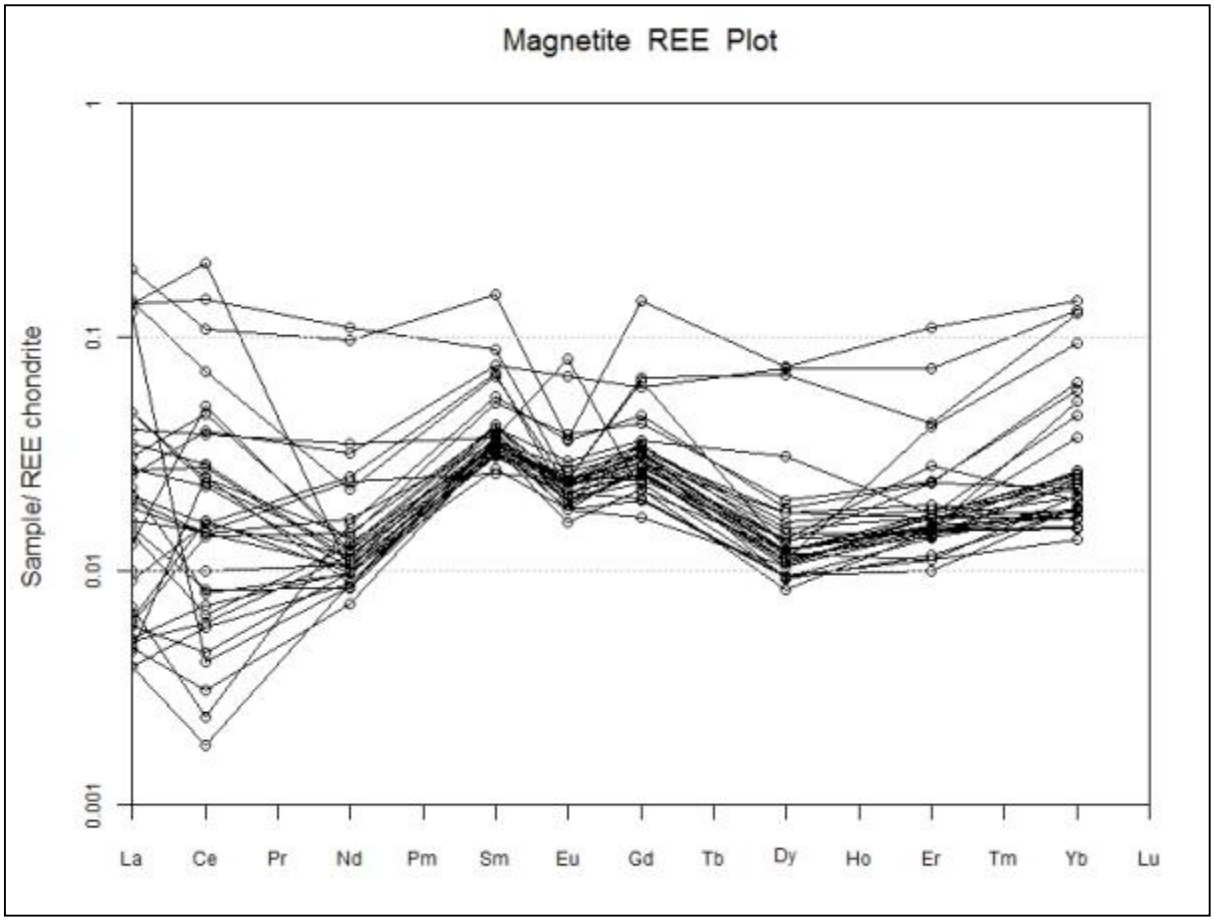

Figure 7: Rare earth element plot of magnetite. Very large Ce anomaly indicating redox change. Small negative Eu anomaly not seen in hematite samples. Several samples close to detection limit and must be viewed with caution.

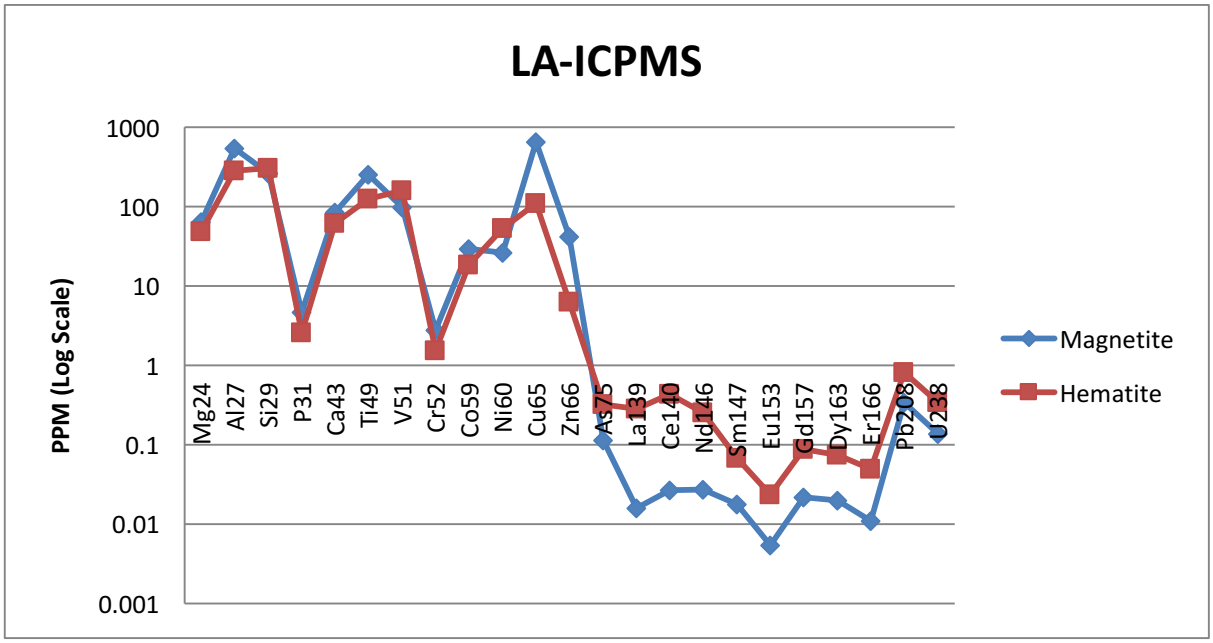

Figure 8: LA-ICPMS data comparing magnetite and hematite using all elements analysed. Trace elements can be seen to have some minor variations between the two minerals. The rare earth element section of the graph can be seen to show a large difference between the two minerals.

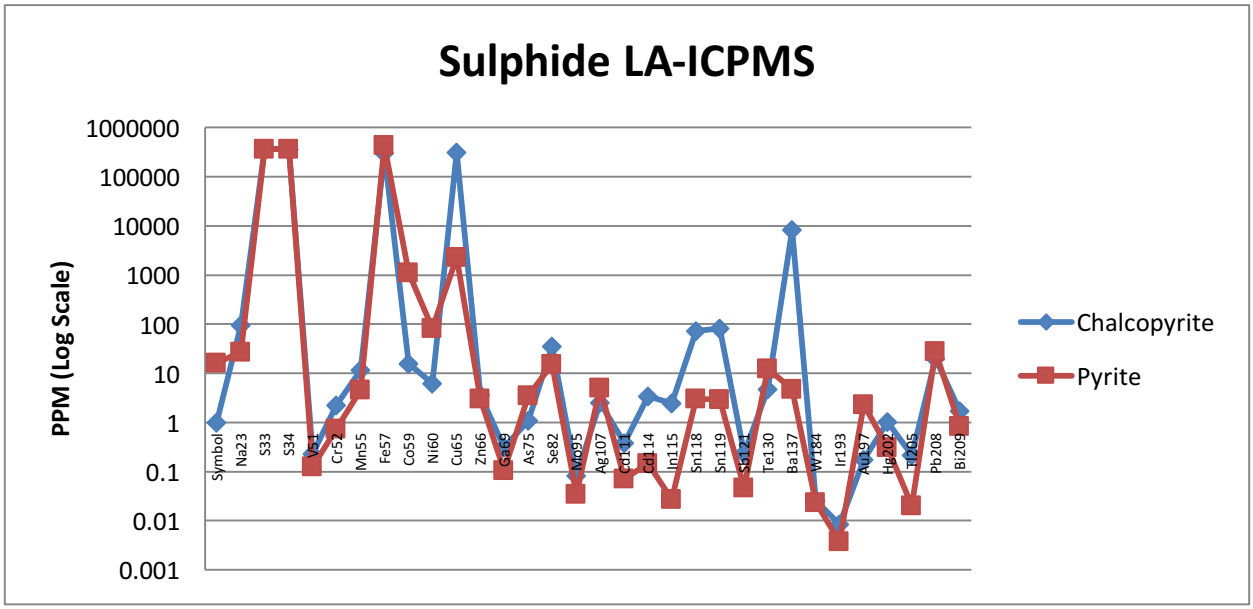

Figure 9: PPM counts from LA-ICPMS data. Chalcopyrite seen to have higher concentrations than pyrite in many different elements.

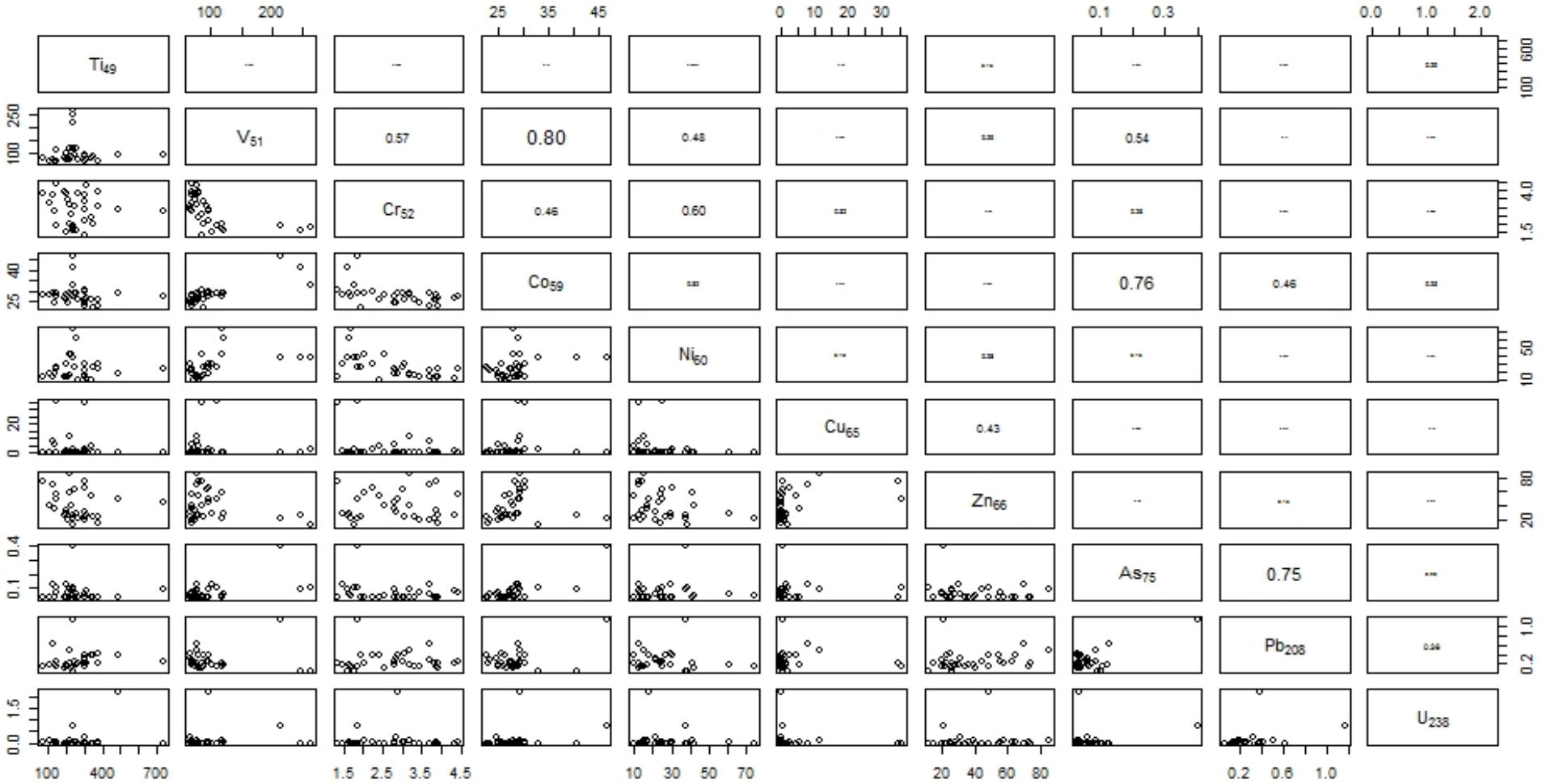

Figure 10: Magnetite correlation plot with all major elements.

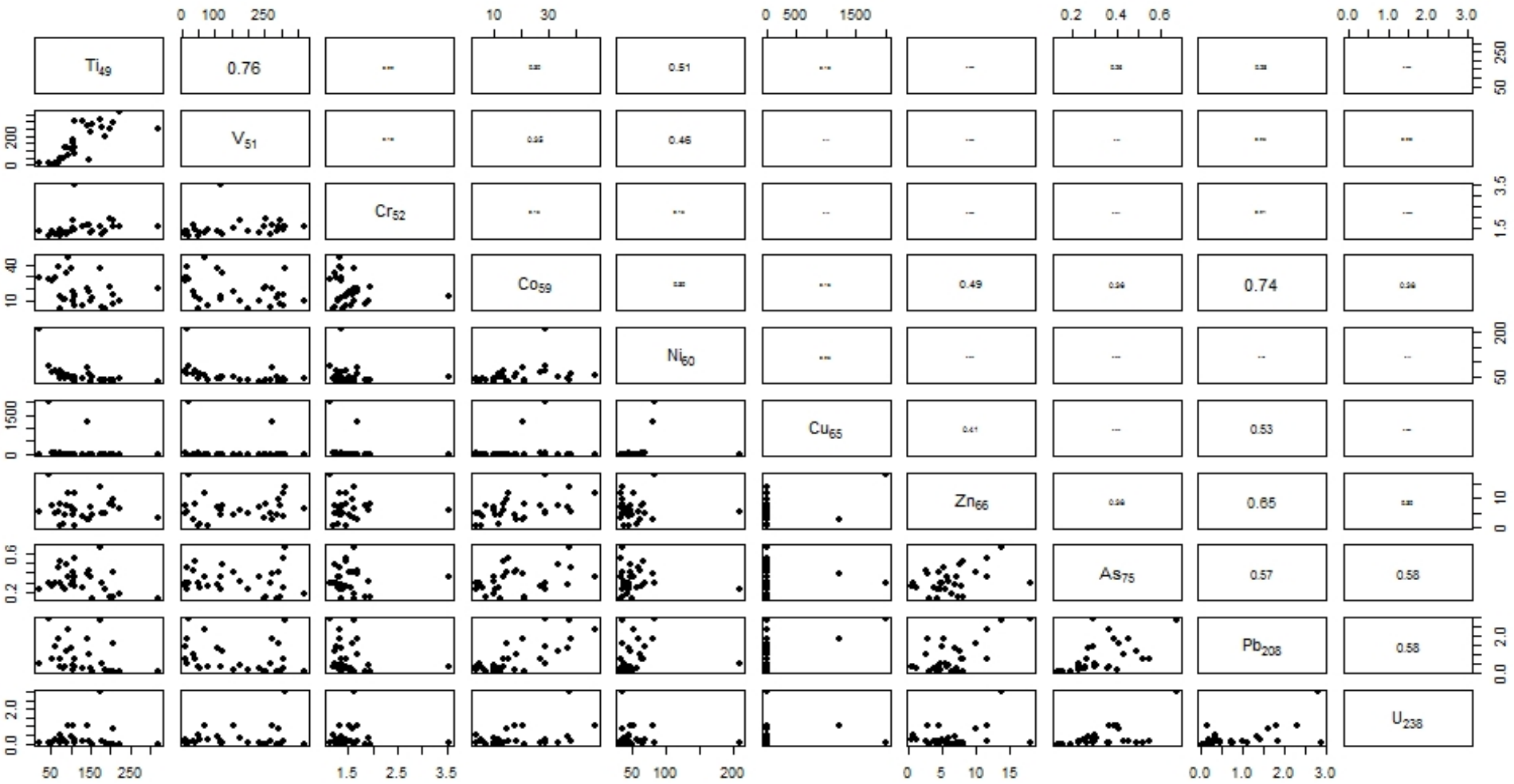

Figure 11: Hematite correlation plot with all major elements.

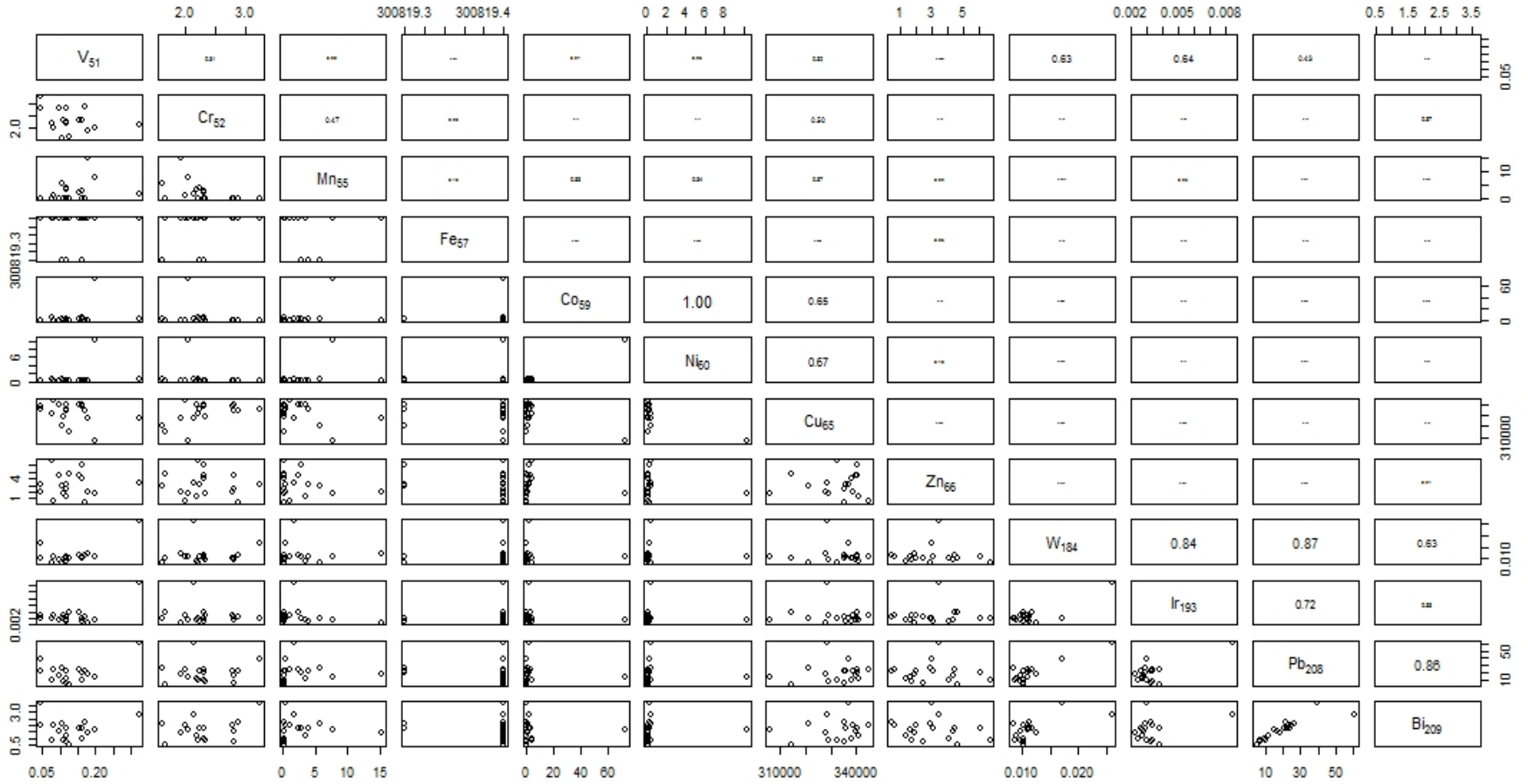

Figure 12: Chalcopyrite correlation plot with all major and minor elements.

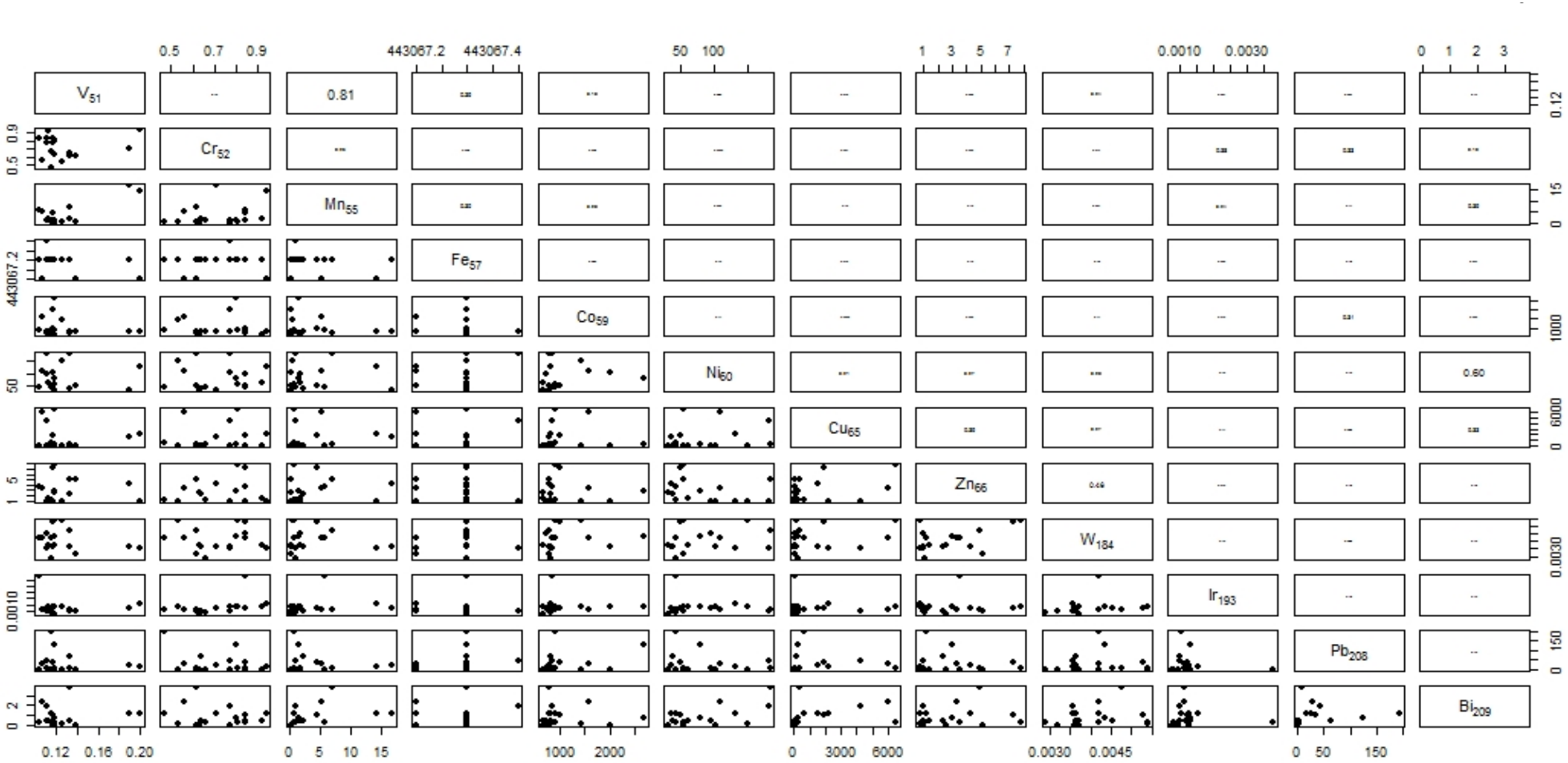

Figure 13: Pyrite element correlation plot with all major and minor elements.

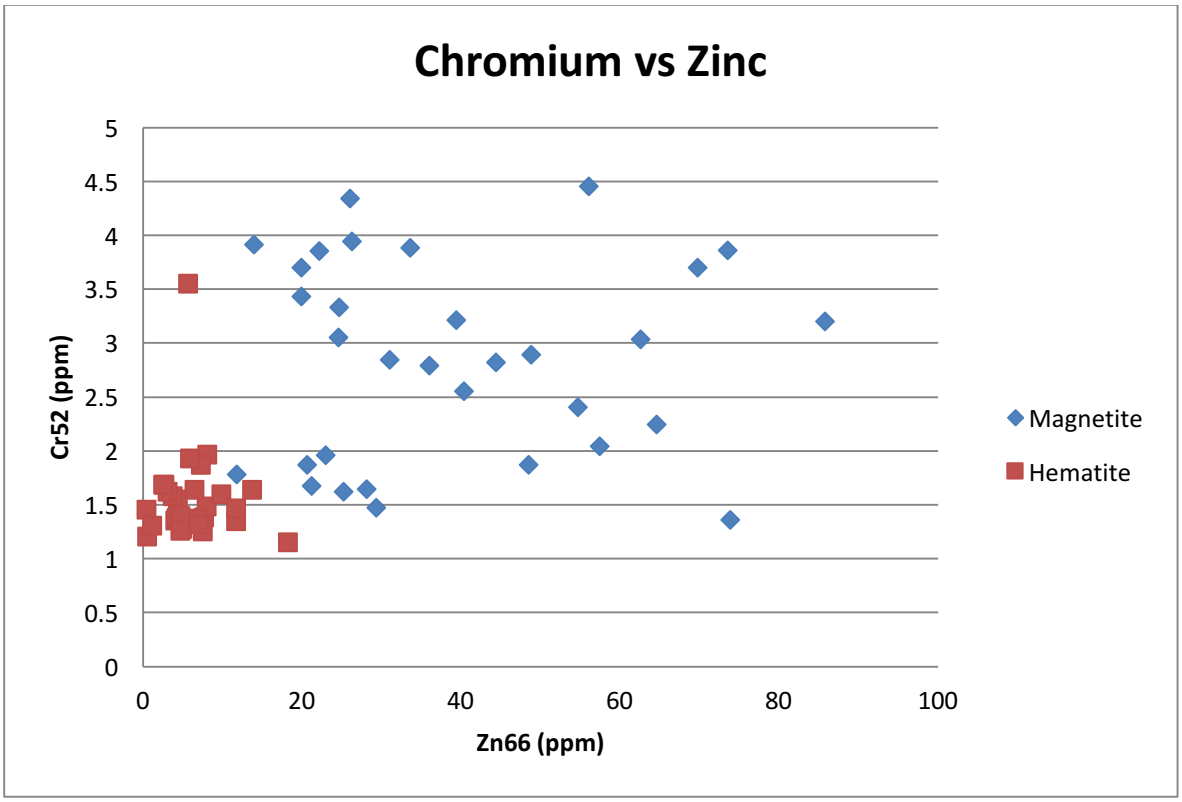

Figure 14: magnetite and hematite graph of chromium vs zinc. The magnetite can be seen to consistently higher values of chromium and zinc. The variation of the magnetite is very large compared to that of hematite. The hematite has much lower values compared to magnetite and the values appear to be very uniform.

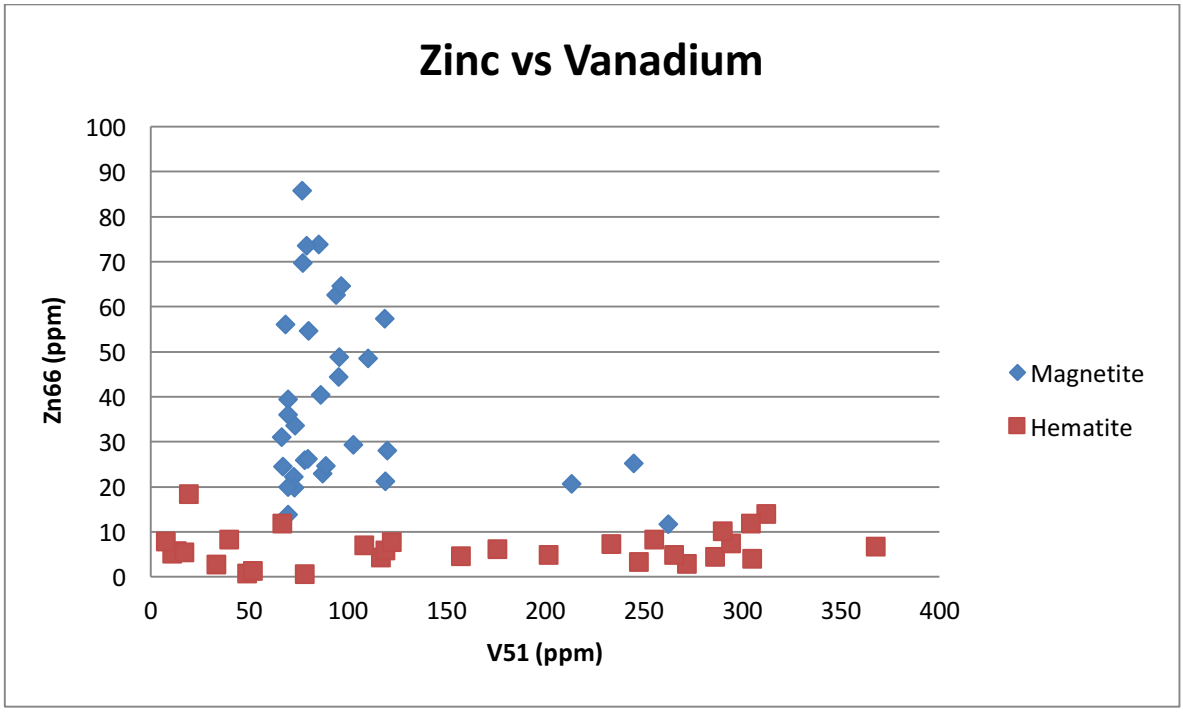

Figure 15: This graph shows the relationship between magnetite and hematite between zinc and Vanadium. The hematite consistently has a lower value of zinc compared to magnetite but has a large variation of vanadium. The magnetite appears to have a consistent level of vanadium but a large range of zinc.

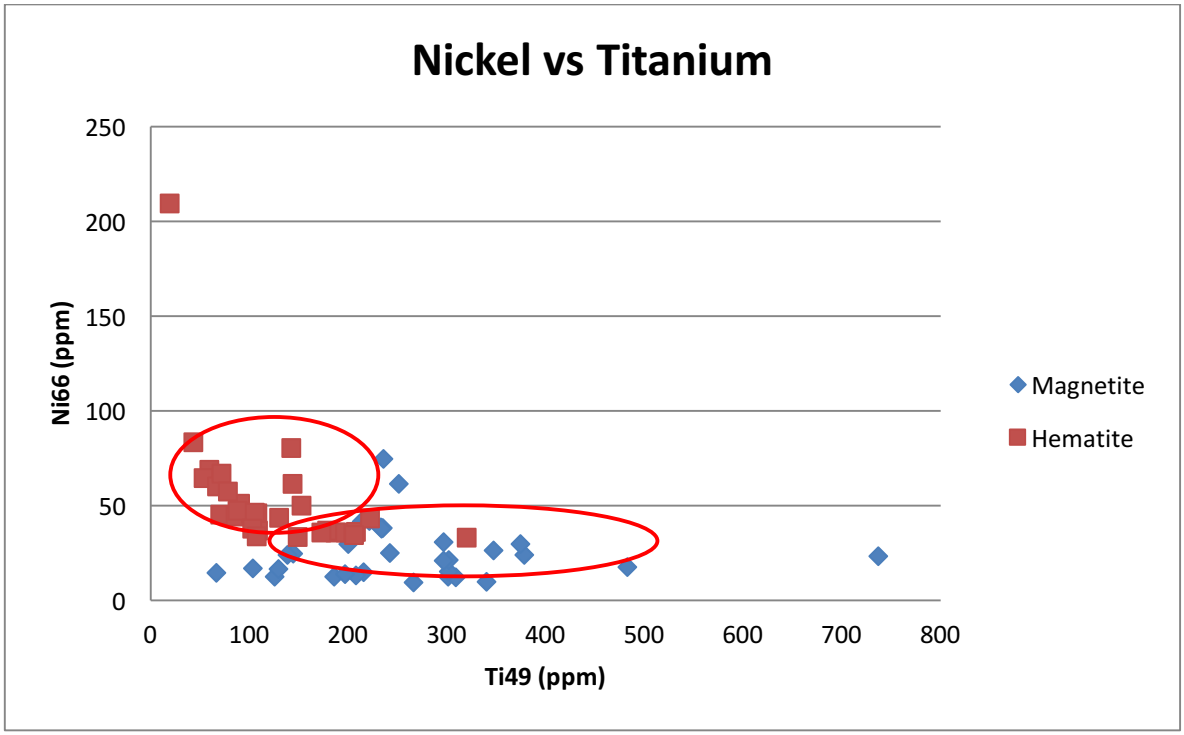

Figure 16: Magnetite and hematite graph shows Ni versus Ti. The two different minerals can be seen to form two different zones within the plot area.

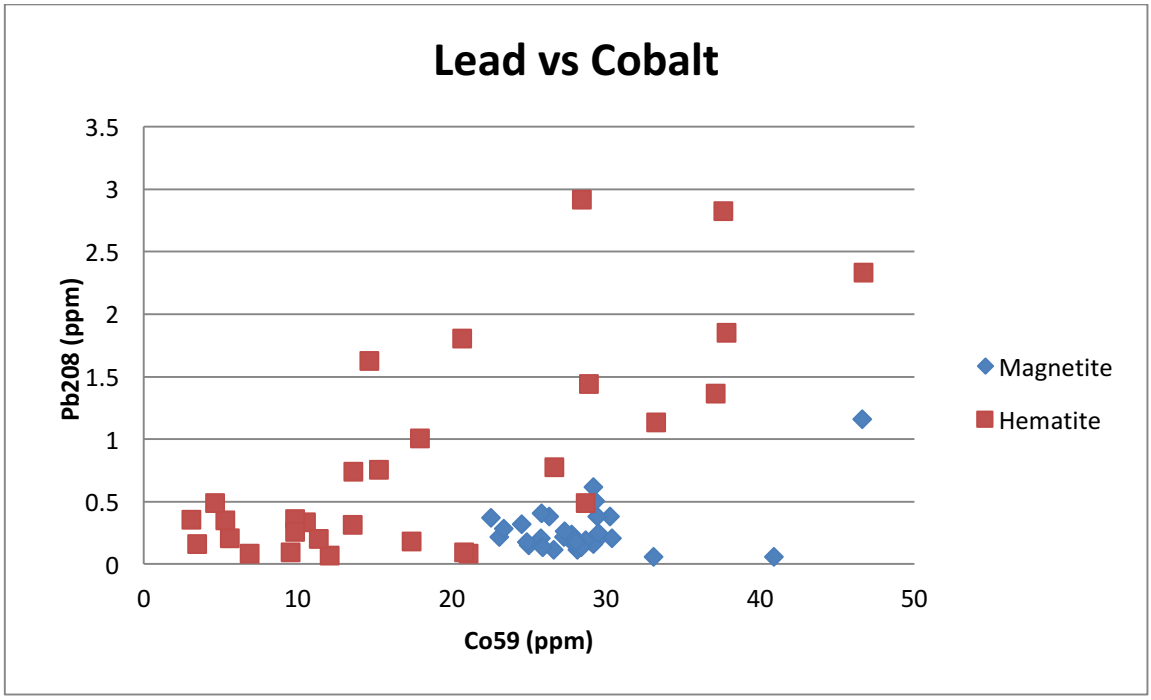

Figure 17: Magnetite and hematite graph with cobalt (Co) versus lead (Pb). The Pb and Co contents of magnetite are very consistent, a tight range can clearly be seen. The hematite values have a slight correlation between lead and cobalt.

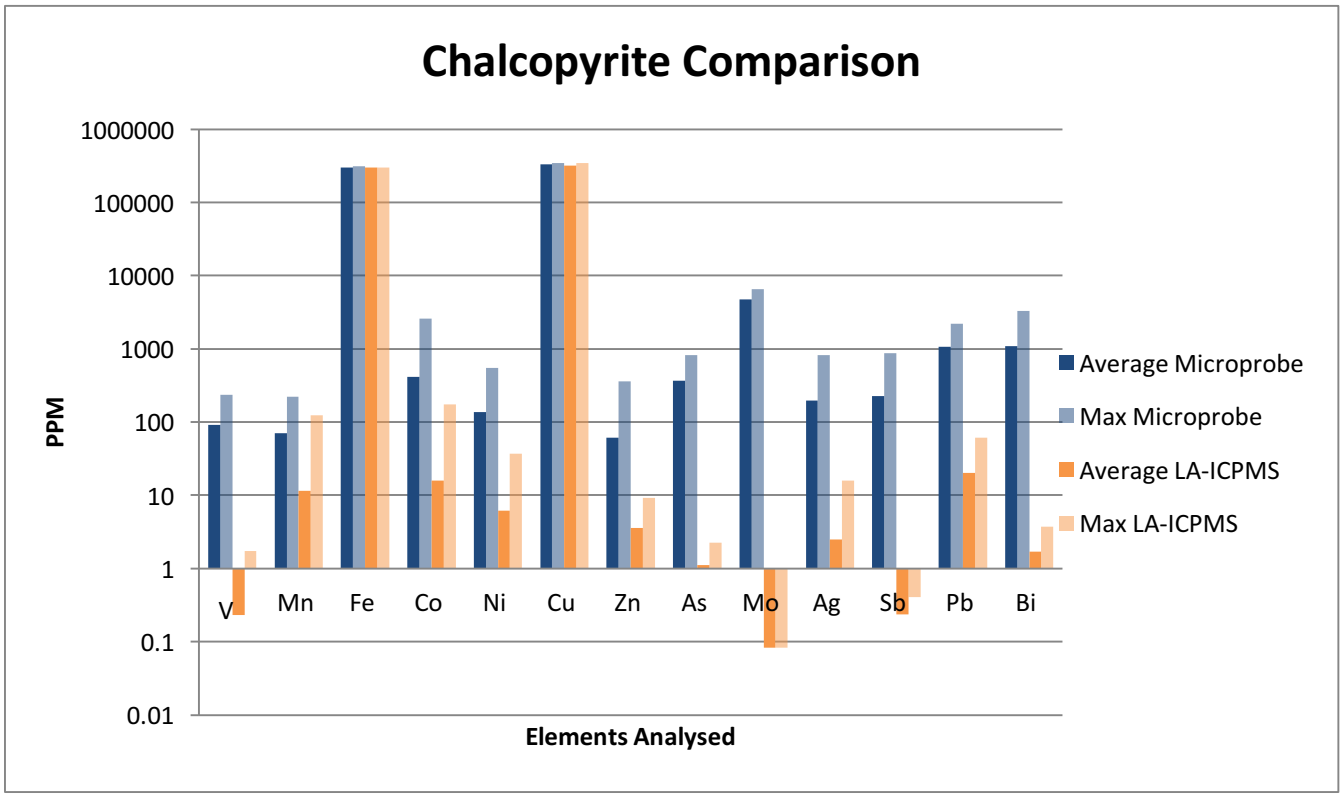

Figure 18: Chalcopyrite comparison between the two analytical techniques (Microprobe vs. LA-ICPMS).

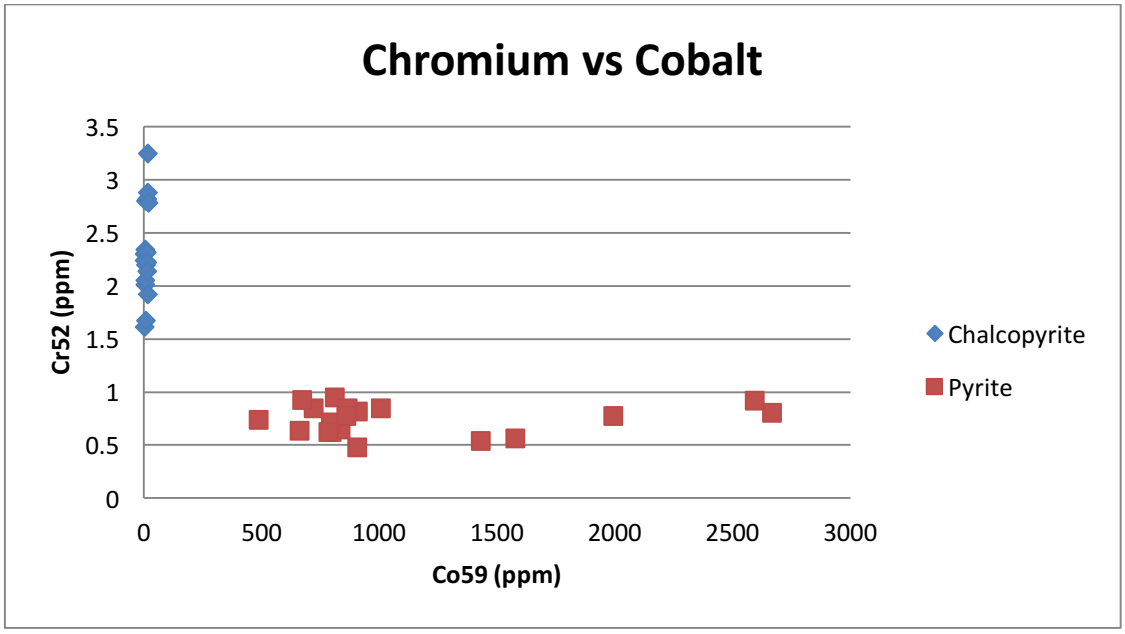

Figure 19: Chromium versus Cobalt in Chalcopyrite and Pyrite. Chalcopyrite showing high concentrations of chromium and very low cobalt. pyrite very high in Cobalt but chromium levels low.

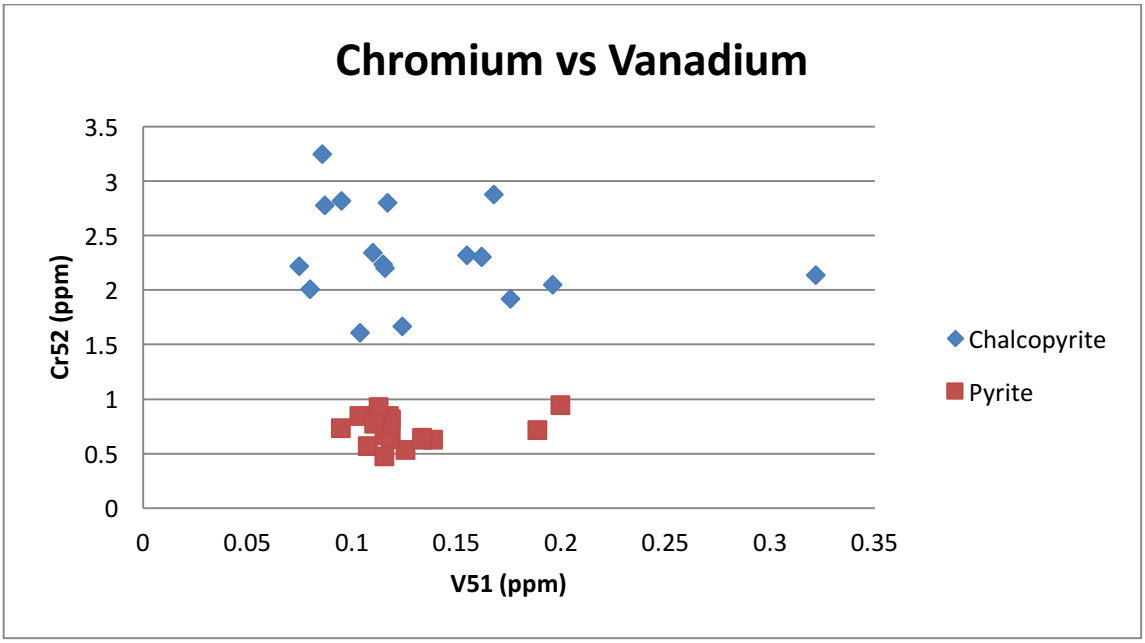

Figure 20: Both pyrite and chalcopyrite with low amounts of vanadium but varying amounts of chromium.

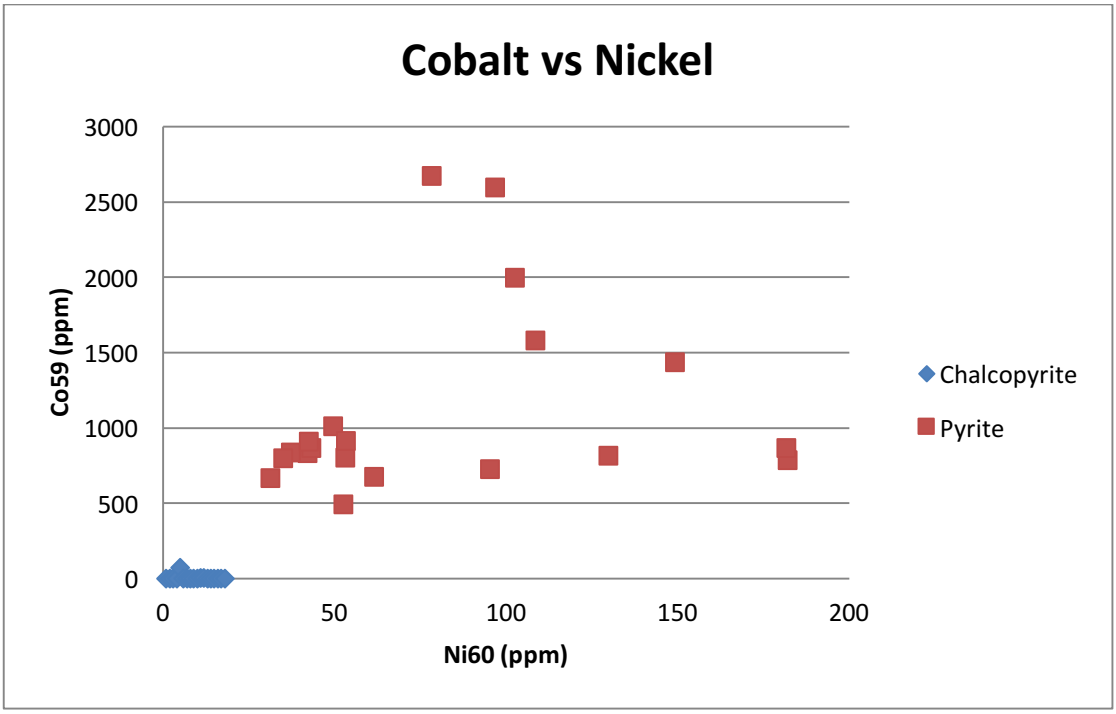

Figure 21: Chalcopyrite and pyrite data from the microprobe, showing levels in cobalt and nickel are much higher in pyrite.

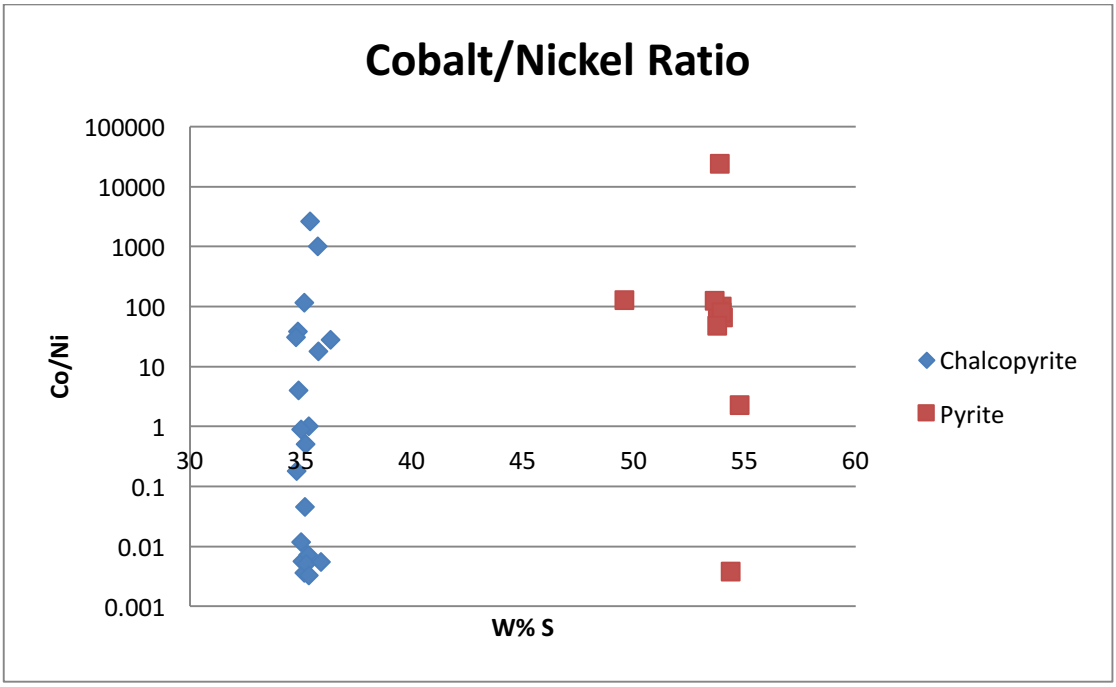

Figure 22: Cobalt- Nickel ratio of sulphides. Both pyrite and chalcopyrite have similar ratios.

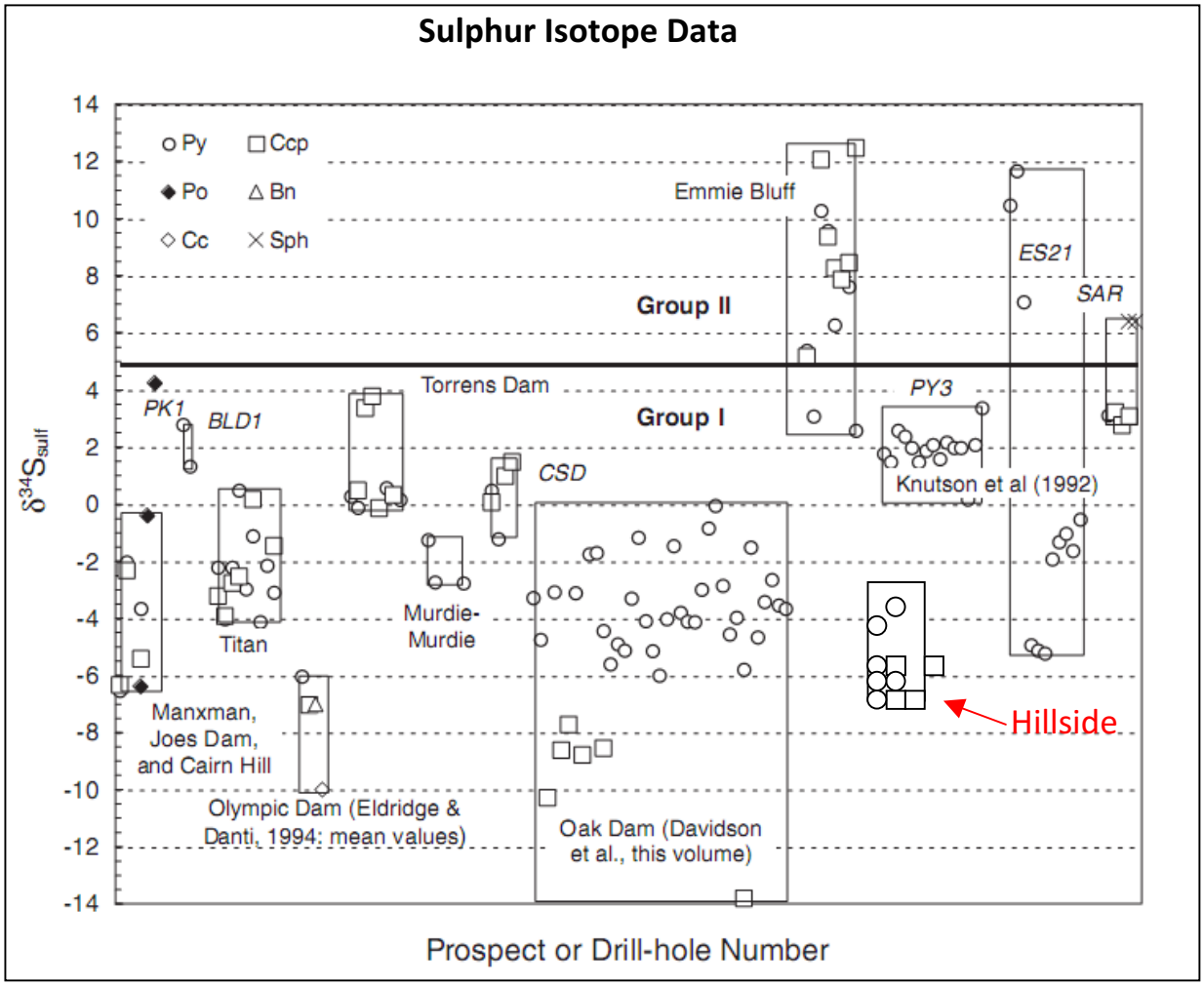

Figure 23: Sulphur isotope data for several deposits/ prospects in the Olympic Dam domain. (Bastrakov et al 2007)

REE Plot of Arthurton Granite

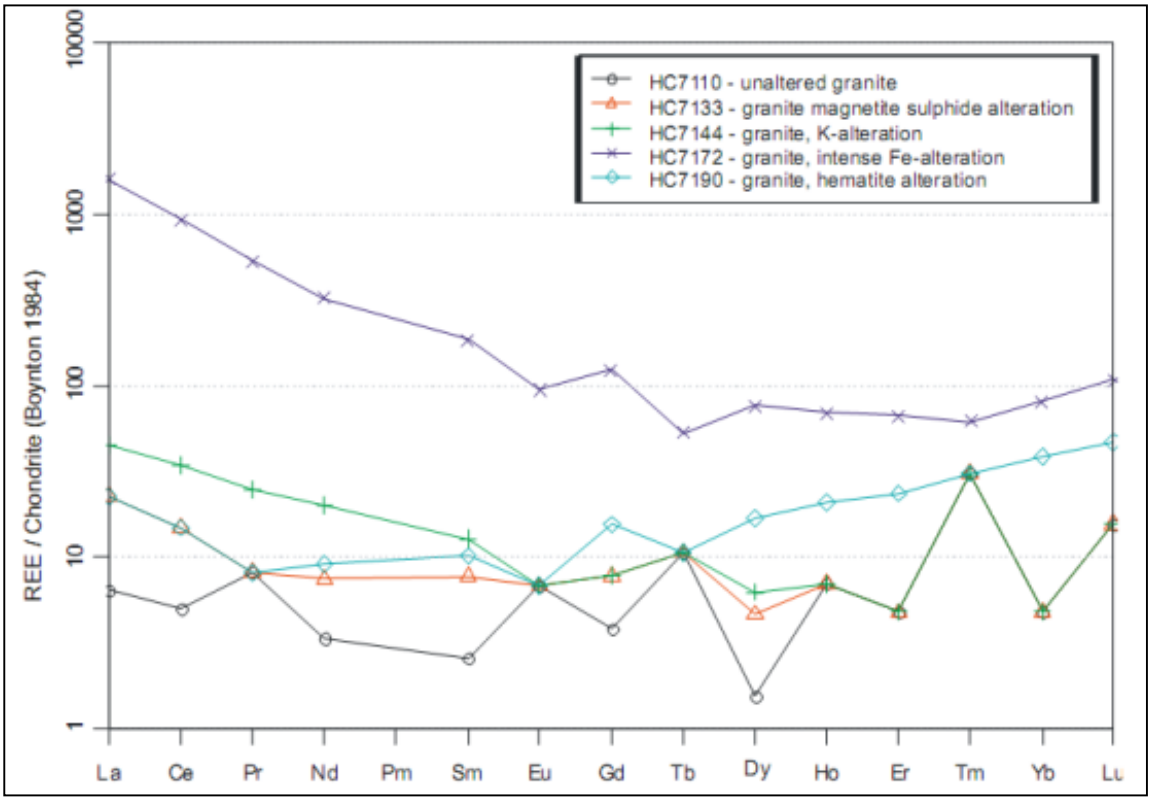

Figure 24: A REE plot of granite samples collected from C. Taylor 2009. This shows the relatively flat shape of the REE plot (Taylor 2009).

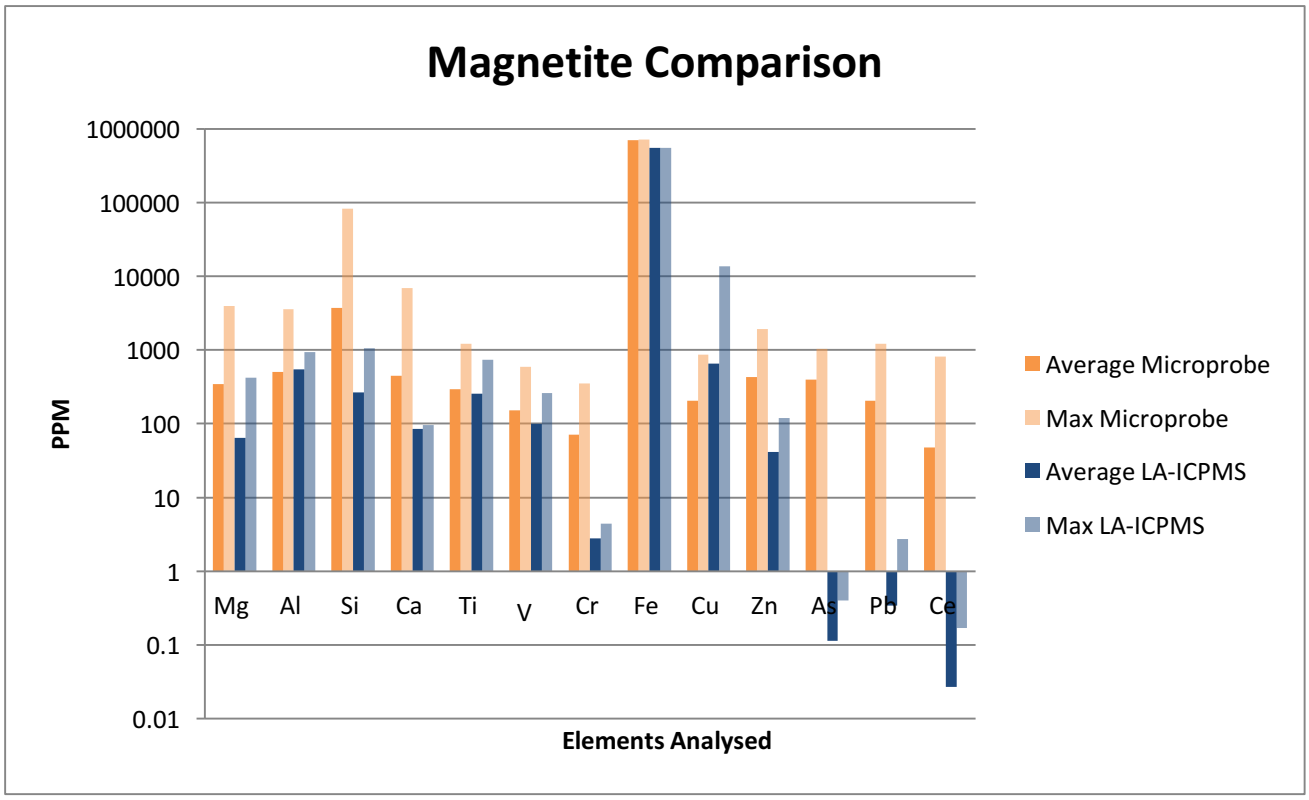

Figure 25: Magnetite comparison of analytical techniques (Microprobe vs. LA-ICPMS).

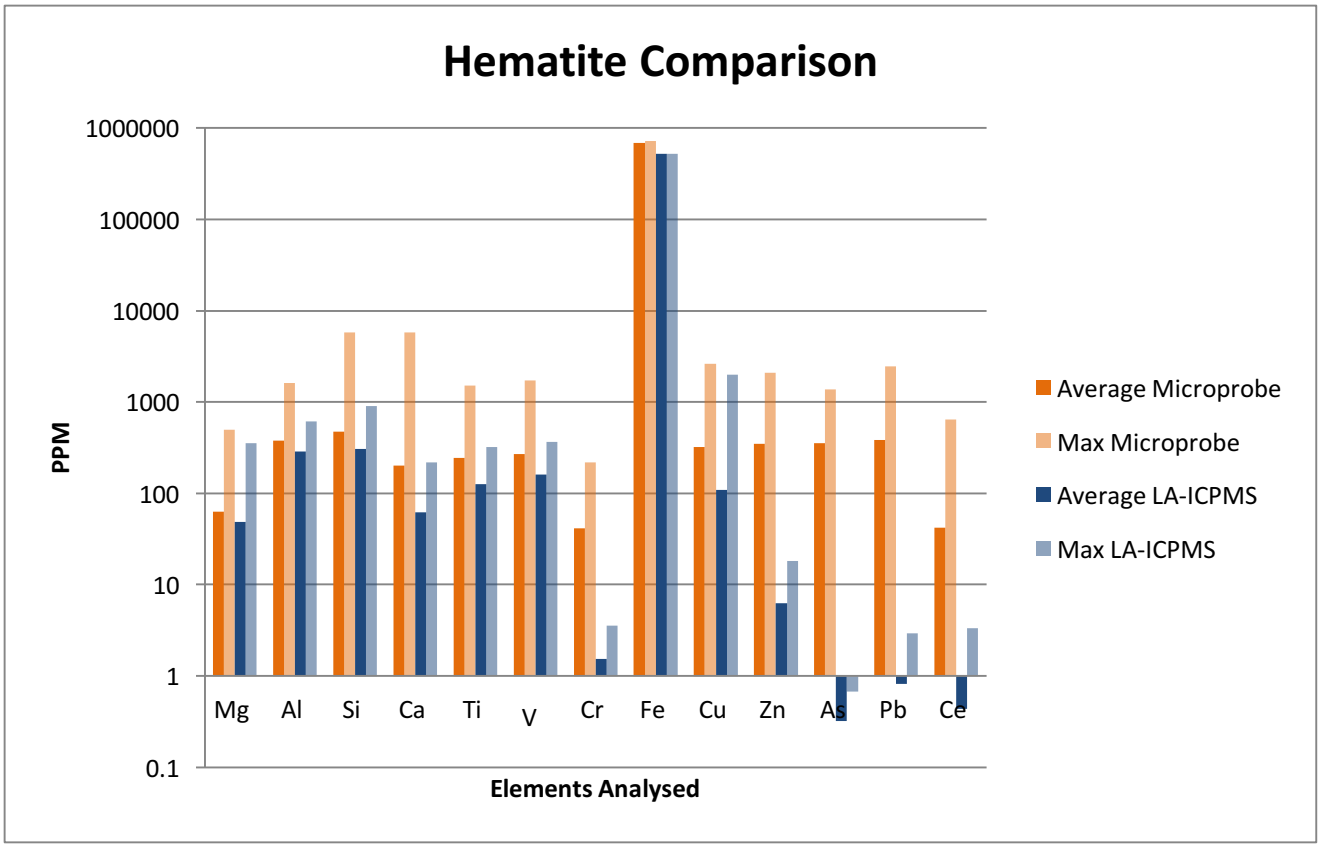

Figure 26: Hematite comparison of analytical methods (Microprobe vs. LA-ICPMS).

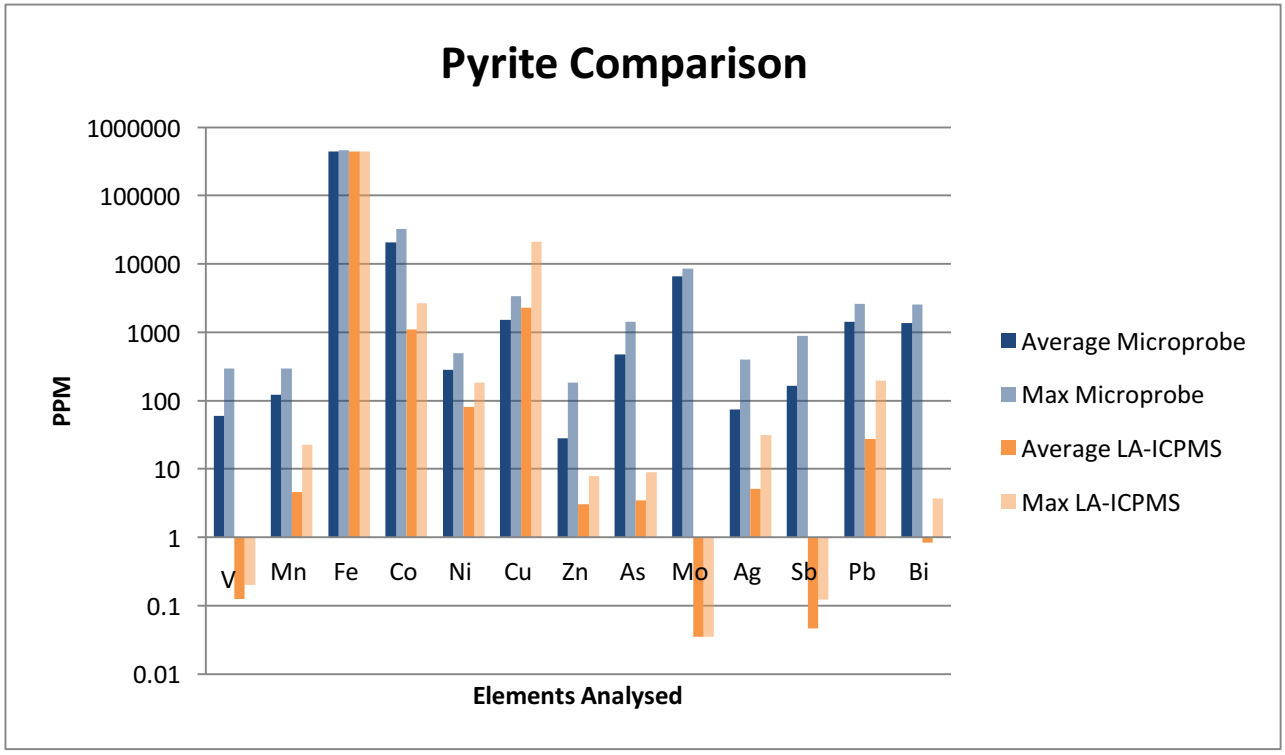

Figure 27: Pyrite comparisons between the two analytical techniques (Microprobe vs. LA-ICPMS).

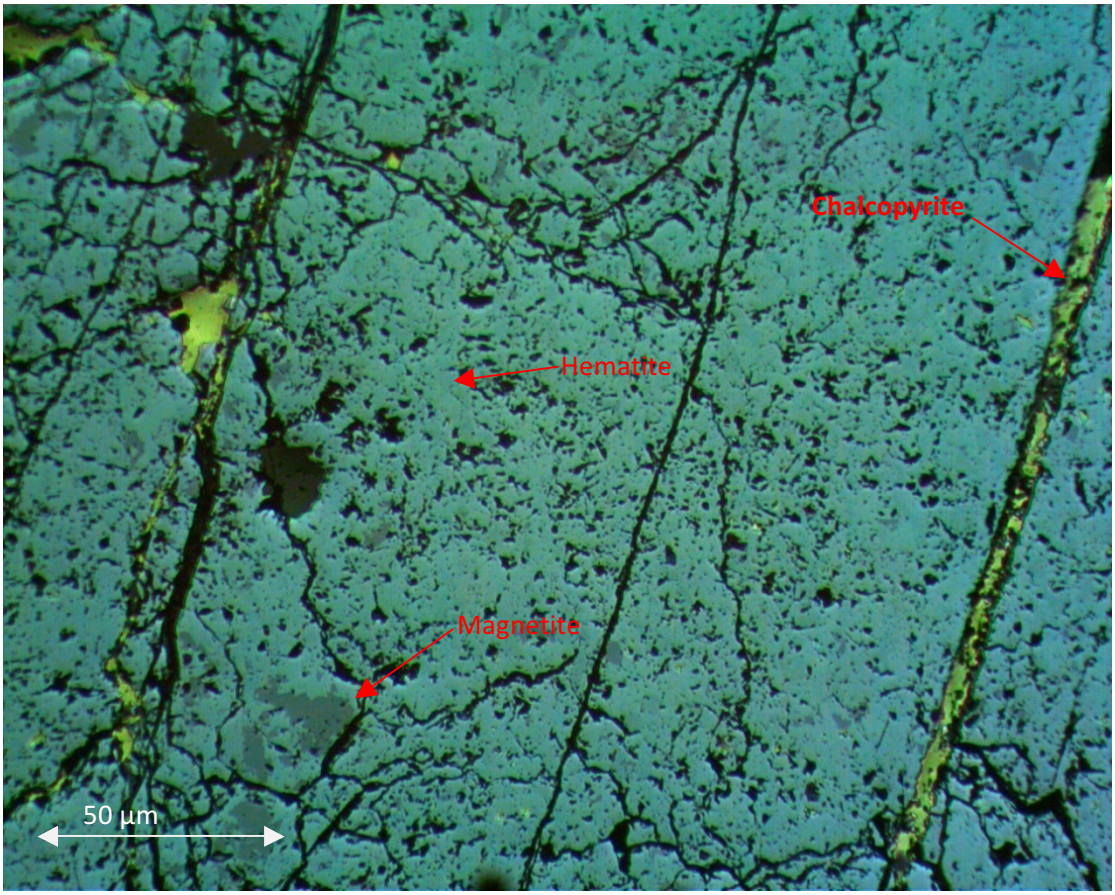

Figure 28: Hematite with chalcopyrite infilling hematite grain fractures.

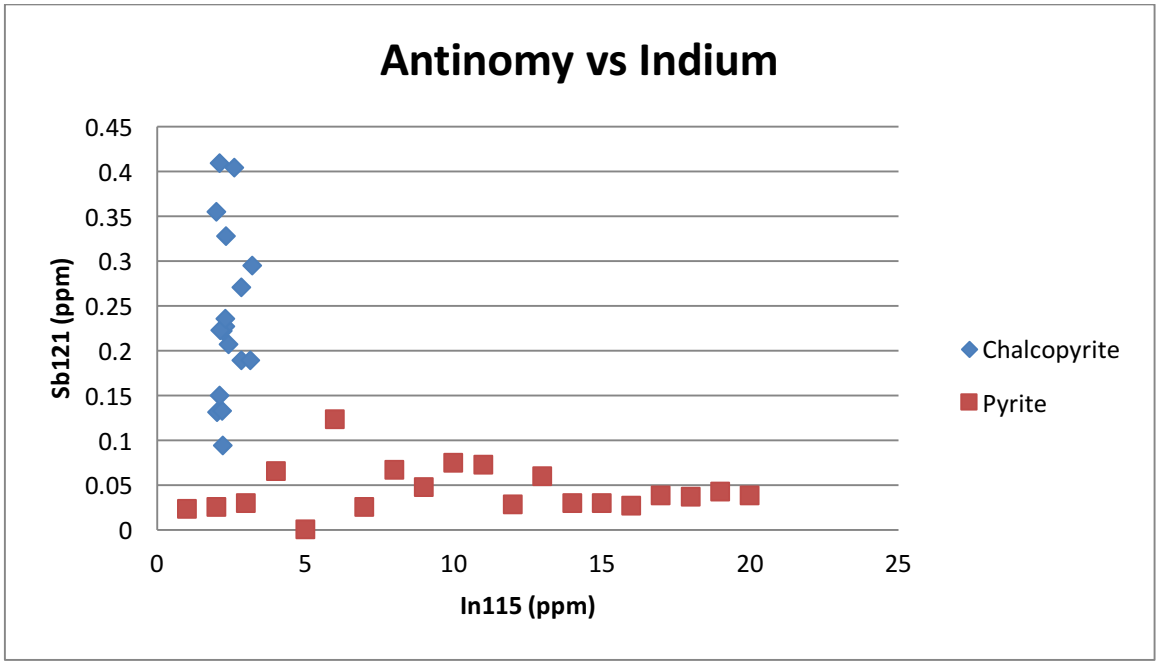

Figure 29: Chalcopyrite and pyrite. Antinomy vs indium shows a clear variation in the concentration of indium in pyrite but low concentration and little variation in chalcopyrite. Antinomy has a distinct variation in chalcopyrite but low concentration and little variation in pyrite.

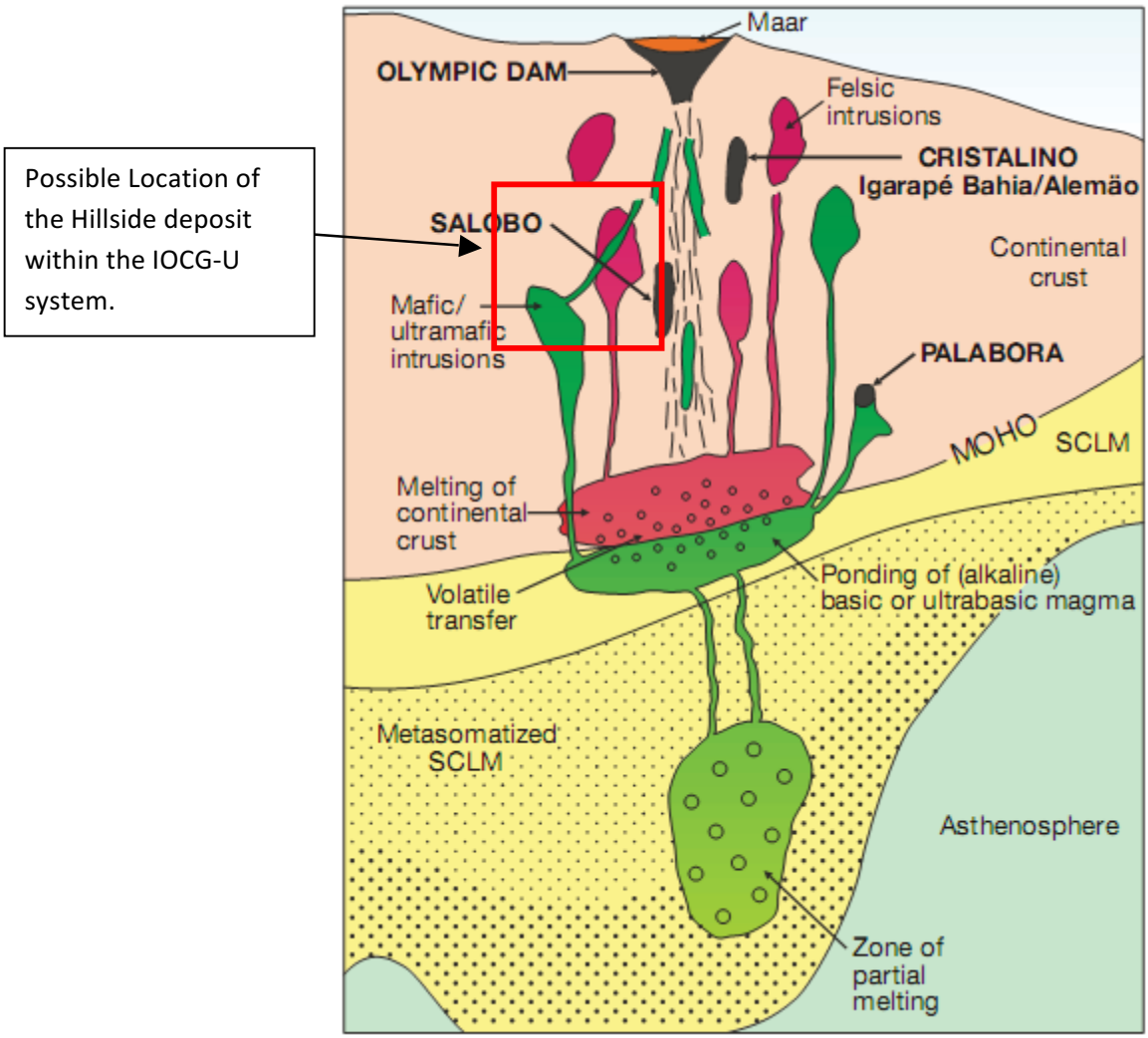

Figure 30: IOCG-U system and locations of known deposits within the system. (Groves et al 2010)

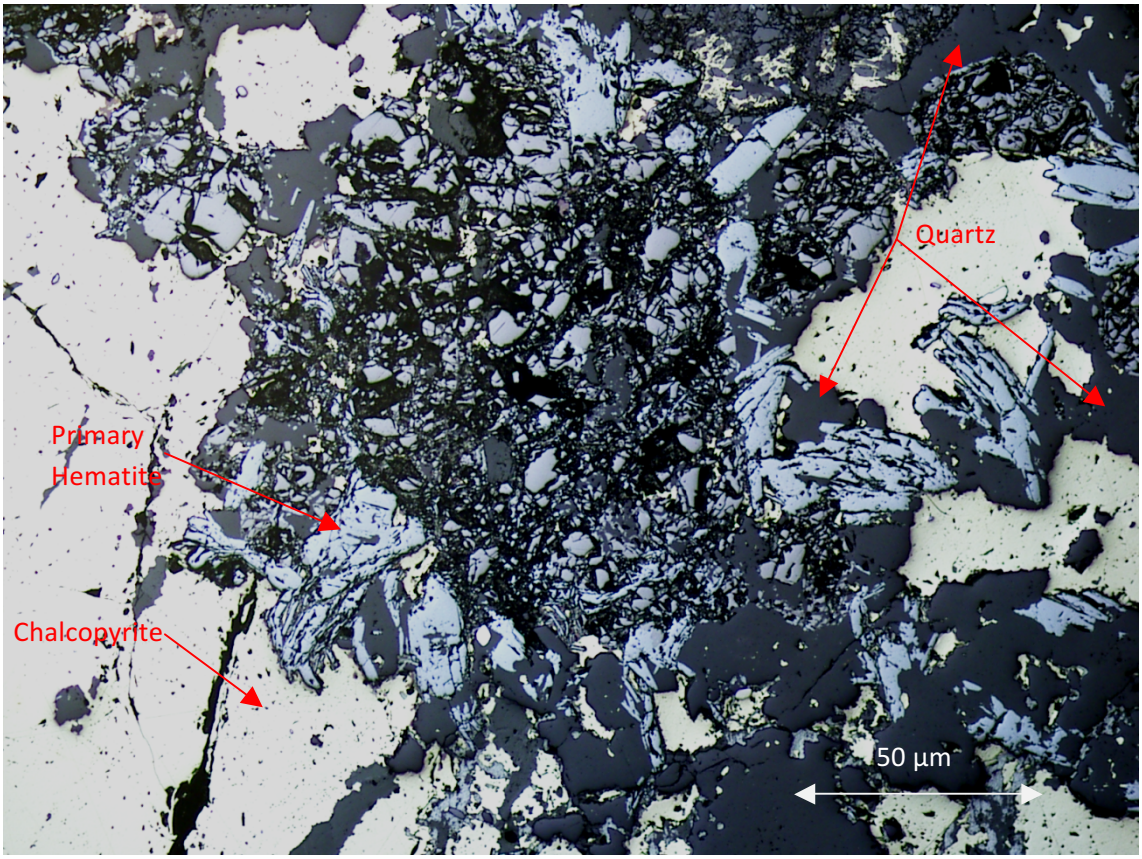

Figure 31:Primary hematite within quartz rich zone. Surrounded by chalcopyrite, hematite always has a small quartz ring surrounding the grains.

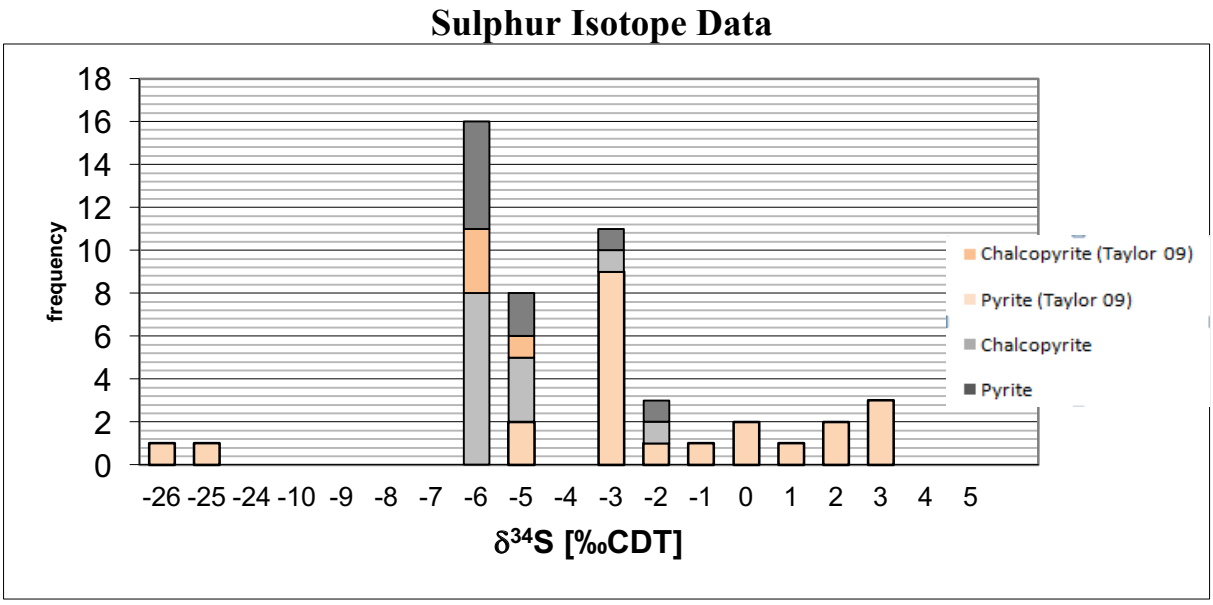

Figure 32: Sulphur isotope data from this study and Taylor (2009).

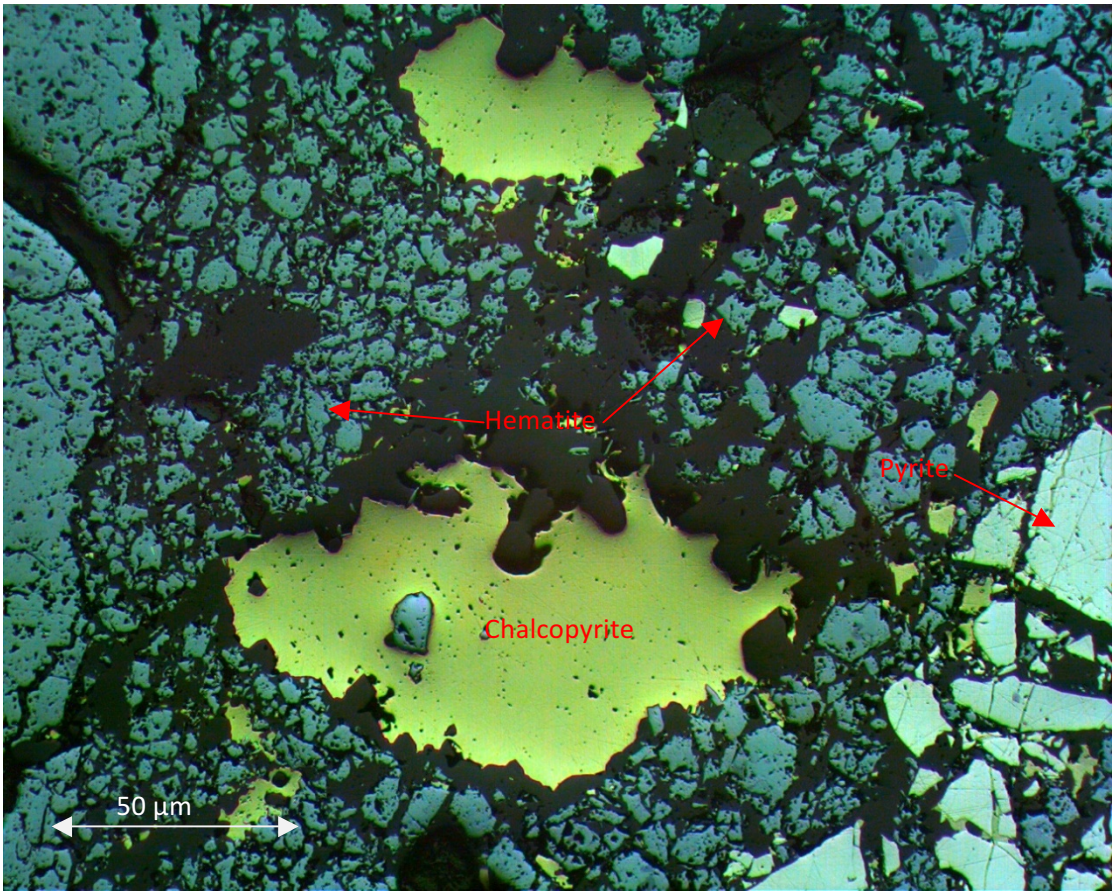

Figure 33: Chalcopyrite filling in space with primary hematite within quartz.

Magnetite (ppm)	Na	Mg	Al	Si	S	K	Ca	Ti	V	Cr	Mn	Fe	Cu	Zn	As	Ce	Pb
Min	3	2	2	1	1	1	1	1	1	1	1	585563	1	1	2	1	1
Lower Quartile	7	70	259	94.5	1	50.5	25.5	162.5	67	10.5	288.5	703784.5	46.5	237.5	358	1	1
Average	76.82	341.64	505.71	3704.68	39.14	96.61	451.00	291.57	152.64	71.07	276.25	696246.07	206.61	429.21	393.11	47.93	204.54
Standard Deviation	157.33	809.91	862.67	15566.63	56.20	114.30	1334.90	337.91	187.82	97.92	215.44	24614.62	282.87	527.48	296.36	164.50	354.17
Upper Quartile	65.5	210.25	440	303	60	159.75	207	417.25	268	133	425.75	707681	391.25	614.25	606.75	1	191
Max	681	3973	3570	82287	172	412	6922	1219	593	355	664	720307	873	1910	1028	819	1206

Table 1: Magnetite electron microprobe data summary.

Hematite (ppm)	Na	Mg	Al	Si	S	K	Ca	Ti	V	Cr	Mn	Fe	Cu	Zn	As	Ce	Pb
Min	3	2	2	1	1	1	1	1	1	1	1	644252	1	1	2	1	1
Lower Quartile	41	2	286	184.5	23	16	39	110	200.5	1	55	684326	62.5	99	300	1	190
Average	80.13	62.63	379.04	475.11	57.50	97.24	200.07	246.20	268.13	41.04	190.96	684974.72	319.02	346.46	356.48	41.85	385.30
Standard Deviation	110.81	100.27	352.32	1015.22	71.81	147.42	851.65	329.60	339.69	60.53	242.42	11834.94	501.22	481.69	339.12	126.40	564.28
Upper Quartile	101.25	87.5	556	301	100.25	152	135	312.25	287.5	59	376	689135.8	537.5	514.75	585.5	1	508
Max	539	501	1614	5824	252	708	5820	1503	1714	217	752	716611	2617	2099	1376	644	2476

Table 2: Hematite electron microprobe data summary.

Chalcopyrite (ppm)	P	S	V	Mn	Fe	Co	Ni	Cu	Zn	As	Mo	Ag	Cd	Sb	Pb	Bi
Min	15	347795	1	1	296365	1	1	308963	1	3	0	1	1	1	1	1
Lower Quartile	250.5	351939	87	37	300583	31.5	112	332285	1	328	5081	78.5	1	80.5	937	922.5
Average	263	352810	90.6	70.9	301723	414.05	136.3	331515	60.85	368.2	4720.95	198.35	111.25	224.25	1065.05	1078.85
Standard Deviation	168.3	3997	80.1	83.6	4251	796.1	141.3	8453	108.0	304.1	1404.1	255.0	198.1	296.4	569.1	830.0
Upper Quartile	333.25	353803	158	132.25	304553	249.25	198.25	336898	53	579.25	5632.25	283	140.25	367	1200.75	1145.25
Max	635	363347	238	223	312660	2611	550	342835	360	823	6495	816	761	870	2218	3318

Table 3: Chalcopyrite electron microprobe data summary.

Pyrite (ppm)	P	S	V	Mn	Fe	Co	Ni	Cu	Zn	As	Mo	Ag	Cd	Sb	Pb	Bi
Min	1	536795	1	1	435621	1	1	253	1	2	5762	1	1	1	329	1
Lower Quartile	1	539900	1	102	443255	23955	269	1265	1	370	6411	1	1	1	1393	1325
Average	46.22	540489	59.33	123.11	447020	20474.89	281.11	1517.22	28.33	470.11	6530.56	74.78	113.22	164.11	1426.56	1371.89
Standard Deviation	83.44	3482	102.32	121.85	10267	11883.27	148.30	1016.85	61.74	428.73	829.36	150.18	173.33	298.46	834.70	804.47
Upper Quartile	64	540660	99	236	446340	27328	367	1918	1	587	6536	1	175	135	2052	2105
Max	257	548051	297	293	464497	32240	496	3368	183	1411	8471	400	420	896	2620	2528

Table 4: Pyrite electron microprobe probe data summary.

Magnetite (ppm)	Mg24	Al27	Si29	P31	Ca43	Ti49	V51	Cr52	Fe57	Co59	Ni60	Cu65	Zn66	As75
Min	8.43	306.54	96.17	2.23	73.20	66.80	66.66	1.36	551891	22.50	9.52	0.24	11.73	0.0580
Lower Quartile	24.07	529.19	161.44	4.41	84.88	235.57	82.76	2.87	551891	27.96	22.34	1.10	32.28	0.0870
Average	57.39	545.75	249.89	4.66	84.88	260.12	99.87	2.83	551891	28.38	25.22	5.58	39.26	0.1080
Standard Deviation	82.28	125.69	219.04	1.67	16.52	124.24	48.93	0.92	0	4.71	14.87	10.59	19.99	0.0873
Upper Quartile	69.14	618.89	265.59	5.63	90.72	302.20	98.30	3.70	551891	29.30	30.11	4.59	55.03	0.1060
Max	424.07	941.43	1055.78	9.11	96.56	737.56	262.74	4.45	551891	46.58	74.69	35.77	85.74	0.4000

Magnetite (ppm)	La139	Ce140	Nd146	Sm147	Eu153	Gd157	Dy163	Er166	Yb172	Pb208
Min	0.0028	0.0025	0.0099	0.0133	0.0050	0.0157	0.0100	0.0035	0.0056	0.06
Lower Quartile	0.0083	0.0128	0.0172	0.0147	0.0055	0.0171	0.0230	0.0089	0.0129	0.21
Average	0.0159	0.0268	0.0271	0.0177	0.0055	0.0217	0.0200	0.0109	0.0163	0.34
Standard Deviation	0.0168	0.0363	0.0219	0.0068	0.0006	0.0102	0.0067	0.0072	0.0088	0.48
Upper Quartile	0.0148	0.0270	0.0303	0.0173	0.0057	0.0223	0.0237	0.0138	0.0246	0.37
Max	0.0600	0.1680	0.0660	0.0296	0.0059	0.0370	0.0240	0.0231	0.0300	2.75

Table 5: Magnetite LA-ICPMS data summary.

Hematite (ppm)	Mg24	Al27	Si29	P31	Ca43	Ti49	V51	Cr52	Fe57	Co59	Ni60	Cu65	Zn66	As75
Min	2.10	70.93	144.72	1.80	25.38	20.29	8.09	1.14	520798	3.12	32.98	0.14	0.47	0.1330
Lower Quartile	16.30	283.34	234.76	2.37	44.80	108.72	140.20	1.42	520798	14.98	45.16	1.09	5.66	0.2975
Average	48.96	285.31	304.40	2.58	61.76	126.70	161.17	1.54	520798	18.41	53.22	109.67	6.30	0.3208
Standard Deviation	85.33	115.03	211.94	0.66	44.50	64.90	116.21	0.43	0	11.86	32.60	420.46	3.89	0.1298
Upper Quartile	27.13	348.13	321.46	2.72	66.44	168.98	270.59	1.63	520798	27.99	59.18	5.03	7.69	0.3975
Max	352.09	615.97	897.96	4.18	219.18	321.17	368.13	3.54	520798	46.70	209.25	2002.18	18.26	0.6700

Hematite (ppm)	La139	Ce140	Nd146	Sm147	Eu153	Gd157	Dy163	Er166	Yb172	Au197	Pb208	U238
Min	0.0306	0.0055	0.0540	0.0200	0.0061	0.0269	0.0144	0.0110	0.0105	0.0000	0.0663	0.00
Lower Quartile	0.1740	0.2340	0.1270	0.0406	0.0144	0.0530	0.0409	0.0314	0.0322	0.0000	0.4195	0.13
Average	0.2824	0.4358	0.2549	0.0672	0.0233	0.0876	0.0747	0.0497	0.0574	0.0001	0.8184	0.34
Standard Deviation	0.3268	0.6223	0.3247	0.0667	0.0199	0.0774	0.0725	0.0488	0.0633	0.0001	0.8341	0.60
Upper Quartile	0.3450	0.4673	0.2890	0.0785	0.0318	0.1153	0.0963	0.0588	0.0715	0.0001	1.3018	0.31
Max	1.6600	3.3500	1.6800	0.2710	0.0872	0.3590	0.3550	0.2370	0.2970	0.0001	2.9100	2.99

Table 6: Hematite LA-ICPMS data summary.

Magnetite (ppm)	Mg24	Al27	Si29	P31	Ca43	Ti49	V51	Cr52	Fe57	Co59	Ni60	Cu65	Zn66	As75
Min	8.43	306.54	96.17	2.23	73.20	66.80	66.66	1.36	551891	22.50	9.52	0.24	11.73	0.0580
Lower Quartile	24.07	529.19	161.44	4.41	84.88	235.57	82.76	2.87	551891	27.96	22.34	1.10	32.28	0.0870
Average	57.39	545.75	249.89	4.66	84.88	260.12	99.87	2.83	551891	28.38	25.22	5.58	39.26	0.1080
Standard Deviation	82.28	125.69	219.04	1.67	16.52	124.24	48.93	0.92	0	4.71	14.87	10.59	19.99	0.0873
Upper Quartile	69.14	618.89	265.59	5.63	90.72	302.20	98.30	3.70	551891	29.30	30.11	4.59	55.03	0.1060
Max	424.07	941.43	1055.78	9.11	96.56	737.56	262.74	4.45	551891	46.58	74.69	35.77	85.74	0.4000

Magnetite (ppm)	La139	Ce140	Nd146	Sm147	Eu153	Gd157	Dy163	Er166	Yb172	Pb208
Min	0.0028	0.0025	0.0099	0.0133	0.0050	0.0157	0.0100	0.0035	0.0056	0.06
Lower Quartile	0.0083	0.0128	0.0172	0.0147	0.0055	0.0171	0.0230	0.0089	0.0129	0.21
Average	0.0159	0.0268	0.0271	0.0177	0.0055	0.0217	0.0200	0.0109	0.0163	0.34
Standard Deviation	0.0168	0.0363	0.0219	0.0068	0.0006	0.0102	0.0067	0.0072	0.0088	0.48
Upper Quartile	0.0148	0.0270	0.0303	0.0173	0.0057	0.0223	0.0237	0.0138	0.0246	0.37
Max	0.0600	0.1680	0.0660	0.0296	0.0059	0.0370	0.0240	0.0231	0.0300	2.75

Table 7: Magnetite LA-ICPMS data summary.

Chalcopyrite (ppm)	Na23	S33	S34	V51	Cr52	Mn55	Fe57	Co59	Ni60	Cu65	Zn66	Ga69	As75	Se82	Mo95
Min	8.84	348425	323270	0.08	1.61	0.31	300819	0.10	0.27	306035	1.39	0.04	0.53	29.32	0.08
Lower Quartile	90.05	367796	358934	0.12	2.27	2.44	300819	1.26	0.46	335489	3.11	0.13	0.94	35.25	0.08
Average	103.03	384486	367699	0.14	2.33	3.55	300819	6.11	2.05	332493	3.42	0.11	0.97	35.80	0.08
Standard Deviation	87.43	36002	39189	0.06	0.43	4.21	0	18.39	4.07	10003	1.58	0.06	0.47	4.72	#DIV/0!
Upper Quartile	152.83	391151	388557	0.16	2.67	3.97	300819	2.43	0.49	339380	4.42	0.15	1.17	37.48	0.08
Max	252.68	477928	457749	0.32	3.25	15.31	300819	72.40	10.36	344699	6.74	0.21	1.88	47.88	0.08

Chalcopyrite (ppm)	Ag107	Cd111	Cd114	In115	Sn118	Sn119	Sb121	Te130	Ba137	Au197	Hg202	Tl205	Pb208	Bi209
Min	0.78	0.15	0.05	0.01	0.96	1.05	0.03	0.68	1.06	0.03	0.23	0.01	4.53	0.36
Lower Quartile	1.57	0.30	0.46	2.29	4.01	5.00	0.22	1.36	2.62	0.08	1.07	0.18	19.13	1.69
Average	2.51	0.39	3.40	2.42	73.74	81.94	0.23	4.70	8304.80	0.17	1.04	0.22	20.21	1.69
Standard Deviation	3.26	0.31	9.30	0.95	171.83	225.39	0.10	14.40	28745.95	0.29	0.29	0.19	13.86	0.91
Upper Quartile	2.31	0.37	0.93	2.64	40.04	11.00	0.31	1.94	5.31	0.13	1.21	0.32	24.27	2.03
Max	15.72	1.00	40.68	5.40	716.05	816.85	0.41	65.79	99585.44	1.25	1.64	0.55	61.31	3.73

Table 8: Chalcopyrite LA-ICPMS data summary.

Pyrite (ppm)	Na23	S33	S34	V51	Cr52	Mn55	Fe57	Co59	Ni60	Cu65	Zn66	Ga69	As75	Se82	Mo95
Min	2.54	347070	344655	0.10	0.47	0.22	443067	488.34	31.54	1.6	0.93	0.02	0.77	10.31	0.04
Lower Quartile	15.06	367793	359333	0.12	0.75	1.58	443067	848.53	57.61	247.5	2.56	0.04	3.55	13.99	0.04
Average	27.01	366275	361254	0.13	0.73	4.64	443067	1111.27	81.54	2277.6	3.02	0.10	3.50	15.33	0.04
Standard Deviation	26.05	10570	10531	0.03	0.14	6.36	0	625.01	47.99	4828.3	2.16	0.11	2.43	4.07	#DIV/0!
Upper Quartile	44.72	373113	370673	0.13	0.84	5.49	443067	1114.61	104.33	1989.6	4.14	0.19	4.54	16.74	0.04
Max	77.85	382088	383806	0.20	0.94	22.50	443067	2669.44	182.36	20927.2	7.86	0.26	8.88	24.00	0.04

Pyrite (ppm)	Ag107	Cd111	Cd114	In115	Sn118	Sn119	Sb121	Te130	Ba137	Au197	Hg202	Tl205	Pb208	Pb208	Bi209
Min	0.05	0.07	0.03	0.00	0.39	0.34	0.02	0.20	0.23	0.01	0.23	0.00	0.05	0.05	0.02
Lower Quartile	2.15	0.07	0.08	0.02	1.52	1.46	0.04	6.53	2.16	0.17	0.31	0.02	4.88	4.88	0.48
Average	5.10	0.07	0.15	0.03	3.06	2.91	0.05	12.20	4.75	2.28	0.31	0.02	27.78	27.78	0.84
Standard Deviation	7.82	#DIV/0!	0.14	0.03	3.19	3.27	0.03	15.57	5.38	4.56	0.05	0.02	49.56	49.56	0.93
Upper Quartile	7.63	0.07	0.21	0.03	4.38	4.05	0.06	13.18	6.43	1.16	0.33	0.02	29.10	29.10	1.16
Max	31.21	0.07	0.62	0.12	11.21	12.59	0.12	57.30	19.21	14.34	0.40	0.06	194.14	194.14	3.74

Table 9: Pyrite LA-ICPMS data summary.

Hole ID	Sample No.	Sample ID	Minerals	$\delta^{34}S$ Value	std. dev.
HDD044	233	BT14	Pyrite	-6.1	0
HDD044	172.4	BT02	Pyrite	-6.1	0
HDD044	221	BT06	Chalcopyrite	-6	0
HDD044	297.5	BT12	Pyrite	-3.8	0
HDD044	197	BT13	Pyrite	-6.6	0.1
HDD044	163.6A	BT07	Chalcopyrite	-6.3	0
HDD044	163.6B	BT07	Chalcopyrite	-6.3	0
HDD044	157	BT03	Pyrite	-2.6	0
HDD044	164A	BT10	Pyrite	-5.3	0
HDD044	164B	BT10	Pyrite	-5	0.1
HDD044	184	BT08	Pyrite	-6.6	0
HDD044	175	BT01	Chalcopyrite	-5.8	0
HDD044	155.5	BT09	Pyrite	-6.3	0

Table 10: Sulphur isotope data.

Samples Collected from Hillside

Sample	Hole	Depth (M)	Rock Type	Description
BT01	HDD044	175	Garnet Skarn	Banded red rock alteration. Some layering, layering paralellel to core axis, strong brecciation, major structure towards base.
BT02	HDD044	172.4	Garnet Skarn	Magnetite replaced by garnet, "garnet skarn". Some K-feldspar+magnetite alteration, CPX replaced by clays, garnet replaced by magnetite.
BT03	HDD044	157	Garnet Skarn	Magnetite replaced by garnet, "garnet skarn". Some K-feldspar+magnetite alteration, CPX replaced by clays, garnet replaced by magnetite.
BT04	HDD044	148	Skarn	Banded skarn hedenburgite, hematite, K-feldspar banded-massive. Trace sulphide at base massive magnetite+pyrite banded sample.
BT05	HDD044	273.5	Garnet Skarn	CPX with chalcopyrite in small hematite rich veins. Garnet skarn, sulphur present. Magnetite with red rock alteration, CPX rich zone "K-feldspar, hematite, CPX alteration skarn with chalcopyrite."
BT06	HDD044	221	CPX Skarn	CPX skarn with remanent garnet skarn.
BT07	HDD044	163.6	Garnet Skarn	Magnetite replaced by garnet, "garnet skarn". Some K-feldspar+magnetite alteration, CPX replaced by clays, garnet replaced by magnetite.
BT08	HDD044	184	Feldspar Skarn	Banded red rock alteration. Some layering, layering paralellel to core axis, strong brecciation, major structure towards base.
BT09	HDD044	155.2	CPX/K-Feldspar skarn	CPX/K-Feldspar skarn, slight red rock alteration, hematite, calcareous with slight garnet, garnet skarn.
BT10	HDD044	164	Garnet Skarn	Magnetite replaced by garnet, "garnet skarn". Some K-feldspar+magnetite alteration, CPX replaced by clays, garnet replaced by magnetite.
BT11	HDD044	126	CPX Skarn	CPX rich skarn quartz flooding, brecciated quartz in magnetite matrix. 121-125.5 K-feldspar, spotted magnetite CPX skarn "CPX to chlorite and clay" small structure. 125.8-128.6 minor garnet skarn, CPX dominated skarn.
BT12	HDD044	277.5	CPX Skarn	CPX rich skarn quartz flooding, brecciated quartz in magnetite matrix. 121-125.5 K-feldspar, spotted magnetite CPX skarn "CPX to chlorite and clay" small structure. 125.8-128.6 minor garnet skarn, CPX dominated skarn.
BT13	HDD044	197	Garnet Skarn	Garnet skarn in parts. Magnetite veins, banded red rock alteration. Metasediment. 188-189 some garnet, carbonate, magnetite.187-188 K-feldspar veins.
BT14	HDD044	233	CPX Skarn	K-feldspar, magnetite ±CPX skarn.
BT15	HDD044	170	Garnet Skarn	Magnetite replaced by garnet, "garnet skarn". Some K-feldspar+magnetite alteration, CPX replaced by clays, garnet replaced by magnetite.

Table 11: Sample collected from Hillside and specimen notes from the field.

Age:	**Subgroup 1** *IOCG sensu stricto*	**Subgroup 2** *Iron-oxide (p)*	**Subgroup 3** *Alkaline Intrusion*	**Subgroup 4** *Skarn*	**Subgroup 5** *High-grade Au (Cu)*
Cenozoic		El Laco		Iron Springs	
		Cerro de Mercado		Cortez, Yerington	
Mesozoic	Candelaria	Chilean iron belt		Hangkow	
	Manto verde	Peruvian iron belt		Cornwall, Grace	
	Raul-condestable			Korshunovsk, Tagar	
Paleozoic				Kachar, Sarbai, Sokolovsk	
				Teyskoe, Ampalyskoe	
				Tashtagol	
				Magnitogorsk	
				Goroblagodat, Peschansk	
				Chogart	
Neoproterozoic		Kasempa		Jabal Isas	
Mesoproterzoic	Olympic Dam	Benson Mines			
	Ernest Henry	Pea Ridge	Bayan Obo		Starra
	Mt. Elliot/Swan	Acropolis	O'Okiep		Tick Hill
Paeloproterozoic		Kiruna	Palabora	**Hillside**	Warrego
		Malmberget		Grangesberg	Nobles Nob
		Svappavaara			White Devil
Neoarchean	Salobo				
	Cristallino				
	Sossego-Sequrinho				

Table12: Classification of IOCG-U style deposits from around the world (Groves et al 2010).

Eu/Eu*	LaN/YbN	LaN/SmN	CeN/YbN	CeN/SmN	EuN/YbN	Sum REE
1.1	5.0	3.2	2.8	1.9	1.6	1.2

Table 13: Hematite REE summary.

Eu/Eu*	LaN/YbN	LaN/SmN	CeN/YbN	CeN/SmN	EuN/YbN	Sum REE
0.749091	1.103636	0.78	0.970909	0.700606	1.013636	0.086061

Table 14: Magnetite REE summary.

Appendix A

Petrographic Study

Hole ID: HDD026 **Sample Number**: HDD026 363.2 **Depth**: 363.2 **Reason For sampling**: Collcted by Graham Teale **Hand specimen description**: Sulphide rich with large garnet grains.	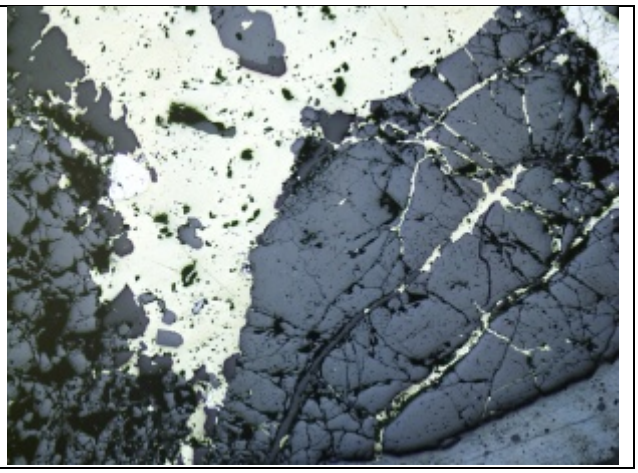

Minerals:
Magnetite
Hematite
Chalcopyrite
Pyrite

Description:
Sulphide dominated, chalcopyrite is the most common sulphide. Pyrite also present within the chalcopyrite rich zone, with indication of chalcopyrite intruding the pyrite grains. Sulphides present throughout entire sample. Pyrite grains highly fractured and have been in filled by chalcopyrite. Original pyrite grain shape is also identifiable and most pyrite grains appear to have grown into very euhedral shapes. A very small amount of hematite is present within the iron oxide domain. There are no traces of magnetite within some of the hematite grains and the hematite grains are in a tabular shape indicating they may be a primary hematite and a non-replacement hematite growth.

Hole ID:HDD016 **Sample Number**: HDD016 379.4 **Depth**: 379.4 **Reason For sampling**: Collcted by Graham Teale **Hand specimen description**: FeO matrix with red rock alteration. Small vein running through sample.	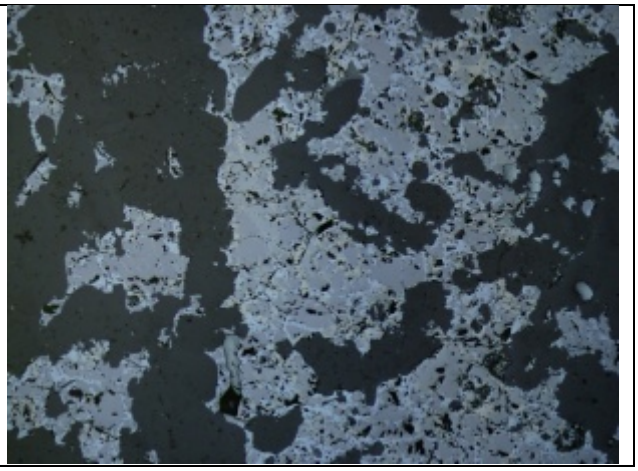

Minerals:
Magnetite
Hematite
Shpalerite
Pyrite
Chalcopyrite

Description:
Very iron oxide rich and very low in sulphides. Alteration very minor apart from the “red rock” alteration. Magnetite slightly replaced around the grain boundaries to hematite. Small amounts of chalcopyrite throughout slide in very small grains sometimes only several microns across. Pyrite also present in small amounts normally associated with chalcopyrite. Previously euhedral pyrite grains highly fractured and fractures in filled by chalcopyrite. Hematite replacement of magnetite appears to follow fractures within the magnetite.

Hole ID:HDD016 **Sample Number**: HDD016 389.5 **Depth**: 389.5 **Reason For sampling**: Collcted by Graham Teale **Hand specimen description**: Oxide dominated with a large amount of epidote within grain boundaries.	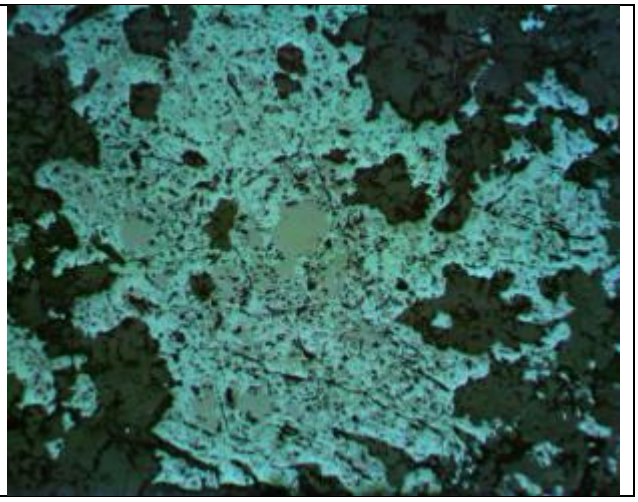

Minerals:
Magnetite
Hematite
Chalcopyrite

Description:
The iron oxides are mostly magnetite that is in the early stages of being replaced by hematite. The large grains of magnetite have been broken into smaller grains by silica intrusions. This has allowed for the replacement of magnetite by hematite to follow these fractures caused by the silica intrusion. The amount of replacement appears to vary with some magnetite grains with small amounts of replacement around the rims and other almost 100% replaced. There are small amounts of chalcopyrite but the relationship with the iron oxides unclear in this sample. This could be due to the fact that this chalcopyrite is very late in the deposits development and is associated with a late fluid influx not the mineralizing fluids.

Hole ID: HDD026 **Sample Number**: HDD026 394.4 **Depth**: 394.4 **Reason For sampling**: Collected by Graham Teale **Hand specimen description**: Fine grains of Fe oxides and sulphides with a large quartz vein in the middle.	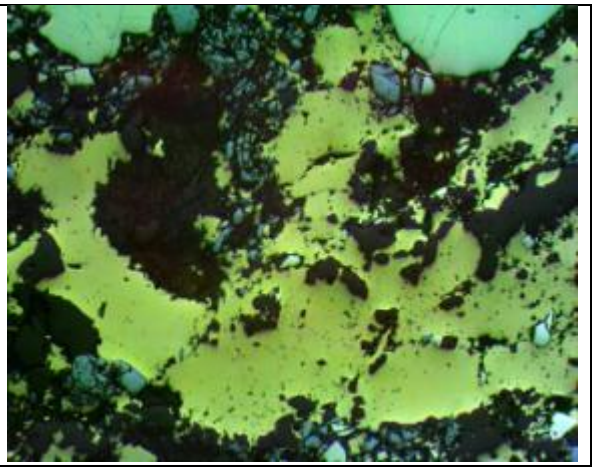

Minerals:
Chalcopyrite
Pyrite
Hematite
Magnetite
Gold

Description:
Highly brecciated and very fine grained in parts. Iron oxides are much finer grained compared to the sulphides. Very small gold grains can be seen within the chalcopyrite rich zones. Slight signs of bladed hematite in areas. Magnetite appears to be strongly replaced by hematite with very little remanent magnetite remaining. On the edges of the quartz veins an increased amount of chalcopyrite in present which may indicate some transport of the chalcopyrite within the quartz veins. Chalcopyrite influx makes up the matrix in some parts with pyrite and some iron oxides within chalcopyrite zone. There is little to no sign of pyrite being replaced by chalcopyrite.

Hole ID: HDD037 **Sample Number**: HDD037 256.1B **Depth**: 256.1 **Reason For sampling**: Collected by Graham Teale **Hand specimen description**: Sulphide rich with quartz and magnetite surrounding sulphide zone.	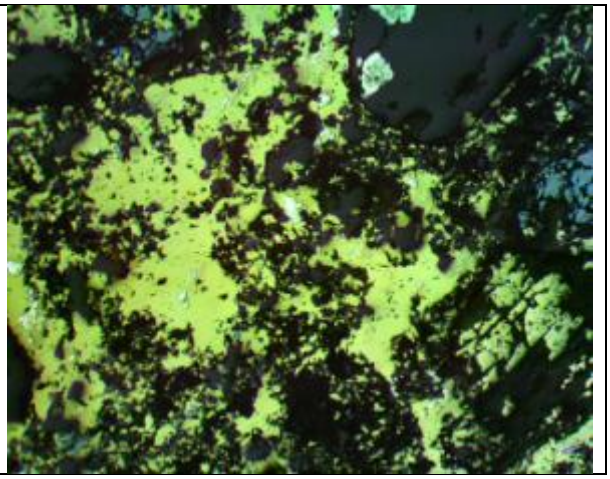

Minerals
Chalcopyrite
Pyrite
Hematite
Magnetite
Sphalerite

Description:
A very large amount of pyrite and chalcopyrite. A rich pyrite band boarders a magnetite + quartz rich area with a very small amount of chalcopyrite and almost no hematite. Throughout the chalcopyrite rich area hematite appears to be replacing magnetite more commonly than normal, a clear relationship is present. Strongly brecciaed coarse grained minerals present throughout the entire sample. Hematite can also be founded within chalcopyrite grains, confirming chalcopyrite entered system after iron oxides but the timing of the replacement is still not defined.

Hole ID: HDD016 **Sample Number**: HDD016 379.4 **Depth**: 379.4 **Reason For sampling**: Collected by Graham Teale **Hand specimen description**: Silica dominated with strong “red rock alteration”	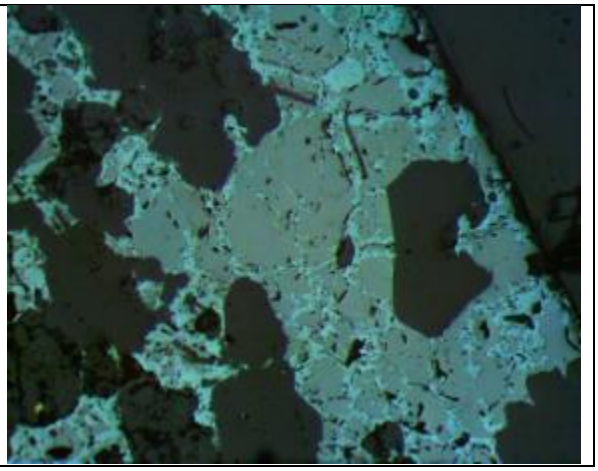

Minerals:
Hematite
Magnetite
Chalcopyrite
Pyrite

Description:
Very iron oxide rich, very low in sulphides. Not a large amount of alteration, strong “red rock alteration” throughout. Magnetite slightly altered around the edges to hematite, small amounts of chalcopyrite throughout the slide in very small grains sometimes. Pyrite also present in small amounts and normally within the intrusion of chalcopyrite.

Hole ID: HDD016 **Sample Number**: HDD016 387.9 **Depth**: 387.9 **Reason For sampling**: Collected by Graham Teale **Hand specimen description**: Fe oxide and sulphide rich. Green mineral also present may be epidote.	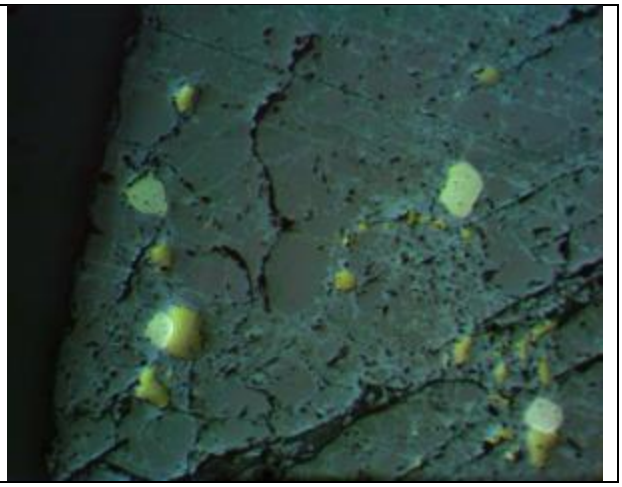

Minerals:
Magnetite
Hematite
Pyrite
Chalcopyrite

Description:
Large amount of magnetite with a limited amount of replacement to hematite. The small amount of hematite replacement appears to follow the joints within the magnetite. The hematite replacement appears to be stronger in the areas chalcopyrite is present. Zone of sulphides within the iron oxides zones common throughout sample. The sulphide zones are dominated by pyrite but are commonly found with some chalcopyrite. The pyrite zones are normally much larger than the scattered chalcopyrite grains.

Hole ID: HDD044 **Sample Number**: BT014B **Depth**: 233 **Reason For sampling**: Sulphide/ Fe oxide interaction **Hand specimen description**: Sulphide dominated with large iron oxide grains.	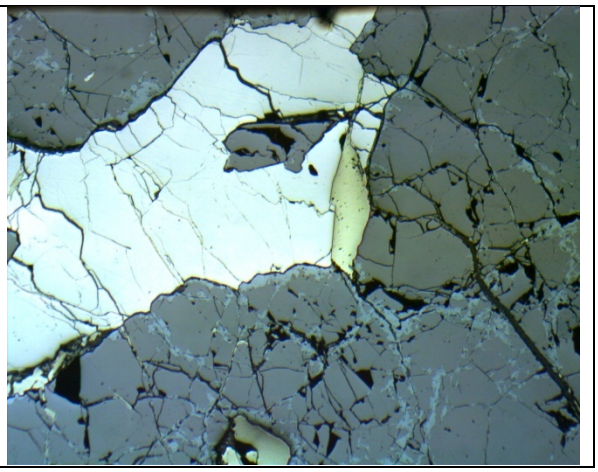

Minerals
Hematite
Magnetite
Chalcopyrite
Pyrite
Sphalerite

Description:
Very iron oxide and sulphide dominated sample. Magnetite in pristine condition with very early stages of replacement from hematite around the grain boundaries. Hematite replacement also appears to be present in zones with no fractures and moves through the magnetite grains. A wave front of hematitic replacement can be observed indicating that the magnetite grains are porous and are allowing fluid to flow through and replace it in sections. Chalcopyrite appears to have in filled small fractures within the magnetite grains. This may be due to the late carbonate veining stage causing an influx in chalcopyrite being deposited.

Hole ID: HDD040 **Sample Number**: HDD040 150.5 **Depth**: 150.5 **Reason For sampling**: Graham Teales samples **Hand specimen description**: very large grains of chalcopyrite with pyrite large hematite grain surrounded by possible garnets.	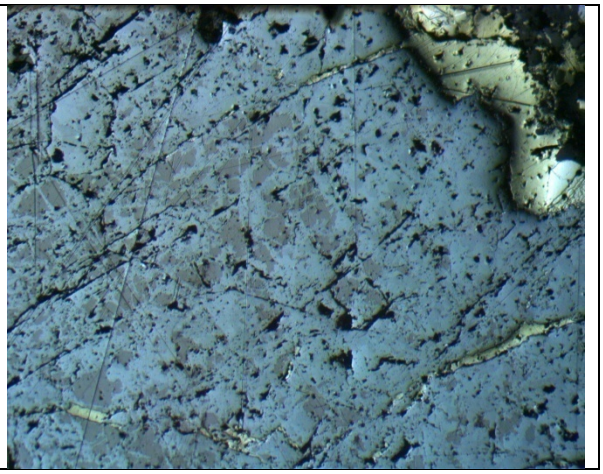

Minerals:
Chalcopyrite
Pyrite
Hematite
Magnetite

Description:
Very large iron oxide grains that appears to have originally been magnetite but is in late stages of hematite replacement. Slide dominated by chalcopyrite but several pyrite grains within the chalcopyrite matrix. This shows the replacement of pyrite to chalcopyrite. Fractured magnetite grains almost complete replaced by hematite, accelerated due to the fractures. Highly brecciated with a chalcopyrite matrix. Chalcopyrite found within some magnetite crystals with hematite replacement. The large iron oxide grain in the centre of the slide is surrounded by chalcopyrite. This large grain has the largest amount of hematite replacement seen.

Hole ID: HDD044 **Sample Number**: BT014B **Depth**: 233m **Reason For sampling**: Iron oxide analysis. Iron oxide- sulphide relationship. **Hand specimen description**: Iron oxide and sulphide dominated.	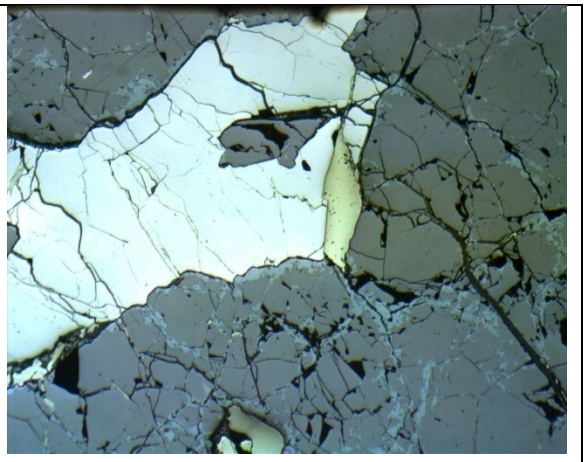

Minerals:
Magnetite
Hematite
Chalcopyrite
Pyrite
Sphalerite

Description:
Very iron oxide and sulphide dominated. Magnetite in very early stages of replacement by hematite. Hematite moves along porous zone within the magnetite grain. Chalcopyrite also appears to have in filled the fractures within magnetite.

Hole ID: HDD044 **Sample Number**: BT10B **Depth**: 164 **Reason For sampling**: Iron oxide sampling. **Hand specimen description**: Iron oxide and sulphur dominated with quartz intrusions.	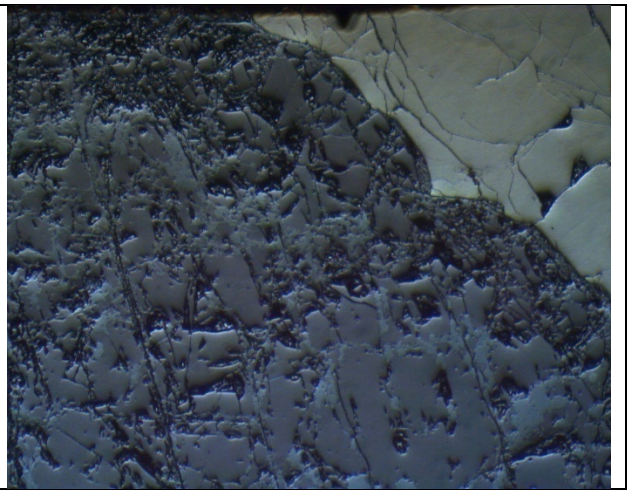

Minerals:
Hematite
Magnetite
Chalcopyrite
Pyrite

Description:
Iron oxide and sulphide dominated. Quartz intrusions that appear to have hematite in tabular grain shape that may have been formed from the influx of fluid that formed the quartz. Chalcopyrite can also be found within the quartz in very sparse concentrations. The Fe oxides appear to be magnetite dominated with very little hematite replacement. Very large magnetite grains have slight hematite replacement along fractures within the grains. A strong line where hematite replacement is stronger. No fractures are visible along this area so it can be assumed that this may be a more porous zone.

Hole ID: HDD044 **Sample Number**: BT15B **Depth**: **Reason For sampling**: Iron oxide analysis **Hand specimen description**: Very Iron rich, spotted with chalcopyrite.	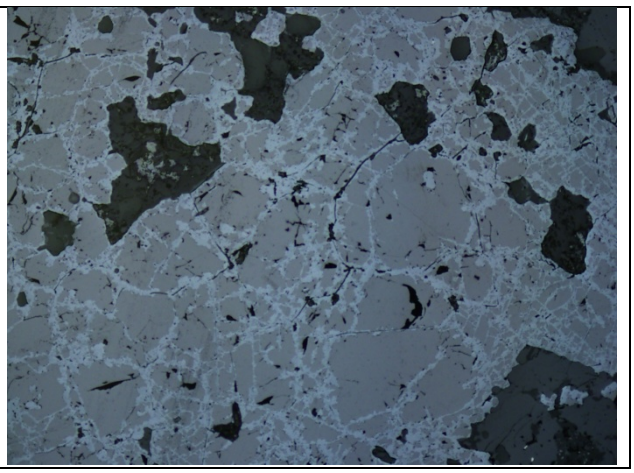

Minerals:
Magnetite
Hematite
Chalcopyrite
Pyrite

Description:
Large amount of magnetite that has been replaced by hematite at the edges of the grains. The hematite replacement appears to follow micro fractures within the magnetite or the porosity of the magnetite. Very small amounts of pyrite with strong cubic grain structure. Very fine grained iron oxides seen throughout the slide.

Hole ID: HDD044 **Sample Number**: BT07B **Depth**: 163.6m **Reason For sampling**: Sulphide analysis. **Hand specimen description**: Sulphides within iron oxide.	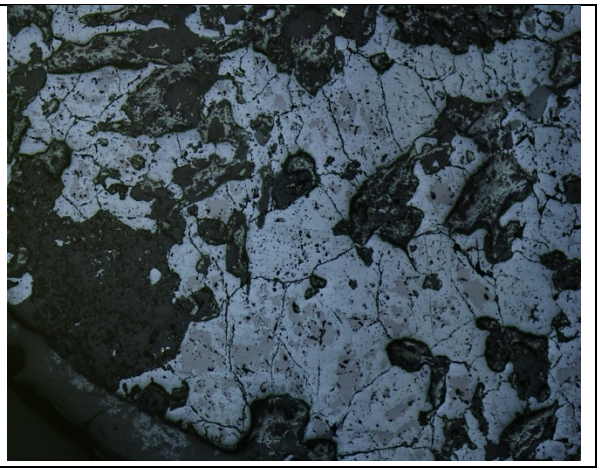

Minerals:
Chalcopyrite
Pyrite
Magnetite
Hematite

Description:
Dominated by sulphides with a large amount of iron oxides also present. Pyrite crystals within the sample appear to be fractured and chalcopyrite is seen to infill the fractures. Hematite can also be seen around the edge of the chalcopyrite grains. The hematite is in bladed form which indicates that it is primary hematite. This may have been injected with the

chalcopyrite. Where the chalcopyrite reaches the iron oxide hematite replacement of magnetite is dominate. Within the magnetite rich zone hematite replacement is obviously not as common.

Hole ID: HDD044 **Sample Number**: BT09B **Depth**:155.2 **Reason For sampling**: Sulphide – iron oxide relationship. **Hand specimen description**: Strongly brecciated sulphides.	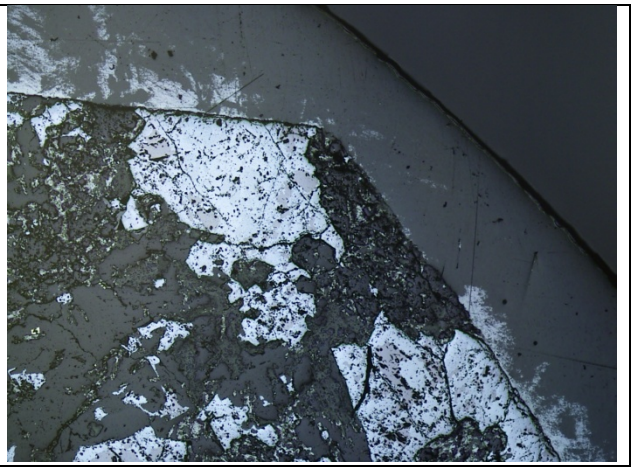

Minerals:
Pyrite
Chalcopyrite
Magnetite
Hematite

Description:
Large amounts of sulphides. Pyrite appears to have been strongly brecciated and in filled by chalcopyrite. The chalcopyrite appears to be controlled by the location of the pyrite. The iron oxide grains have little sulphides grains within them. The iron oxide rich areas are highly brecciated with hematite replacement strong on the edges of the sulphides but much weaker and almost non-existant the further away. Large vein cuts through the length of sample. Very little inclusions within the magnetite grains. Large magnetite grains ideal sampling.

Hole ID: HDD044 **Sample Number**: BT04B **Depth**: 148m **Reason For sampling**: K-feldspar rich skarn, **Hand specimen description**: K-feldspar rich with iron oxides present.	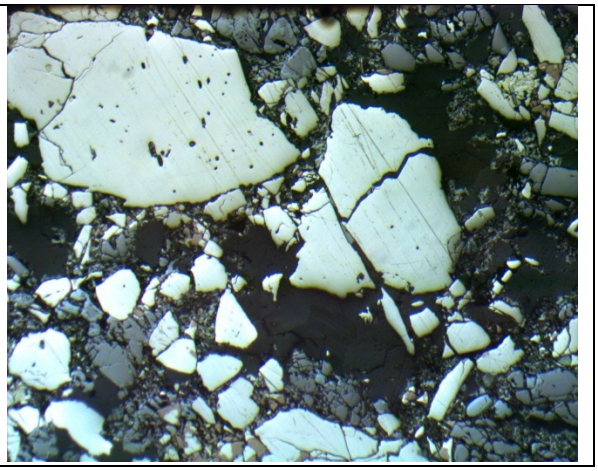

Minerals:
Magnetite
Hematite
Sphalerite
Chalcopyrite
Pyrite

Description:
Very Si rich, with some traces of Fe oxides. Magnetite dominated but hematite replacement in late stages. Sphalerite also present in a small abundance. Large magnetite grains can also be seen with hematite replacement at it's edges. Some very small magnetite grains have been effected stronger than the large grains.

Hole ID: HDD016 **Sample Number**: HDD016 542.7 **Depth**: 542.7m **Reason For sampling**: Graham Teale samples. **Hand specimen description**: Fe oxide rich "some red rock alteration"	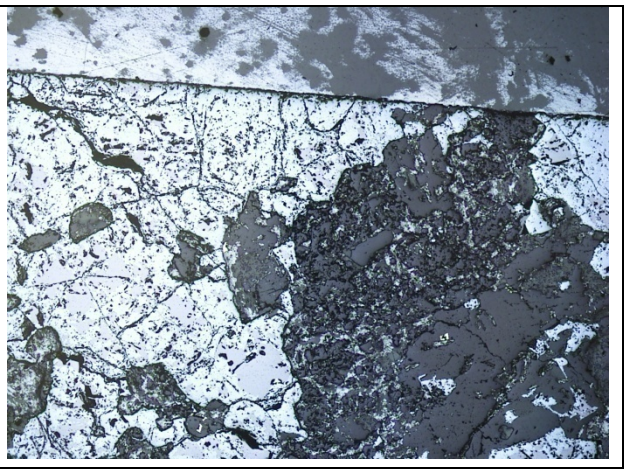

Minerals:
Magnetite
Hematite
Chalcopyrite
Pyrite

Description:
Dominated by iron oxides. Hematitic replacement in its advanced stages. Yet large magnetite grains are still present. Magnetite does not appear to make contact with the edge of any iron oxide grains. Magnetite replacement also appears to not follow fractures within the rock but is more likely to be from the porosity within the magnetite grains. Some bladed hematite can be observed in sections. Also within what looks like carbonate are very small hematite grains that almost look as if they have been dusted. Carbonate vein can be seen cutting iron oxides. Hematite grains appear to flow along veins.

Hole ID: HDD044 **Sample Number**: BT06B **Depth**: 221m **Reason For sampling**: Iron oxide – sulphide relationship. **Hand specimen description**: Garnet skarn, chalcopyrite rich.	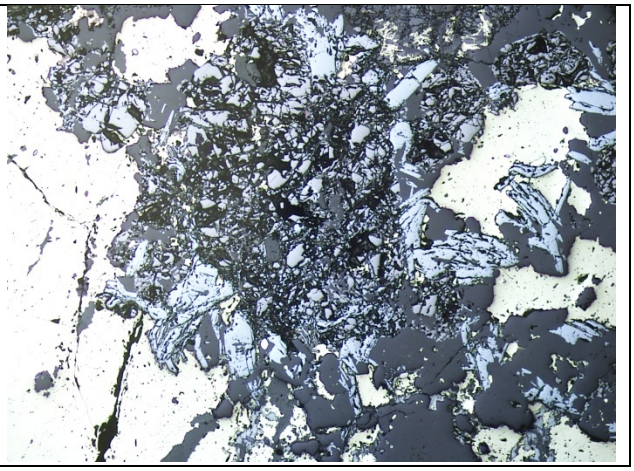

Minerals:
Chalcopyrite
Pyrite
Sphalerite
Magnetite
Hematite

Description:
Very sulphur and iron oxide dominated. Rich in sphalerite compared to previous samples. Hematite concentrated around the chalcopyrite rich areas. Hematite sometimes has a tabular texture indicating primary hematite. Chalcopyrite with large number of fractures. Large pyrite grains that have been fractured and in fill by chalcopyrite. Very small amount of hematite with tabular grain shape. Sphalerite can show ghost grains that are fractured grains

that hold original shape. Large amount of brecciated magnetite with very little hematite replacement. Any replacement is very hard to see.

Polished Thin Sections

Hole ID: HDD **Sample Number**: HDD037 256.1B **Depth**: 256.1m **Reason For sampling**: Graham Teale samples **Hand specimen description**: Large amount of “red rock alteration”, amphibole rich.	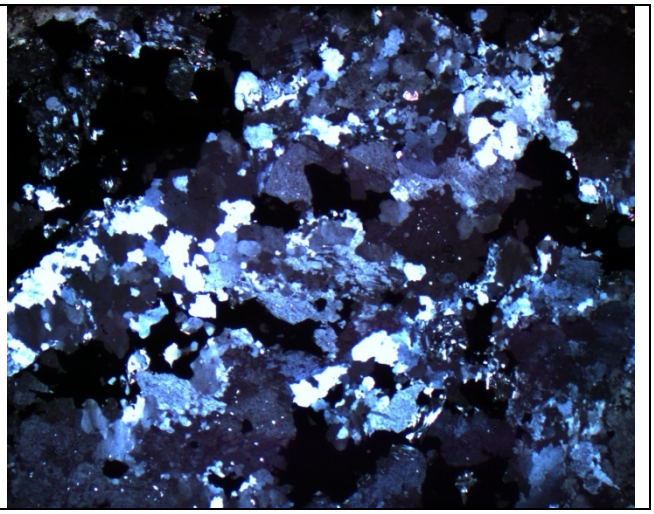

Minerals:
Amphibole (hornblend)/ Chloritised biotite
“red rock alteration”
Quartz
Plagioclase
Chlorite

Description:
Sulphide rich with a large amount of quartz. Quartz grain size varies greatly with very fine grain bands in sections and very course plagioclase grains alternativly. Within the finer section of quartz clear banding can be seen with chloritised biotite running through some layers. Banding orientation similar throughout but not always present. Plagioclase does not appear to have a uniform orientation within the slide. Chlorite/biotite appear to form matrix of sulphides. Chlorite appear to be very late. Quartz and plagioclase formed first out of the minerals in the slide with biotite and sulphides.

Interp: Metasediments brecciated and mineralized.

Hole ID: HDD016 **Sample Number**: HDD016 379.4 **Depth**: 379.4m **Reason For sampling**: Graham Teale samples **Hand specimen description**: Silica dominated with "red rock" alteration.	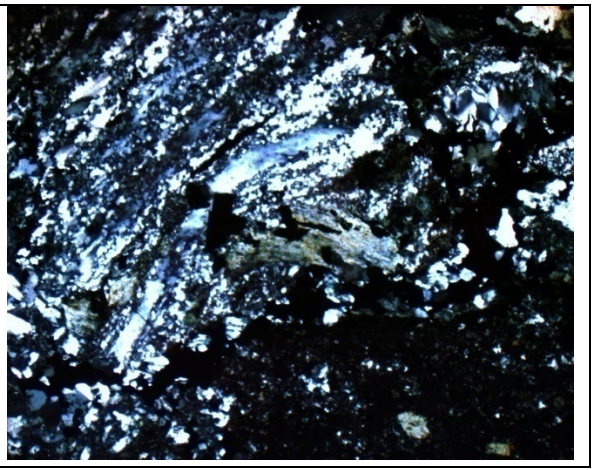

Minerals:
Chlorite
Quartz
Sulphides
K-feldspar
CPX

Description:
Very fine grained quartz throughout slide. Brecciation appears to be uniform throughout slide. Chlorite and K-feldspar related to the "red rock alteration" found to be zoned together. Small veins running the length of the slide. Variation of fine grained to coarse grain immediate to each other. High bifringence mineral presence in veins and in several sections throughout the slide.

Hole ID: HDD026 **Sample Number**: HDD026 363.2 **Depth**: 363.2m **Reason For sampling**: Graham Teale samples **Hand specimen description**: very sulphide rick rocks with what appears to be garnet.	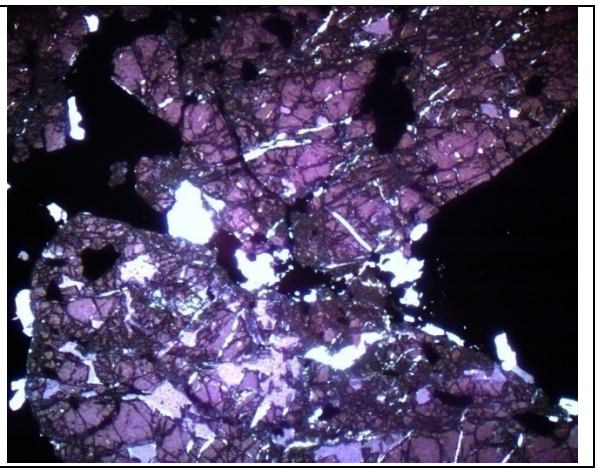

Minerals:
Garnet
Plagioclase
Quartz

Description:
Sulphur dominated with very large grains of garnet throughout. Plagioclase and garnet appear to be commonly found in the garnet sulphide contact zone. Veins throughout the garnet filled with high bifringence mineral may be kyanite. Garnet extremely fractured with sulphide minerals running through fractures. Slight corresponding fracture orientation is visible throughout the slide.